FINITE ELEMENT METHOD WITH WEIGHTED EXTENDED B-SPLINES FOR ELECTROMAGNETICS

by

Gökhan Apaydın

B.S., Electrical and Electronic Engineering, Boğaziçi University, 2001

M.S., Electrical and Electronic Engineering, Boğaziçi University, 2003

Submitted to the Institute for Graduate Studies in
Science and Engineering in partial fulfillment of
the requirements for the degree of
Doctor of Philosophy

Graduate Program in
Boğaziçi University
2007

ACKNOWLEDGEMENTS

I would like to thank my thesis supervisor Prof. Selim Şeker for his invaluable guidance, interest, and motivation throughout my study. I am grateful to him. I would like to thank Prof. Niyazi Arı for his contribution, experience, and patient explanation of my numerous questions throughout my stay in Switzerland. This thesis could not have been completed without their assistance, contributions, and suggestions.

I would also like to thank the other members of the thesis committee; Prof. Avni Morgül, Prof. Tayfun Günel, Prof. Yorgo Istefanopulos, and Prof. Kadri Özçaldıran for their constructive comments and advice.

Finally, I would like to thank my family for their support throughout my study of education. I also thank my wife, Bilge for her contribution. Life does not have a meaning without them.

ABSTRACT

FINITE ELEMENT METHOD WITH WEIGHTED EXTENDED B-SPLINES FOR ELECTROMAGNETICS

This thesis presents fundamental overview of electromagnetics and finite element method (FEM) with weighted extended basis splines (web-splines), which is a new developed finite element method for electromagnetic problems.

The developed method is discussed in detail. The advantages of FEM with web-spline method are illustrated by using several electromagnetic applications. The wave equation is solved by using web-spline method and compared with the previous studies in the literature. The results of the simulation are shown to have excellent agreements. Thus, this thesis proves that the FEM with web-spline method can be used in electromagnetic applications with good accuracy. The method does not need any mesh generation as in the standard FEM, and more accurate results are obtained by using less memory in computations.

ÖZET

ELEKTROMANYETİK İÇİN AĞIRLIKLI GENİŞLETİLMİŞ B-SPLINE İLE SONLU ELEMAN YÖNTEMİ

Bu tez, elektromanyetik problemler için geliştirilmiş yeni sonlu eleman yöntemi olan ağırlıklı genişletilmiş b-spline sonlu eleman yöntemini ve elektromanyetiğin genel hatlarını sunuyor.

Geliştirilen yöntem ayrıntılı olarak tartışılmaktadır. Çeşitli elektromanyetik uygulamalar kullanılarak ağırlıklı genişletilmiş b-spline yöntemi ile sonlu eleman yönteminin avantajları açıklanmaktadır. Ağırlıklı genişletilmiş b-spline yöntemi kullanılarak dalga denklemi çözülüp literatürde bulunan daha önceki çalışmalarla karşılaştırılmaktadır. Benzetim sonuçları mükemmel uyuşma gösterdi. Böylelikle, bu tez elektromanyetik uygulamaların daha doğru şekilde ağırlıklı genişletilmiş b-spline sonlu eleman yönteminin kullanılmasını ispatlar. Bu yöntem normal sonlu elaman yönteminde kullanılan ağ oluşturmaya ihtiyaç duymaz ve hesaplamalarda daha az hafıza kullanılarak daha doğru sonuçlar elde edebilmektedir.

TABLE OF CONTENTS

LIST OF FIGURES

LIST OF TABLES

LIST OF SYMBOLS/ABBREVIATIONS

a	The maximum diameter of circle circumscribing domain
$\mathbf{B}$	Magnetic flux density vector
B	Basis function
$\mathbf{D}$	Electric flux density vector
e	Error
$\mathbf{E}$	Electric field intensity vector
f	Frequency
F	Load matrix
h	Grid width
$\mathbf{H}$	Magnetic field intensity vector
I	Set of inner b-splines
j	Imaginary unit
$\mathbf{J}$	Electric current density vector
J	Set of outer b-splines
K	Stiffness matrix
$\widetilde{k}$	Wave number
m	Dimension
M	Mass matrix
$\mathbf{n}$	The normal unit vector
n	Degree of functions
R	Reflection coefficient
T	Thickness
u	Time harmonic magnetic and electric field
u_e	Exact solution
$\widetilde{u}$	Approximated solution
U	Matrix consisting of coefficients
v	Smooth function
w	Weight function

Δ	Laplace operator
∇	Gradient
$\nabla\cdot$	Divergence
$\nabla\times$	Curl
Ω	Defined region
$\partial\Omega$	Boundary of the region
β	Loss parameter
γ	Smoothing parameter
δ	Size of boundary strip
ε	Permittivity
ε_r	Relative permittivity
θ	Direction angle of wave
κ	Diffusion coefficient
μ	Permeability
ρ	Electric charge density
σ	Electric conductivity
ω	Wave angular frequency

BC	Boundary Condition
BEM	Boundary Element Method
CAD	Computer Aided Design
FDM	Finite Difference Method
FEM	Finite Element Method
FVM	Finite Volume Method
GUI	Graphical User Interface
MOM	Method of Moments
PDE	Partial Differential Equation
TE	Transverse Electric
TM	Transverse Magnetic
WEB-SPLINES	Weighted Extended Basis Splines

1. INTRODUCTION

Electromagnetics has played an important role in shaping our daily lives. The ambition of mankind to make use of electromagnetic waves has resulted in drastic improvements in the communications technologies over the last few decades. We now enjoy the ability to communicate real time over large distances, using satellite links, and the mobile life styles enabled by portable wireless communications devices. Radar technologies, which are used to track moving objects, support air-traffic control systems.

It was in 1831 when Faraday made a ground-breaking discovery. He observed the relationship between electric currents and magnetism. He thus proposed the three laws of electro-magnetic induction [1]. In 1873, Maxwell introduced the classical electromagnetics theory through developing mathematical expressions which characterize the relationship between electric and magnetic fields [2]. These equations are still widely used in physics and the study of electromagnetic waves. Recent discoveries regarding the nature of these waves, coupled with the advances in computing technology have provided simple means of solving complex equations.

The use of wireless communications devices entails some undesired effects as well. Such effects are mostly due to the fact wireless is a broadcast medium and therefore it is not possible to direct the electromagnetic waves precisely. Extensive use of cell phones, for example, has raised concerns regarding the possible harmful effects to human health. As radio waves originating from the cell phone hit the skull, they are scattered and part of their energy is absorbed into the body. The effects of this phenomenon are still an open research question. Another interesting side effect of wireless communication technologies can be seen in the use of laptops in air-craft. The signals for the personal laptop can interfere with the signaling between the aircraft and the control tower, leading to potentially disastrous situations. Many other examples for such undesired effects can be produced. To combat such undesired effects, the true nature of electromagnetic waves need to be studied, and computationally inexpensive

tools need to be developed. It is only through such tools that the engineering community can design systems which can coexist and do not create undesired interference.

Maxwell's equations have yielded some partial differential equations (PDE) which model the behavior of the electromagnetic waves. These equations are widely used in engineering designs and are often difficult to solve analytically. Thus, numerical computation techniques which promote faster and more accurate solution techniques have been developed. There are some numerical techniques, the most important ones being Method of Moments (MOM) or Boundary Element Method (BEM), Finite Difference Method (FDM), and Finite Element Method (FEM).

The choice of the solution method often depends on the specific application it is used for. For example, FEM and FDM methods are particularly useful in studying inhomogeneous materials as they consider a discretization approach.

FDM was developed by Yee in 1966 [3]. His idea is to divide the considered domain in order to take the values of points and convert the partial derivatives to difference equations. The idea is coming from Taylor expansions. The finite differences are used to approximate derivatives. In this method, continuous equations are replaced with their finite difference of values of selected points. However, FDM is difficult to implement for complex objects.

FEM stands out as the most widely used method when studying complex geometries and boundaries, irregular domains or inhomogeneous media with different boundary conditions. It uses piecewise continuous functions and numerical meshes. More specifically it is based on the use of basis functions and numerical integration to solve the linear system equation. More details about the FEM method can be found in Chapter 2. It is important to note that FEM increases the computation time as well as the memory usage.

MOM or BEM achieves better performance in terms of computation time and memory usage. It only considers the elements along the boundaries of the domains,

rather than the interior regions [4], and the equations are governed by the boundary conditions. This method is not very useful in studying inhomogeneous media; as such media require the examination of the interior region.

FDM provides fast solution in time domain. However, it cannot provide good solutions for complex objects, because it provides a point wise approximation. Table 1.1 summarizes the comparison between fundamental techniques to solve partial differential equations.

Table 1.1. Comparison of numerical methods to solve partial differential equations

Method	BEM	FDM	FEM
Complex domain	Good	Poor	Best
Regular domain	Good	Good	Good
Computational time	Good	Good	Poor
Inhomogeneous domains	Poor	Poor	Best
Complex boundary conditions	Good	Poor	Good

For FEM, mesh generation causes consumption in computation time for higher dimensions. In the past years, many researches have developed mesh generation and meshless FEM [5, 6, 7, 8].

This study presents on the use of b-splines in the FEM method. The spline functions are often used in approximation, data fitting, computer aided design (CAD), and many other applications [9, 10]. The contributions of Carl De Boor, de Casteljau, and Bezier have played an important role for splines. The b-splines can be used as basis functions for their flexibility and continuity between points. However, boundary conditions have caused problems considering stability. Many researches have been done about this issue [11, 12, 13].

1.1. Contribution of the Thesis

The advances of mathematics have supported the development of electromagnetic theory in the history of electromagnetics [14]. This study uses web-spline method of numerical solution for solving the PDE for electromagnetics for the first time. The objective is to use the web-spline finite element method for electromagnetic problems such as two dimensional wave equation, reflection, and waveguide problems, which are intensively studied in literature. The analyses presented in this study show the suitability of the proposed method to the complex electromagnetic problems. A Matlab based graphical user interface for the web-spline is also presented in this work.

1.2. Outline of the Thesis

The outline of the thesis is as follows. Chapter 2 begins with the overview of electromagnetics, PDE, and FEM. After introducing the general background of FEM, it explains the b-splines.

Using FEM and b-splines, the steps of FEM with web-spline method are studied in Chapter 3. Finite element basis functions are constructed by using web-splines without mesh generation. Then, finite element assembly and solution are studied.

Chapter 4 focuses on some applications of electromagnetics in one dimension. This chapter shows why the b-splines are used for constructing basis functions. The simulation results using FEM with b-splines are compared with the exact results and the general FEM methods.

Chapter 5 shows the applications of electromagnetics in two dimensions such as wave equations and waveguides; then it presents the simulation results. Solutions of problems with various parameters using weighted extended b-splines are tested and compared with the standard FEM solutions. The advantages of FEM with web-spline method are shown by using error analysis.

Chapter 6 shows Graphical User Interfaces (GUI) for web-splines. These interfaces are designed to simplify the study of the user. Therefore, Matlab functions are executed by clicking an icon easily.

This study comes to a conclusion with a discussion on the advantages and disadvantages of the proposed model in the last chapter.

The Appendix presents some vector identities, integral theorems; and gradient, curl relationships among various coordinate systems. Then, a short overview of the programs, which are provided for this thesis in Matlab, follows.

The computer platform used for all simulation results is a Hewlett Packard notebook computer with a Pentium 2.0 GHz main processor and 1.5 GB of RAM.

2. THEORETICAL BACKGROUND

2.1. Information about Electromagnetics

2.1.1. Overview of the Maxwell's Equations

The Maxwell's equations are four differential equations which show the classical properties of electromagnetic fields using electric (**E**) and magnetic field intensity vector (**H**). The equations can be summarized in Table 2.1 [15]. For the equations; ρ is the electric charge density (C/m^3), (**J**) is the electric current density vector (A/m^2), (**D**) and (**B**) show the electric and magnetic flux density vectors (C/m^2, Wb/m^2) respectively. The first two equations are related to the divergence of vectors, and the others are related to the curl operation of vectors. The divergence and curl operations for various coordinate systems are given in Appendix A.

Table 2.1. The Maxwell's equations using differential form

Name	Differential form
Gauss's Law	$\nabla \cdot \mathbf{D} = \rho$
Gauss's Law for magnetism	$\nabla \cdot \mathbf{B} = 0$
Faraday's Law	$\nabla \times \mathbf{E} = -\frac{\partial \mathbf{B}}{\partial t}$
Maxwell-Ampere's Law	$\nabla \times \mathbf{H} = \mathbf{J} + \frac{\partial \mathbf{D}}{\partial t}$

The relations between these vectors are shown in the following equations as:

$$\mathbf{D} = \varepsilon \mathbf{E} \tag{2.1}$$

$$\mathbf{B} = \mu \mathbf{H} \tag{2.2}$$

$$\mathbf{J} = \sigma \mathbf{E} \tag{2.3}$$

where ε, μ, σ denote the permittivity (F/m), the permeability (H/m), and the electric conductivity (S/m) of the medium.

2.1.2. Wave Equations

The wave equations for the electric and magnetic fields can be obtained by using the Maxwell's equations [16, 17]. Taking the curl of $\nabla \times \mathbf{E}$ given in Table 2.1 divided by μ as:

$$\nabla \times (\frac{\nabla \times \mathbf{E}}{\mu}) = -\nabla \times \frac{\partial \mathbf{H}}{\partial t} \tag{2.4}$$

$$\nabla \times (\frac{\nabla \times \mathbf{E}}{\mu}) = -\frac{\partial}{\partial t}(\nabla \times \mathbf{H}) \tag{2.5}$$

The fourth Maxwell's equation is used for the curl of $\mathbf{H}$ as:

$$\nabla \times (\frac{\nabla \times \mathbf{E}}{\mu}) = -\frac{\partial}{\partial t}(\mathbf{J} + \varepsilon \frac{\partial \mathbf{E}}{\partial t}) \tag{2.6}$$

Using the vector identity given in Appendix (B.1), Equation (2.6) becomes

$$\frac{1}{\mu}\nabla \times \nabla \times \mathbf{E} + \nabla(\frac{1}{\mu}) \times \nabla \times \mathbf{E} + \varepsilon \frac{\partial^2 \mathbf{E}}{\partial t^2} = -\frac{\partial \mathbf{J}}{\partial t} \tag{2.7}$$

For the homogeneous material, the second term in Equation (2.7) vanishes and the vector identity given in Appendix (B.2) is applied as:

$$\frac{1}{\mu}\nabla \times \nabla \times \mathbf{E} + \varepsilon \frac{\partial^2 \mathbf{E}}{\partial t^2} = -\frac{\partial \mathbf{J}}{\partial t} \tag{2.8}$$

$$\nabla(\nabla \cdot \mathbf{E}) - \nabla^2 \mathbf{E} + \mu\varepsilon \frac{\partial^2 \mathbf{E}}{\partial t^2} = -\mu \frac{\partial \mathbf{J}}{\partial t} \tag{2.9}$$

Using the same procedure, the equations for the magnetic field $\mathbf{H}$ are

$$\frac{1}{\varepsilon}\nabla \times \nabla \times \mathbf{H} + \mu\frac{\partial^2 \mathbf{H}}{\partial t^2} = \nabla \times \frac{\mathbf{J}}{\varepsilon} \tag{2.10}$$

$$\nabla(\nabla \cdot \mathbf{H}) - \nabla^2\mathbf{H} + \mu\varepsilon\frac{\partial^2 \mathbf{H}}{\partial t^2} = \nabla \times \mathbf{J} \tag{2.11}$$

Using the Gauss's Law ($\nabla \cdot \mathbf{E} = 0$ and $\nabla \cdot \mathbf{H} = 0$), the wave equation for free source medium ($\rho = 0, \mathbf{J} = 0$) can be shown as follows:

$$-\nabla^2\mathbf{E} + \varepsilon\mu\frac{\partial^2 \mathbf{E}}{\partial t^2} = 0 \tag{2.12}$$

$$-\nabla^2\mathbf{H} + \varepsilon\mu\frac{\partial^2 \mathbf{H}}{\partial t^2} = 0 \tag{2.13}$$

If the electric and magnetic fields are to be time harmonic with the time dependence $e^{j\omega t}$, the wave equations in Equations (2.12) and (2.13) can be written as:

$$-\nabla^2\mathbf{u} - \widetilde{k}^2\mathbf{u} = 0 \tag{2.14}$$

where $\widetilde{k} = \omega\sqrt{\mu\varepsilon}$ is the wave number, ω is the wave angular frequency, $\nabla^2(\Delta)$ is the Laplace operator, and $\mathbf{u}$ shows the time harmonic magnetic and electric field. This is called homogeneous wave equation or Helmholtz's equation, which is the elliptic partial differential equation.

2.1.3. Boundary Conditions

While studying the boundary conditions (BC) for the wave equations, the tangential and normal components of electric and magnetic fields on the surface are to be taken into consideration. At the interface between two media, the boundary conditions

for the electromagnetic fields can be expressed as:

$$\mathbf{n} \times (\mathbf{E_1} - \mathbf{E_2}) = 0 \tag{2.15}$$

$$\mathbf{n} \times (\mathbf{H_1} - \mathbf{H_2}) = \mathbf{J_i} \tag{2.16}$$

$$\mathbf{n} \cdot (\mathbf{B_1} - \mathbf{B_2}) = 0 \tag{2.17}$$

$$\mathbf{n} \cdot (\mathbf{D_1} - \mathbf{D_2}) = \rho_i \tag{2.18}$$

where $\mathbf{n}$ is the normal unit vector pointing from the second medium to the first medium, $\mathbf{J}_i$ is the electric current density at the interface, and ρ_i is the electric charge density at the interface.

If the boundary for the second medium has infinite conductivity, it is called perfect conducting boundary and electromagnetic fields for the second medium are zero.

2.2. Overview of Partial Differential Equations

Partial Differential Equations are equations which contain functions of independent variables and their partial derivatives. The general PDE of second order in m dimensions can be shown as

$$\sum_{p=1}^{m}\sum_{q=1}^{m} a_{pq}\frac{\partial^2 u}{\partial x_p \partial x_q} + \sum_{p=1}^{m}\beta_p \frac{\partial u}{\partial x_p} + \alpha u = f(x) \tag{2.19}$$

where x shows the independent variables with the coefficients $a_{pq}, \beta_p, \alpha; f$ is a forcing function, m is the dimension, and u is the unknown quantity on R^m. The PDE can be defined for the region ($\Omega \in R^m$). They are classified as elliptic, parabolic, and

hyperbolic according to the coefficients. If the eigenvalues of the matrix involved by a_{pq} are non zero and have the same sign, it is called elliptic equation. If they have opposite sign, it is called hyperbolic equation. If at least one of the eigenvalues is zero, it is defined as parabolic equation. Table 2.2 summarizes these classifications of second order PDE and gives some examples [18].

Table 2.2. The classification of partial differential equations

Type	Examples
Elliptic	1. Laplace's equation ($\Delta u = 0$)
Parabolic	2. Diffusion equation ($\frac{\partial u}{\partial t} = \kappa \Delta u$)
Hyperbolic	3. Wave equation given in (2.12)

The boundary of the region ($\partial\Omega$) should be specified to solve the PDE. The general form of the boundary conditions can be shown as

$$ru + s\frac{\partial u}{\partial n} = g(x) \tag{2.20}$$

where $\frac{\partial u}{\partial n}$ shows the derivative in the direction of the outward normal to the region with the coefficients r, s and function g which depends on the boundary conditions. Table 2.3 shows the types of boundary conditions.

Table 2.3. The classification of boundary conditions

Boundary Condition	r	s
Dirichlet BC	nonzero	zero
Neumann BC	zero	nonzero
Cauchy BC	nonzero	nonzero

2.3. Finite Element Method

The numerical techniques have been developed due to the fact that the analytical solutions do not exist for some engineering problems. The FEM has become one of the numerical techniques, which has been applied to obtain numerical solutions for partial differential equations in engineering, physics, and applied mathematics. FEM is useful for complex geometries and inhomogeneous media. Today, there are many developed programs which use FEM to solve partial differential equations. The idea is to use the piecewise continuous equations in order to find the solution. Approximate solutions are constructed for boundary value problems.

The Rayleigh-Ritz and Galerkin methods contributed to develop this method. FEM was firstly used in plane stress analysis by Clough [19]. The first book on FEM was published by Zienkiewicz and Cheung in 1967 [20]. Then, it has been applied to many engineering problems since 1960 [21, 22, 23, 24]. In the past years, many researches have developed mesh generation for FEM. Moreover, meshless FEM has been considered [5, 6, 7, 25, 26]. However, boundary conditions cause problems considering stability.

In electromagnetics, most differential equations with the mixed boundary condition in the domain Ω using Equations (2.19) and (2.20) can be considered as

$$-A\nabla^2 u + \alpha u = f \qquad \text{in } \Omega \tag{2.21}$$

$$ru = 0 \qquad \text{on } \partial\Omega_1 \tag{2.22}$$

$$s\frac{\partial u}{\partial n} + ru = g(x) \qquad \text{on } \partial\Omega_2 \tag{2.23}$$

where $\partial\Omega_1, \partial\Omega_2$ show the homogeneous Dirichlet ($g(x) = 0$) and Cauchy boundaries around the domain respectively.

The idea is to divide the domain, which can be complex, into sub domains (called elements) and to use approximated solutions according to nodes. Nodes are points in the domain. Figure 2.1 shows the nodes and elements for linear, quadratic, and cubic interpolation of standard FEM.

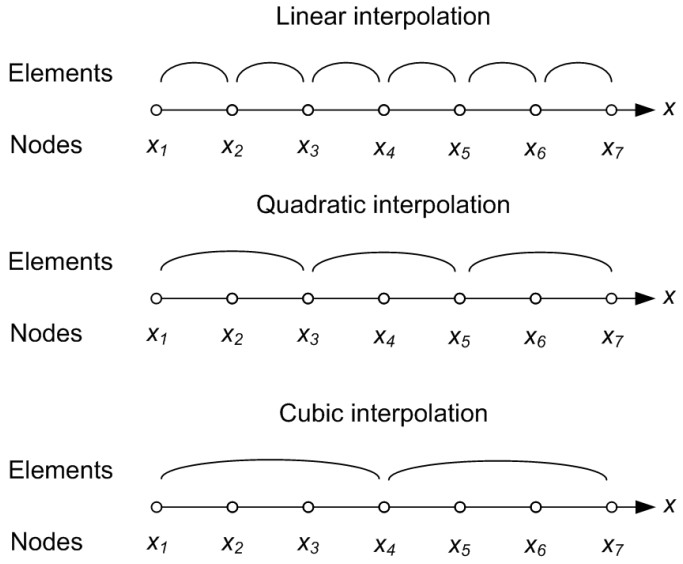

Figure 2.1. Nodes and elements for linear, quadratic, and cubic interpolation

Various approximation methods have been developed for FEM. This study presents Ritz-Galerkin approximation by minimizing the functional with respect to its variables as:

$$\frac{1}{2}\int_{\Omega}(-A\nabla^2 u + \alpha u)ud\Omega - \int_{\Omega} fud\Omega \tag{2.24}$$

Multiplying Equation (2.21) by a smooth function v which vanishes on $\partial\Omega_1$ and integrating by parts using Appendix (B.3):

$$-A\nabla^2 uv + \alpha uv = fv \tag{2.25}$$

$$A\int_{\Omega}\nabla u\cdot\nabla v^t + \alpha\int_{\Omega} uv - A\int_{\partial\Omega}\frac{\partial u}{\partial n}v = \int_{\Omega} fv \tag{2.26}$$

Considering Equations (2.22) and (2.23)

$$A\int_{\Omega}\nabla u\cdot\nabla v^{t}+\alpha\int_{\Omega}uv+Ar\int_{\partial\Omega_2}uv=\int_{\Omega}fv+A\int_{\partial\Omega_2}gv \tag{2.27}$$

Replacing u with the approximated solution $\widetilde{u}$ which consists of p nodes,

$$\widetilde{u}=\sum_{i=1}^{p}c_iB_i \tag{2.28}$$

where c_i indicates the coefficients of basis functions B_i, and replacing v with B_k where $k=1...q$, q is the number of nodes in domain

$$A\int_{\Omega}\nabla(\sum_{i=1}^{p}c_iB_i)\cdot\nabla B_k^{t}+\alpha\int_{\Omega}\sum_{i=1}^{p}c_iB_iB_k+Ar\int_{\partial\Omega_2}\sum_{i=1}^{p}c_iB_iB_k=\int_{\Omega}fB_k+A\int_{\partial\Omega_2}gB_k \tag{2.29}$$

$$\sum_{i=1}^{p}c_i\left[A\int_{\Omega^{(i)}}\nabla B_i\cdot\nabla B_k^{t}+\alpha\int_{\Omega^{(i)}}B_iB_k+Ar\int_{\partial\Omega_2^{(i)}}B_iB_k\right]=\int_{\Omega}fB_k+A\int_{\partial\Omega_2}gB_k \tag{2.30}$$

$$\sum_{i=1}^{p}c_i\left[K_{i,k}+M_{i,k}+R_{i,k}\right]=F_k+G_k \tag{2.31}$$

The basis functions are constructed by using piecewise polynomials such as Lagrange polynomials for N data points as

$$l_j^{n}(x)=\prod_{k=0,k\neq j}^{N-1}\frac{x-x_{j+k}}{x_j-x_{j+k}} \tag{2.32}$$

The linear and quadratic Lagrange functions are obtained respectively as

$$\left\{\begin{array}{c} l_i^{1}(x)=\frac{x-x_{i+1}}{x_i-x_{i+1}},\\ l_{i+1}^{1}(x)=\frac{x-x_i}{x_{i+1}-x_i}\end{array}\right\} \tag{2.33}$$

$$\left\{ \begin{array}{c} l_i^2(x) = \frac{(x-x_{i+1})(x-x_{i+2})}{(x_i-x_{i+1})(x_i-x_{i+2})}, \\ l_{i+1}^2(x) = \frac{(x-x_i)(x-x_{i+2})}{(x_{i+1}-x_i)(x_{i+1}-x_{i+2})}, \\ l_{i+2}^2(x) = \frac{(x-x_i)(x-x_{i+1})}{(x_{i+2}-x_i)(x_{i+2}-x_{i+1})} \end{array} \right\} \tag{2.34}$$

Figures 2.2- 2.3 show the elemental linear and quadratic Lagrange functions respectively.

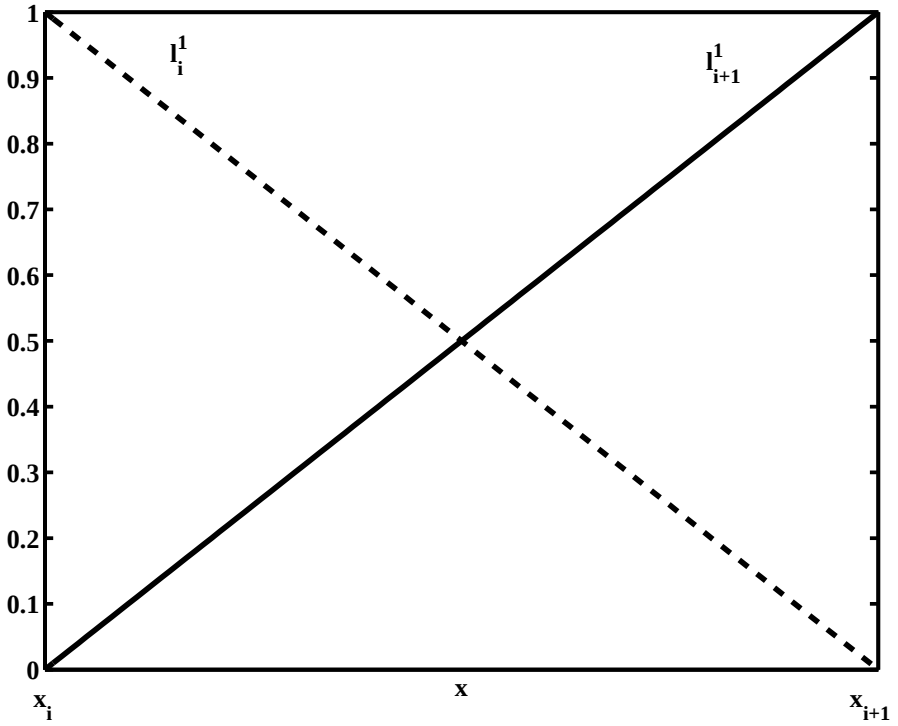

Figure 2.2. The elemental linear Lagrange function

FEM generally uses triangulation with the hat function which is a linear Lagrange function to solve problem easily. According to this consideration, the basis function equals 1 for the selected mesh and vanishes for the triangles which do not contain the selected mesh. So, it looks like a pyramid. However, the maximum diameter of circle circumscribing triangles must be chosen small to provide better approximation. The other way is to choose basis functions of higher degree such as quadrilateral, tetrahedral, hexahedra etc. This situation is a problem for complex objects in two or three dimensions.

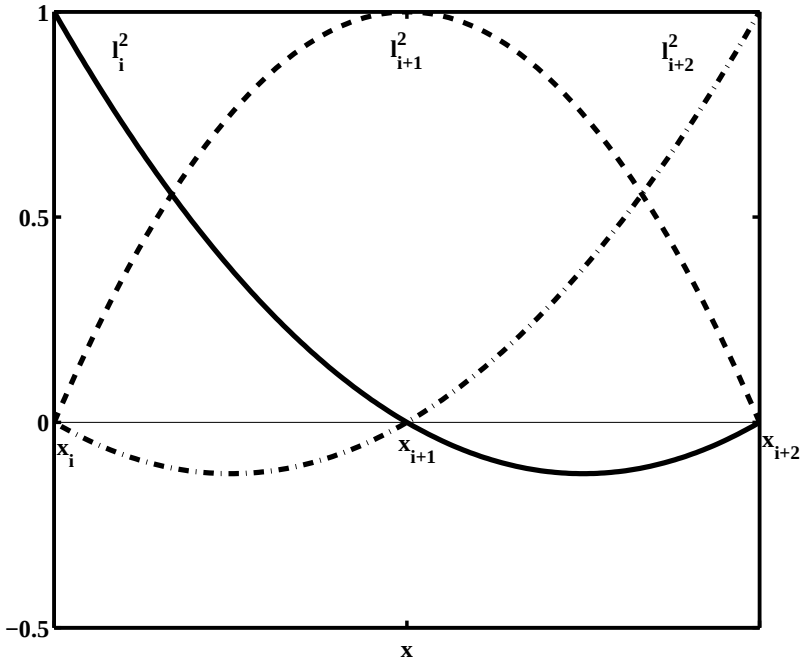

Figure 2.3. The elemental quadratic Lagrange function

After constructing the basis functions and taking the integral of each mesh in Equation (2.30), the linear system is assembled and solved

$$(K + M + R)U = F + G \tag{2.35}$$

where U is the matrix consisting of the coefficients of basis functions, K is the stiffness matrix, M is the mass matrix, F is the load matrix, and R and G are matrices related to the boundary conditions.

2.4. B-splines

The splines are used in approximation, data fitting, computer aided design (CAD), and many other applications [9, 10]. The contributions of Carl De Boor, de Casteljau, and Bezier have played an important role for splines. They have become popular and many papers have been published on basis splines (b-splines). The b-splines, which can be used as basis functions for their flexibility and continuity between points, have been taken into consideration to implement basis functions for FEM. It was proven that

more accurate results are obtained by using b-spline basis functions as shape functions in order to solve two dimensional electromagnetic field problems for regular regions [27]. Hollig has also used b-splines as basis functions to solve boundary value problems using FEM [28]. Using b-splines involving higher order shape functions is simple for the approximation of FEM applications. This method provides to solve electromagnetic problems with high accuracy and can also be applied to irregular domains.

2.4.1. Definition and Properties of B-splines

The standard uniform b-spline of degree n is defined [9]

$$b^n(x) = \int_{x-1}^{x} b^{n-1}(t)dt \tag{2.36}$$

starting from b^0 of the unit interval between zero and one. Table 2.4 explains how to obtain linear, quadratic, and cubic b-splines by using Equation (2.36). Figure 2.4 shows the uniform b-splines of degree one, two and three. These are linear (dotted line), quadratic (dashed line), and cubic (dash-dotted line) b-splines respectively.

Table 2.4. Obtaining the linear, quadratic, and cubic uniform b-splines

n	The uniform b-splines
1	$b^1(x) = \begin{cases} \int_0^x dt = x & x \in [0,1] \\ \int_{x-1}^1 dt = 2-x & x \in [1,2] \\ 0 & otherwise \end{cases}$
2	$b^2(x) = \begin{cases} \int_0^x t\,dt = \frac{1}{2}x^2 & x \in [0,1] \\ \int_{x-1}^1 t\,dt + \int_1^x (2-t)\,dt = -x^2+3x-\frac{3}{2} & x \in [1,2] \\ \int_{x-1}^2 (2-t)\,dt = \frac{1}{2}x^2-3x+\frac{9}{2} & x \in [2,3] \\ 0 & otherwise \end{cases}$
3	$b^3(x) = \begin{cases} \int_0^x \frac{1}{2}t^2\,dt = \frac{1}{6}x^3 & x \in [0,1] \\ \int_{x-1}^1 \frac{1}{2}t^2\,dt + \int_1^x -t^2+3t-\frac{3}{2}\,dt = -\frac{1}{2}x^3+2x^2-2x+\frac{2}{3} & x \in [1,2] \\ \int_{x-1}^2 -t^2+3t-\frac{3}{2}\,dt + \int_2^x \frac{1}{2}t^2-3t+\frac{9}{2}\,dt = \frac{1}{2}x^3-4x^2+10x-\frac{22}{3} & x \in [2,3] \\ \int_{x-1}^3 \frac{1}{2}t^2-3t+\frac{9}{2}\,dt = -\frac{1}{6}x^3+2x^2-8x+\frac{32}{3} & x \in [3,4] \\ 0 & otherwise \end{cases}$

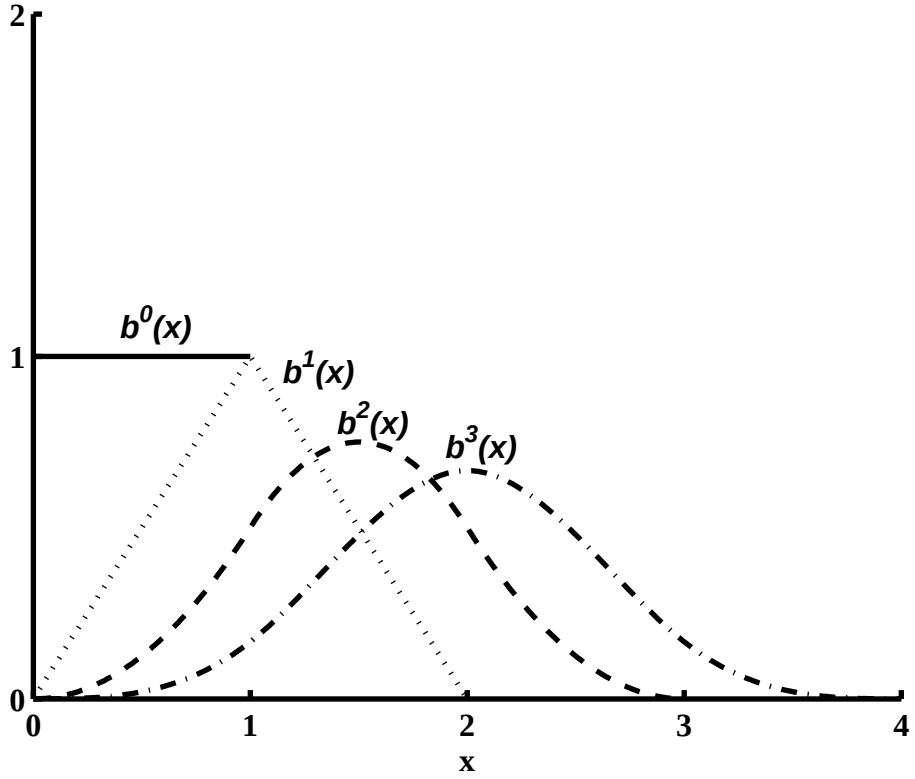

Figure 2.4. The uniform b-splines

The scaled b-spline with grid width h supporting in $[i, i+n+1]h$ is

$$b^n_{i,h}(x) = b^n(x/h - i) \tag{2.37}$$

The basic properties of $b^n_{i,h}(x)$ are given as [9, 10]:

- positive on their supports $[i, i+n+1]h$ and vanishes outside
- $n-1$ times continuously differentiable
- piecewise polynomial of degree n
- symmetric

The derivative of the scaled b-spline and recursion relations are shown as:

$$\frac{d}{dx} b^n_{i,h}(x) = \frac{1}{h}\left[b^{n-1}_{i,h}(x) - b^{n-1}_{i+1,h}(x)\right] \tag{2.38}$$

$$b_{i,h}^{n}(x) = \frac{1}{n}\left[\left(\frac{x}{h} - i\right) b_{i,h}^{n-1}(x) + \left(n + i + 1 - \frac{x}{h}\right) b_{i+1,h}^{n-1}(x)\right] \tag{2.39}$$

Figure 2.5 shows the derivative of cubic b-spline (dashed line).

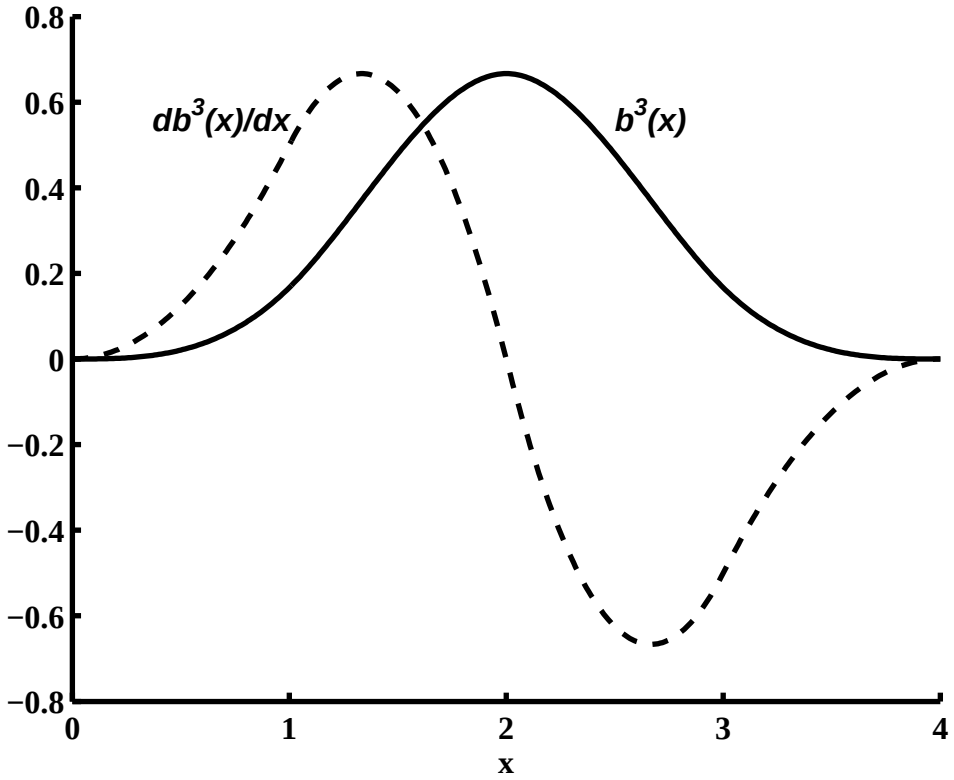

Figure 2.5. The derivative of cubic b-spline

The recursion relation for the cubic b-spline having a grid width ($h = 1$) in terms of quadratic and linear b-splines as

$$b_0^3(x) = \frac{x}{3} b_0^2(x) + \frac{4-x}{3} b_1^2(x) \tag{2.40}$$

$$b_0^3(x) = \frac{x}{3}\left(\frac{x}{2} b_0^1(x) + \frac{3-x}{2} b_1^1(x)\right) + \frac{4-x}{3}\left(\frac{x-1}{2} b_1^1(x) + \frac{4-x}{2} b_2^1(x)\right) \tag{2.41}$$

$$b_0^3(x) = \frac{x^2}{6} b_0^1(x) + \frac{-x^2 + 4x - 2}{3} b_1^1(x) + \frac{(4-x)^2}{6} b_2^1(x) \tag{2.42}$$

Using recurrence, the polynomial representations of b-splines are found in Table 2.5.

Table 2.5. The coefficients and representation of polynomials for various b-splines

n	Representation
1	$b^1_{i,h}(x) = \begin{cases} \frac{x}{h} - i & x \in h[i, i+1] \\ -\left(\frac{x}{h} - (i+1)\right) + 1 & x \in h[i+1, i+2] \end{cases}$
2	$b^2_{i,h}(x) = \begin{cases} \frac{1}{2}(\frac{x}{h} - i)^2 & x \in h[i, i+1] \\ -\left(\frac{x}{h} - (i+1)\right)^2 + \left(\frac{x}{h} - (i+1)\right) + \frac{1}{2} & x \in h[i+1, i+2] \\ \frac{1}{2}\left(\frac{x}{h} - (i+2)\right)^2 - \left(\frac{x}{h} - (i+2)\right) + \frac{1}{2} & x \in h[i+2, i+3] \end{cases}$
3	$b^3_{i,h}(x) = \begin{cases} \frac{1}{6}\left(\frac{x}{h} - i\right)^3 & x \in h[i, i+1] \\ -\frac{1}{2}\left(\frac{x}{h} - (i+1)\right)^3 + \frac{1}{2}\left(\frac{x}{h} - (i+1)\right)^2 + \frac{1}{2}\left(\frac{x}{h} - (i+1)\right) + \frac{1}{6} & x \in h[i+1, i+2] \\ \frac{1}{2}\left(\frac{x}{h} - (i+2)\right)^3 - \left(\frac{x}{h} - (i+2)\right)^2 + \frac{2}{3} & x \in h[i+2, i+3] \\ -\frac{1}{6}\left(\frac{x}{h} - (i+3)\right)^3 + \frac{1}{2}\left(\frac{x}{h} - (i+3)\right)^2 - \frac{1}{2}\left(\frac{x}{h} - (i+3)\right) + \frac{1}{6} & x \in h[i+3, i+4] \end{cases}$

2.4.2. Convolution and Scalar Products of B-splines

The integrals of b-splines can be computed easily with the aid of convolution. The convolution of two b-splines of degree n_1 and n_2 is defined as [28]

$$b^{n_1+n_2+1}(x) = \int_R b^{n_1}(x-y)b^{n_2}(y)dy \tag{2.43}$$

The other significant properties of b-splines are the representation of their scalar product. The scalar product of two b-splines and their derivatives can be shown as

$$s^n_{i-k} = b^n_{i,h} \cdot b^n_{k,h} = hb^{2n+1}(n+1+i-k) \tag{2.44}$$

$$d^n_{i-k} = \frac{1}{h}(2s^{n-1}_{i-k} - s^{n-1}_{i-k-1} - s^{n-1}_{i-k+1}) \tag{2.45}$$

Table 2.6 shows the scalar products of b-splines and their derivatives for the unit grid width [28].

Table 2.6. The scalar products of b-splines and their derivatives

n	s_0^n	s_1^n	s_2^n	s_3^n	d_0^n	d_1^n	d_2^n	d_3^n
1	$\frac{2}{3}$	$\frac{1}{6}$			2	-1		
2	$\frac{11}{20}$	$\frac{13}{60}$	$\frac{1}{120}$		1	$-\frac{1}{3}$	$-\frac{1}{6}$	
3	$\frac{151}{315}$	$\frac{397}{1680}$	$\frac{1}{42}$	$\frac{1}{5040}$	$\frac{2}{3}$	$-\frac{1}{8}$	$-\frac{1}{5}$	$-\frac{1}{120}$

2.4.3. Tensor Product of B-splines

The tensor product of b-splines helps to construct b-splines in two and three dimensions. It is defined by multiplying b-splines of each direction. The tensor product of b-splines of degree n with support $[\mathbf{i}, \mathbf{i}+n]h$, grid index $\mathbf{i}$, and dimension m is

$$b_{i,h}^n(\mathbf{x}) = h^{-m/2} \prod_{d=1}^{m} b_{i_d,h}^n(x_d) \qquad \mathbf{i} \in Z^m, \mathbf{x} \in R^m \tag{2.46}$$

The support of $b_{\mathbf{i},h}^n$ consists of $(n+1)^m$ grid cells $C_{\mathbf{i}} = \mathbf{i}h + [0,h]^m$. $h^{-m/2}$ provides the b-spline to be bounded with respect to L_2 norm $\int_{R^m} |b_{\mathbf{i},h}^2| = 1$. Figures 2.6 and 2.7 show the tensor product b-spline of $n = 2$ for two and three dimensions respectively.

2.4.4. Partial Derivatives of B-Splines

The first order partial derivatives of b-splines are obtained by using Equation (2.38) as a difference of two b-splines with degree $n-1$ divided by h for the unit vectors α [28]

$$\partial^\alpha b_{i,h}^n = \frac{b_{i,h}^{n-\alpha} - b_{i+\alpha,h}^{n-\alpha}}{h} \tag{2.47}$$

The higher order partial derivatives of b-splines obey this rule. Figures 2.8 and 2.9 show the first and second order partial derivatives of cubic b-spline with respect to x

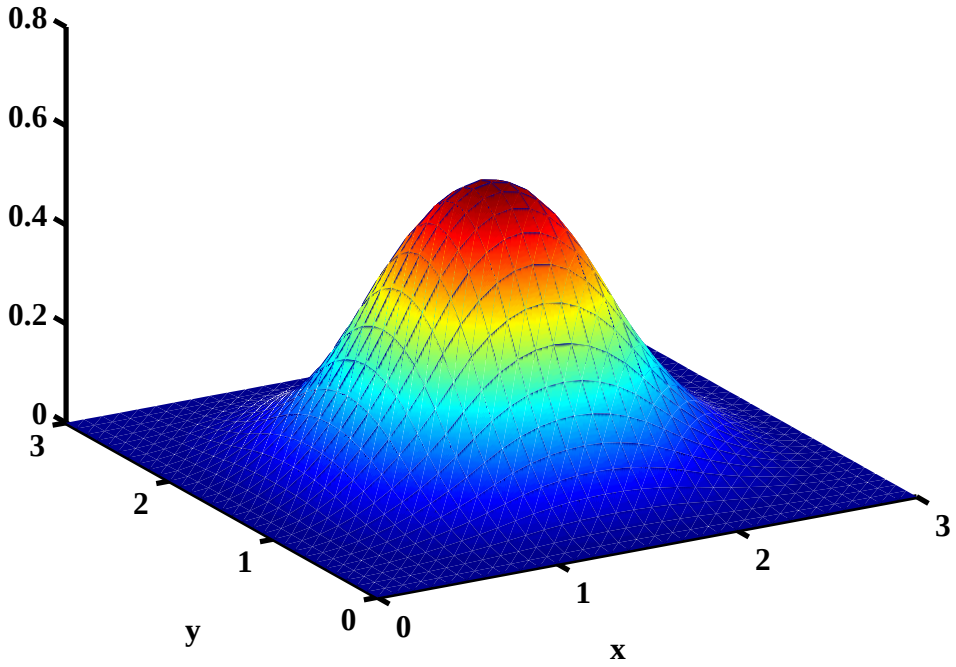

Figure 2.6. Tensor product of quadratic b-spline in 2D

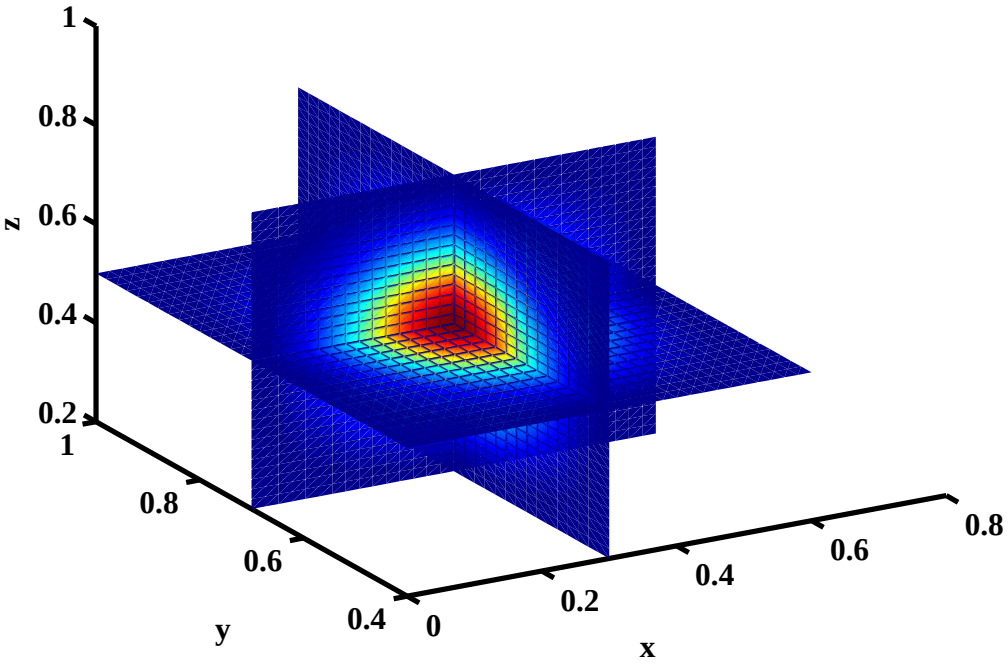

Figure 2.7. Tensor product of quadratic b-spline in 3D

and y respectively, which are obtained by using Equations (2.46) and (2.47) as:

$$\frac{\partial}{\partial x_1} b^n_{\mathbf{i},h} = h^{-m/2} \left[\frac{\partial}{\partial x_1} b^n_{i_1,h} \right] \cdot b^n_{i_2,h} \tag{2.48}$$

$$\frac{\partial^2}{\partial x_2^2} b^n_{\mathbf{i},h} = h^{-m/2} b^n_{i_1,h} \cdot \left[\frac{\partial^2}{\partial x_2^2} b^n_{i_2,h} \right] \tag{2.49}$$

2.5. Error Analysis

The error in finite element approximation is defined as the difference between the exact (u_e) and the approximated solution:

$$e = u_e - \widetilde{u} \tag{2.50}$$

For the accuracy studies, the maximum norm measures the maximum absolute value, the relative error measures the absolute value of error divided by the exact value, and relative L_2-error norm measures the root mean square of integral of a squared error function over the domain (Ω) respectively as:

$$\|e\|_\infty = max|e| \tag{2.51}$$

$$\|e_{rel}\| = |\frac{e}{u_e}| \tag{2.52}$$

$$\|e_{rel}\|_0 = \frac{\sqrt{\int_\Omega e^2 \, d\Omega}}{\sqrt{\int_\Omega u_e^2 \, d\Omega}} \tag{2.53}$$

The convergence rate is significant in order to understand the strength of method

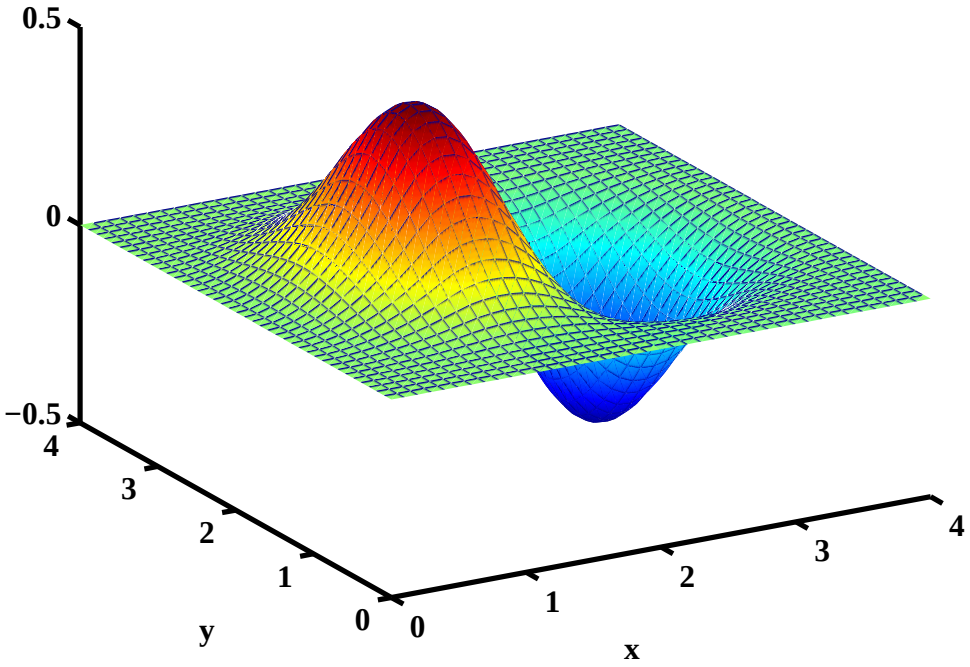

Figure 2.8. First order partial derivative of cubic b-spline with respect to x

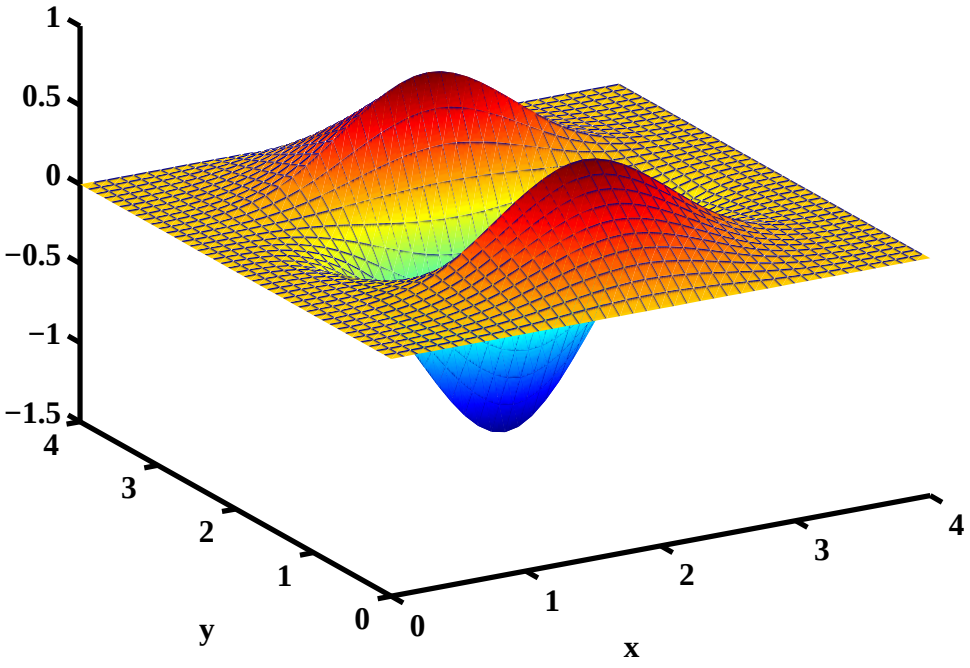

Figure 2.9. Second order partial derivative of cubic b-spline with respect to y

for the numerical computation. It shows how the error reduces when the grid size is divided by two. The grid width is divided by two and taking the logarithms of error ratio with respect to base two gives the convergence rate, which is defined as

$$\text{Convergence rate} = \log_2 \frac{\|e_{h\cdot 2^{1-l}}\|}{\|e_{h\cdot 2^{-l}}\|} \tag{2.54}$$

for the grid widths $h \cdot 2^{-l}$, $l = 1, 2, 3, 4, ...$

3. FEM WITH B-SPLINES

FEM applications use basis functions and meshes. The mesh generation part of FEM causes consumption in computation time for higher dimensions. In the past years, many researches have developed mesh generation. Moreover, meshless FEM are considered by many authors [5, 6, 7, 8, 25, 26].

The b-splines have been taken into consideration to implement basis functions for FEM. Hollig has used b-splines as basis functions to solve boundary value problems using FEM [28]. The approach considers using b-splines for the approximation of functions for FEM applications. However, they have some disadvantages. The boundary conditions have not been modeled easily. The basis should vanish outside the domain; and if homogeneous Dirichlet boundary condition is taken into consideration, the function must be zero on the domain. Secondly, some b-splines which support the domain have a little effect and this causes instability for the approximation. Thirdly, the numerical integration for boundary cells has not been solved easily. New developments have overcome these problems. For the Dirichlet boundary conditions, the weight functions are used. For the instability problem, the extended b-splines, given in Equation (3.1), have been considered. Some numerical integration techniques have been developed in order to solve the boundary integral in two and three dimensions.

Web-spline method is a new type of meshless finite element method for solving two or three dimensional boundary value problems. Web-spline method uses weighted extended b-splines to construct finite elements without using mesh generation. As a result, this method reduces time computation and saves vast amounts of money. Using web-splines, the boundary condition problems and time consuming for mesh generation have been eliminated, and more accurate results are found with faster computation and less memory [29, 30, 31, 32, 33, 34].

3.1. The Flow Diagram

Before explaining web-spline method, the flow chart of FEM using web-spline method is presented. Figure 3.1 shows the flow diagram. First of all, the simulation region and the problem are defined by the storage of inputs for the region, PDE, and boundary conditions. Then, the generation of the grid cells and classification of b-splines are done for the simulation region. The next step is to compute the extension coefficients. If there is homogeneous Dirichlet boundary condition, the weight function for the region is determined. After assembling and solving the system of equations, the approximated solution is computed. At the end, the results are shown as an output.

3.2. Grid generation and Classification of B-splines

For the domain Ω, firstly grid generation is completed. Figure 3.2 shows the grid generation for the given region. The grid width is taken as 0.5.

The next step is to classify b-splines. The relevant b-splines b_k, $k \in (I \cup J)$, which are supporting in the domain, are determined. According to the size of their support, they are classified as inner and outer b-splines. The inner b-splines ($k \in I$) have at least one complete grid cell of their support in the domain. The other ones supporting the domain are called outer b-splines ($k \in J$). For the outer b-splines, the grid cells of their supports are not completely contained in the domain [29, 30, 31, 32, 33, 34]. Figure 3.3 shows some inner and outer b-splines. According to their centers of support, the inner and outer b-splines are marked by ($\bullet$) and ($\circ$) respectively. Figure 3.4 shows all the relevant b-splines for the given domain.

3.3. Extension Coefficients

Although the outer b-splines have a little effect, they are not omitted. This causes instability. So, they are adjoined to the inner b-splines in order to form the extended

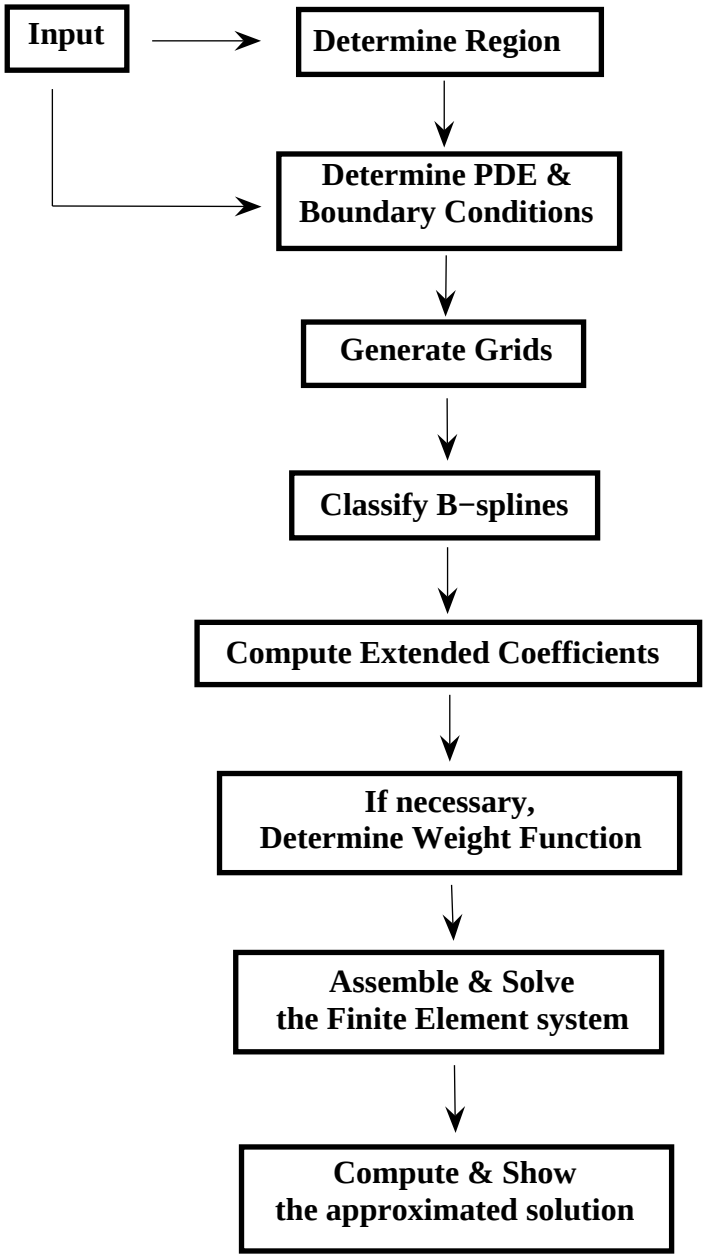

Figure 3.1. The flow diagram of FEM with web-spline method

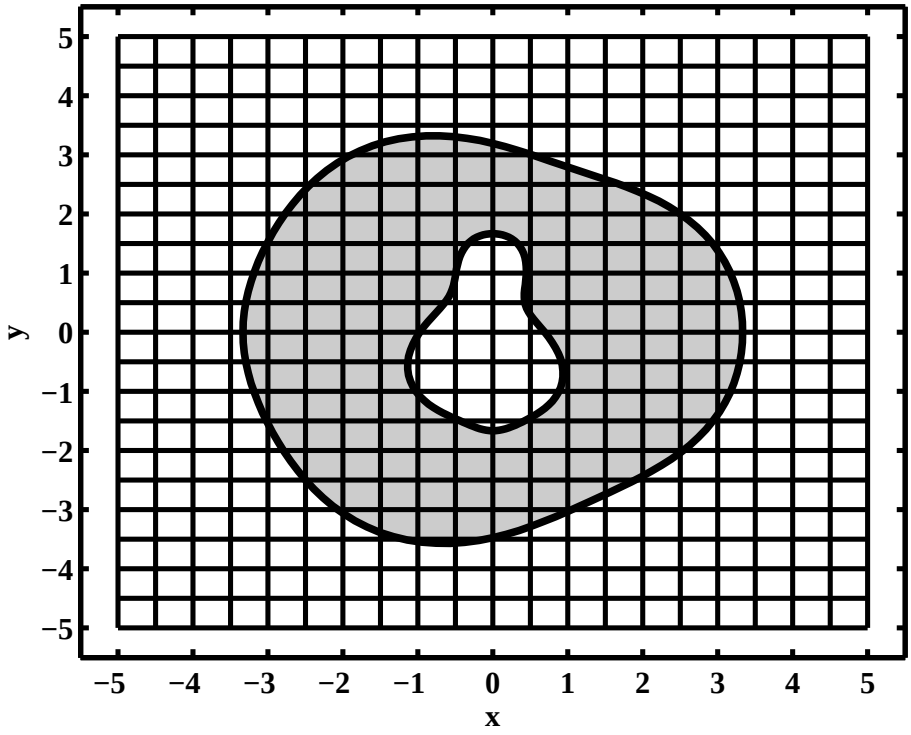

Figure 3.2. Grid generation of web-spline method

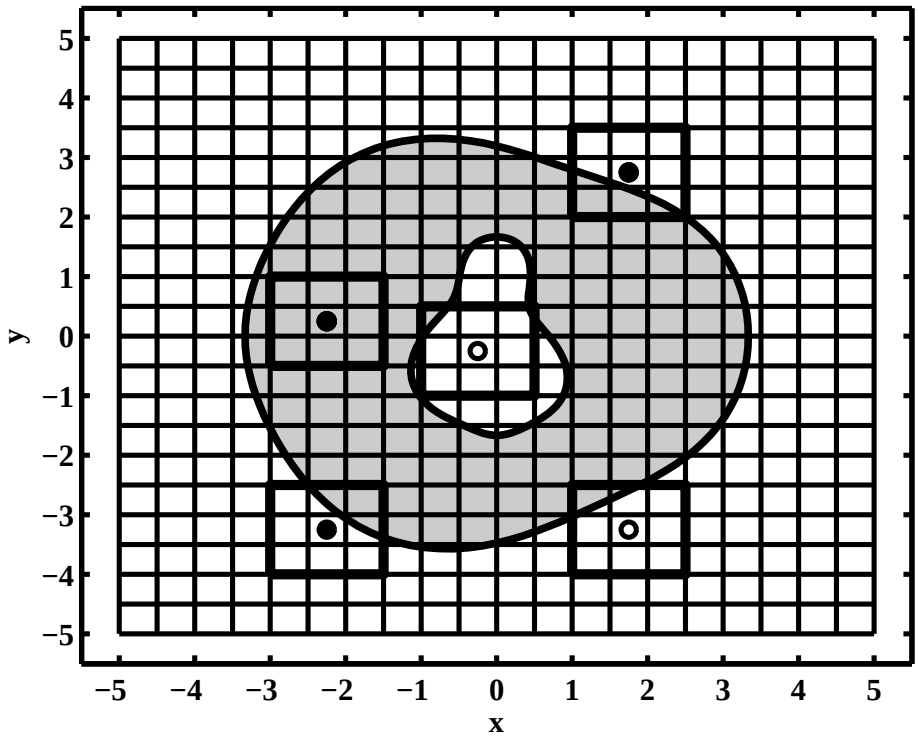

Figure 3.3. Support of inner (•) and outer (○) b-splines

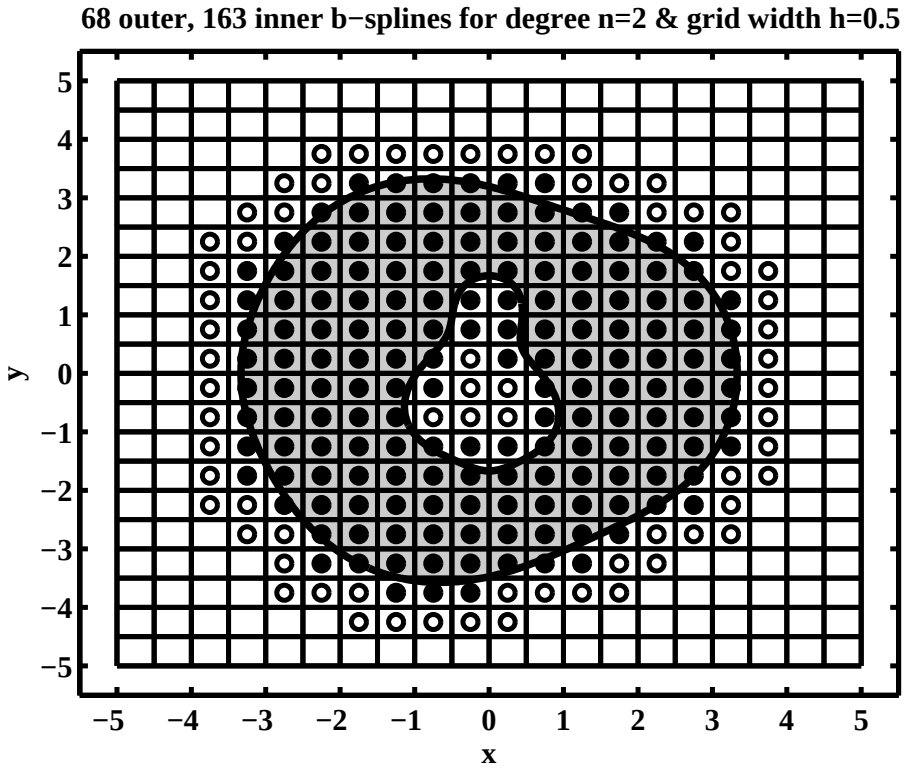

Figure 3.4. All relevant inner (•) and outer (∘) b-splines for the given domain

b-splines having stable basis. The extended b-splines are

$$B_k = b_k + \sum_i e_{k,i}\, b_i \qquad \text{for } k \in I, i \in J(k) \tag{3.1}$$

where $e_{k,i}$ are the extension coefficients. For each outer b-splines, the closest $(n+1)^m$ inner b-splines are affected. The extension coefficients are computed by using Lagrange polynomials as:

$$e_{k,i} = \begin{cases} \displaystyle\prod_{d=1}^{m} \prod_{\mu=0}^{n} \frac{i_d - l_d - \mu}{k_d - l_d - \mu} & \text{for } i = j \in J, k \in I(i), l_d + \mu \neq i_d \\ 1 & \text{for } i = k \in I \\ 0 & \text{otherwise} \end{cases} \tag{3.2}$$

where $l = [l_1, l_2, \ldots] \in Z^m$ is the index for the lower left position of $I(j)$.

Figure 3.5 shows some extension coefficients of the given inner and outer quadratic

b-splines. The values of the coefficients with $k \in I(i)$ are given for the outer b-spline. The left outer b-spline circle ($\circ$) of Figure 3.5 indicates that it involves only three inner b-splines, and the right outer b-spline circle indicates that it involves nine inner b-splines. The coefficients of them are shown in figure. The bullets ($\bullet$) show the inner b-splines with the extension coefficients of the adjoined outer b-splines with $i \in J(k)$.

Equation (3.1) can be used to solve the system with Neumann and Cauchy boundary conditions. However; if Dirichlet boundary conditions are taken into consideration, the extended b-splines are multiplied with the weight function $w(x)$. Multiplying with $1/w(x_k)$ provides the extended b-splines to be normalized where $w(x_k)$ is the value of the weight function at the center of a grid cell which intersects the support of b-spline and the domain completely. The equation for weighted extended b-spline is shown at the end of next section.

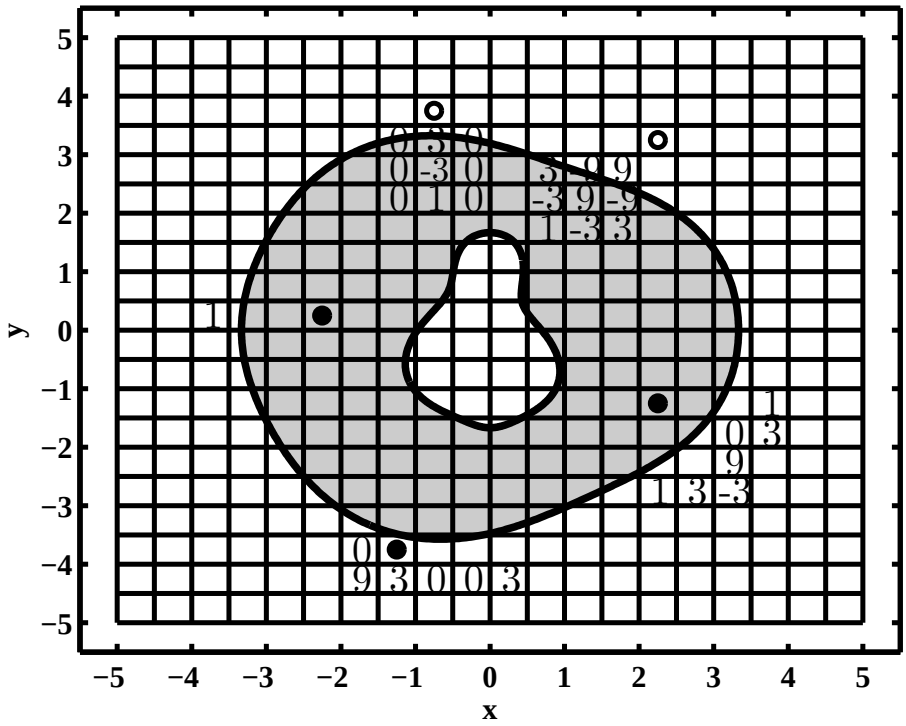

Figure 3.5. The extension coefficients of inner ($\bullet$) and outer ($\circ$) b-splines

3.4. The Weight Function

The weight function is a continuous positive function in the domain and zero on the boundary. It can be constructed by using smooth distance function as [35, 36, 37, 38]:

$$w(x) = \begin{cases} 1 - (1 - \frac{\text{dist}_{(x,\partial\Omega)}}{\delta})^{\gamma} & \text{dist}(x) < \delta \\ 1 & \text{otherwise} \end{cases} \tag{3.3}$$

where δ is the boundary strip, γ is the smoothing parameter, and dist is the function which determines the minimum distance to the boundary.

If analytical equations are used for the boundaries, the weight function can be constructed by using Rvachev's R-functions. The intersection, union, or complement of R-functions can be considered as [35, 36, 37]:

$$w_{\cap}(w_1, w_2) = \frac{1}{1+\tau}\left(w_1 + w_2 - \sqrt{w_1^2 + w_2^2 - 2\tau w_1 w_2}\right) \tag{3.4}$$

$$w_{\cup}(w_1, w_2) = \frac{1}{1+\tau}\left(w_1 + w_2 + \sqrt{w_1^2 + w_2^2 - 2\tau w_1 w_2}\right) \tag{3.5}$$

$$w^c = -w \tag{3.6}$$

respectively where τ is a constant ($-1 < \tau \leq 1$). Taking $\tau = 0$ provides good results in simulations. Figures 3.6 and 3.7 show the examples of constructed weight functions for the given domains using the distance function and Rvachev's R-functions respectively. The first domain is the previous consideration shown in Figure 3.2. The second one in Figure 3.7 uses seven weight functions given in Table 3.1.

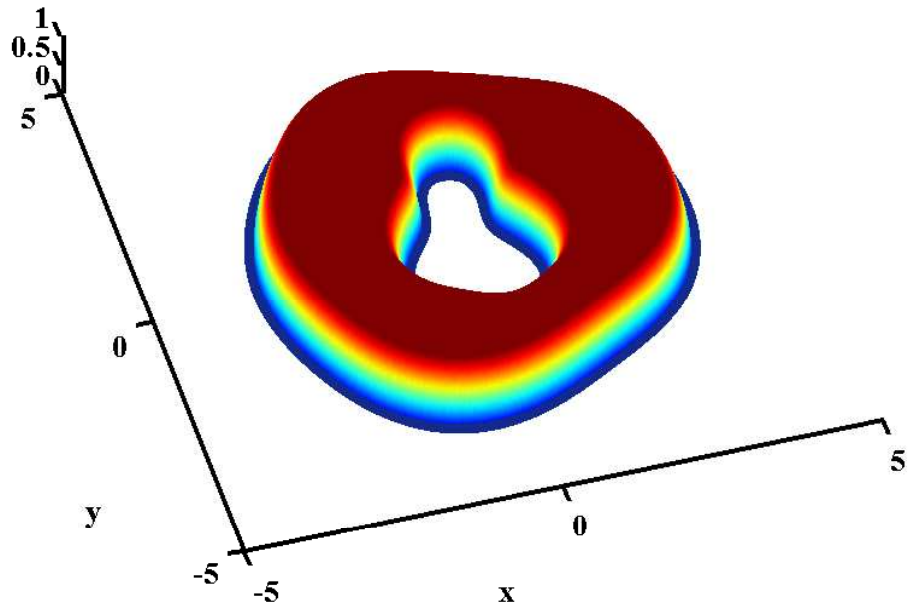

Figure 3.6. The weight function using distance function

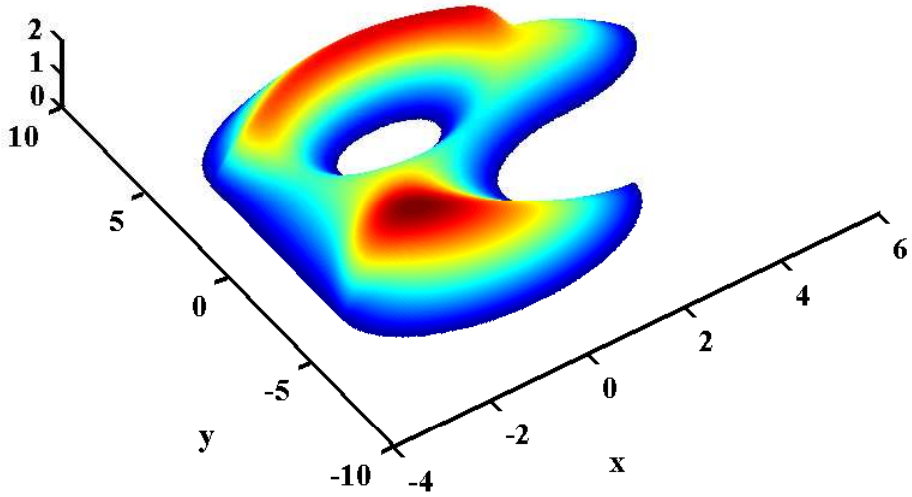

Figure 3.7. The weight function using Rvachev's R-function

Table 3.1. The weight functions and rule for the domain of Figure 3.7

Functions	$w_1 = \frac{9-x^2}{6}, \quad w_2 = \frac{16-y^2}{8}, \quad w_{3^-,4^+} = \frac{9-x^2-(y\mp 4)^2}{6}$ $w_{5^-,6^+} = \frac{4-(x-3)^2-(y\mp 2)^2}{4}, \quad w_7 = \frac{1-x^2-(y-2)^2}{2}$
Rule	$\Omega_R = ((\Omega_1 \cap \Omega_2) \cup \Omega_3 \cup \Omega_4 \cup \Omega_5) \cap \overline{\Omega}_6 \cap \overline{\Omega}_7$

3.5. Weighted Extended B-splines

The weighted extended b-splines are

$$B_k = \frac{w(x)}{w(x_k)} \left(b_k + \sum_i e_{k,i} b_i \right) \qquad \text{for } k \in I, i \in J(k) \tag{3.7}$$

The outer b-splines are coupled with the inner b-splines in order to stabilize basis. If we have a boundary value problem with homogeneous Dirichlet boundary conditions, Equation (3.7) is constructed as a basis function into Equation (2.30). The other boundary conditions use Equation (3.1) as basis function.

Figures 3.8-3.13 show the outer b-splines (∘), extended inner b-splines (▲), and standard inner b-splines (•). Figures 3.8-3.10 and Figures 3.11-3.13 use linear, quadratic, and cubic b-splines with the grid width $h = 0.5$ and $h = 0.25$ respectively. Therefore, the outer b-splines are adjoined to the inner b-splines, which are called extended b-splines. These extended b-splines form a stable basis with the properties of standard finite elements [29, 30, 31, 32, 33, 34]. As seen in figures, the majority of inner b-splines remains unchanged for the small grid width. Web-splines use 20-40 per cent less nodes compared with the weighted splines for this example.

Some b-splines related to extended and weighted extended b-splines are shown in Figures 3.14-3.15 respectively. For the web-splines, all b-splines are multiplied by a weight function which satisfies homogeneous boundary conditions. The second figure obviously shows the effect of weight function. All web-splines vanish on the boundary and are zero outside the domain.

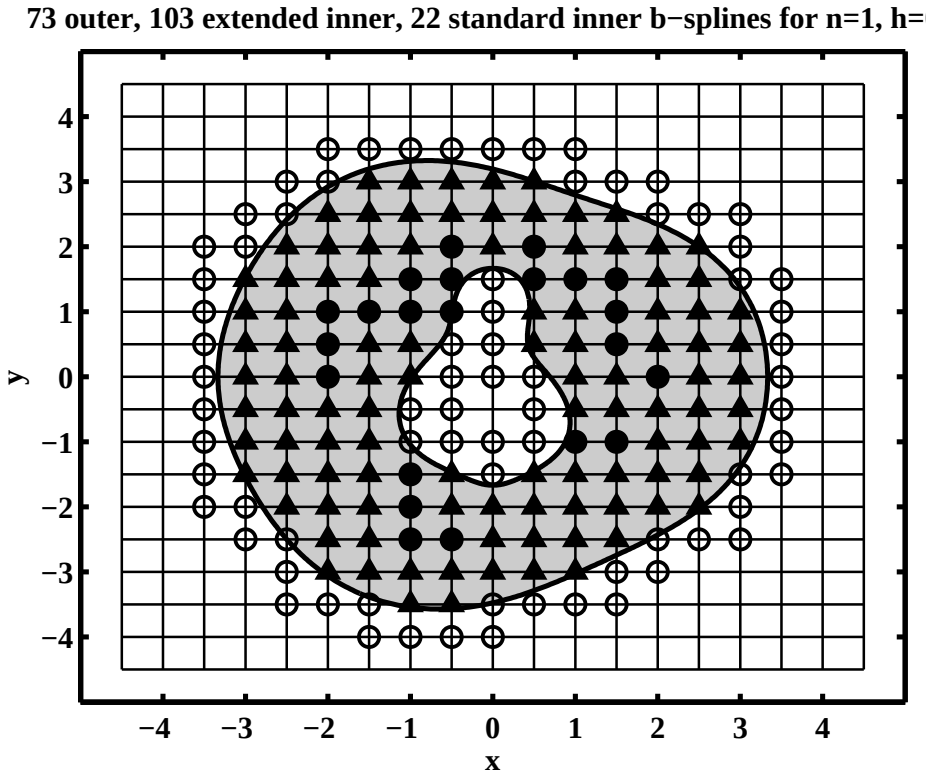

Figure 3.8. Outer (○), extended (▲), and standard (●) linear b-splines for $h = 0.5$

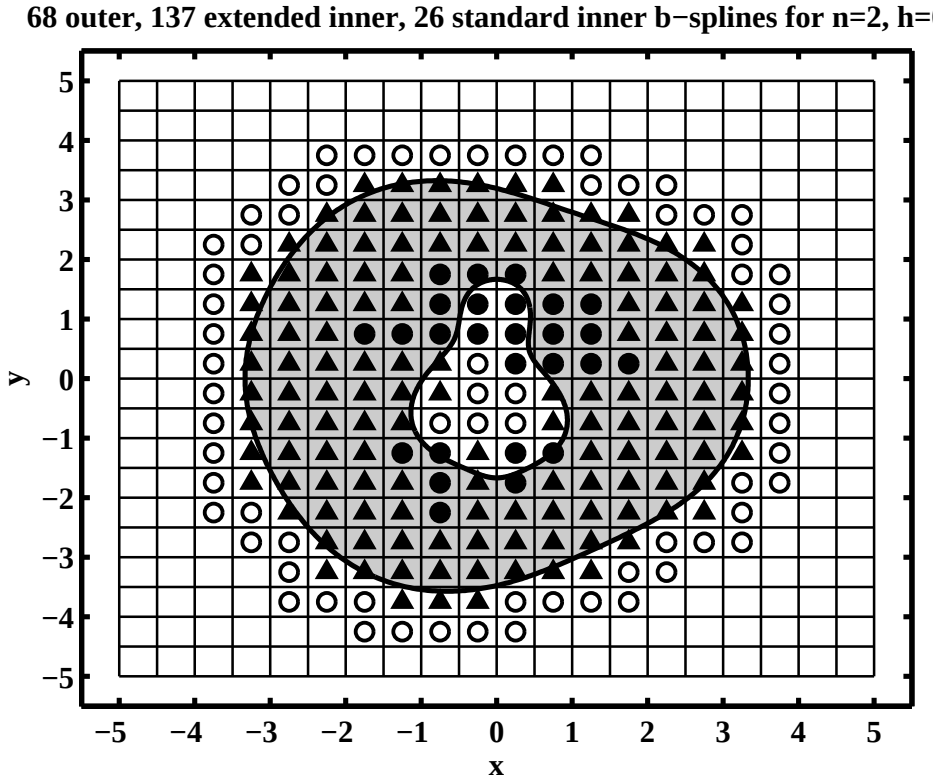

Figure 3.9. Outer (○), extended (▲), and standard (●) quadratic b-splines for $h = 0.5$

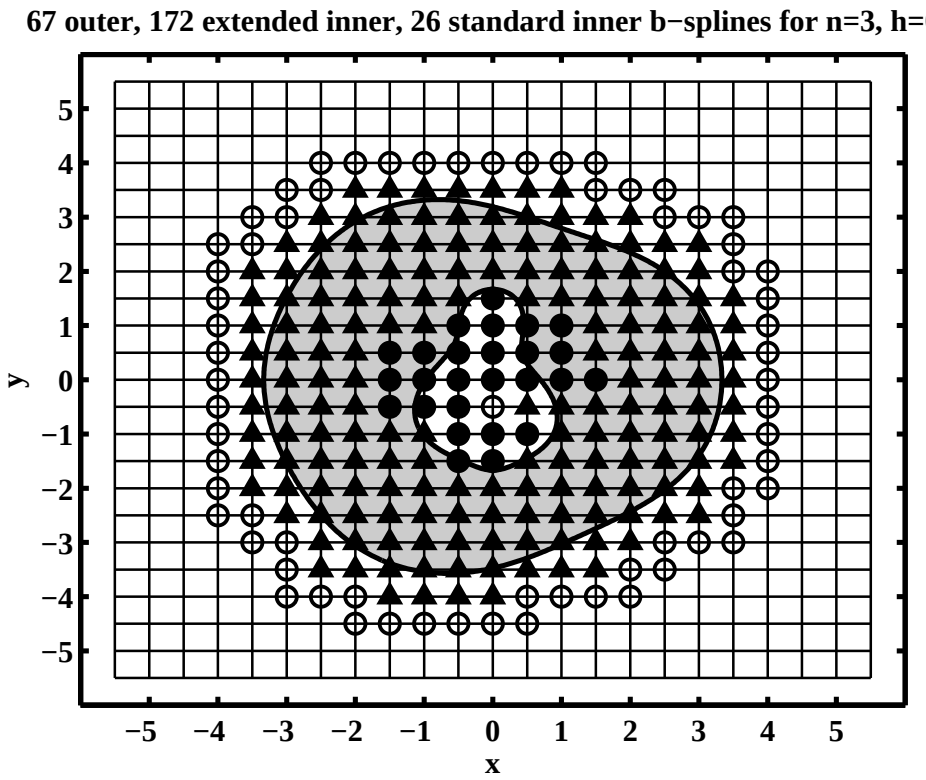

Figure 3.10. Outer (○), extended (▲), and standard (●) cubic b-splines for $h = 0.5$

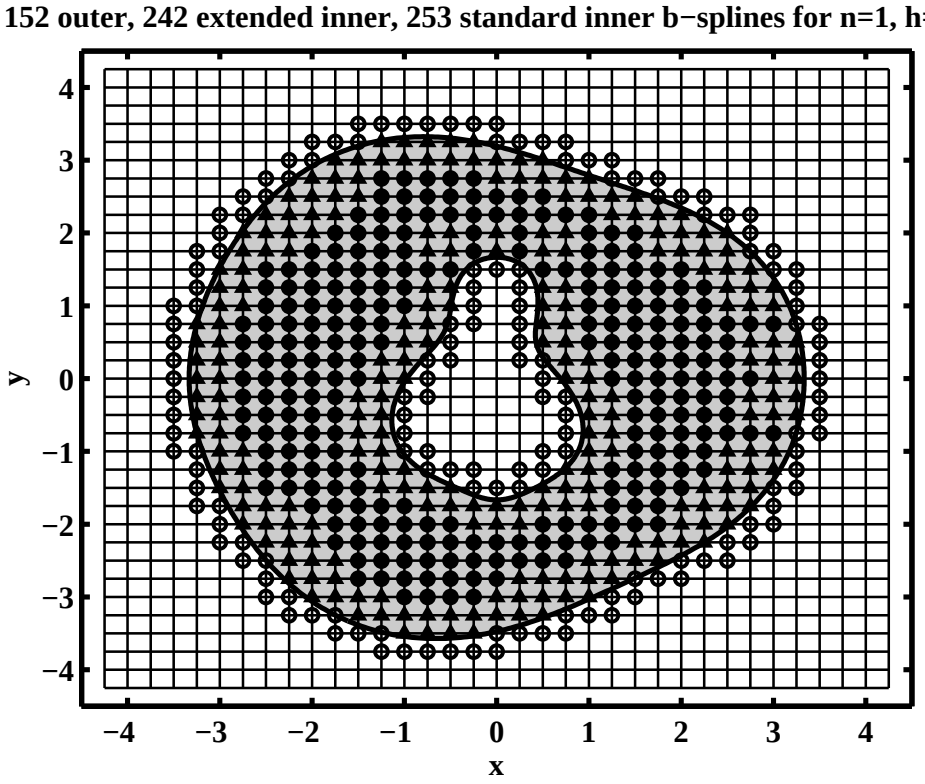

Figure 3.11. Outer (○), extended (▲), and standard (●) linear b-splines for $h = 0.25$

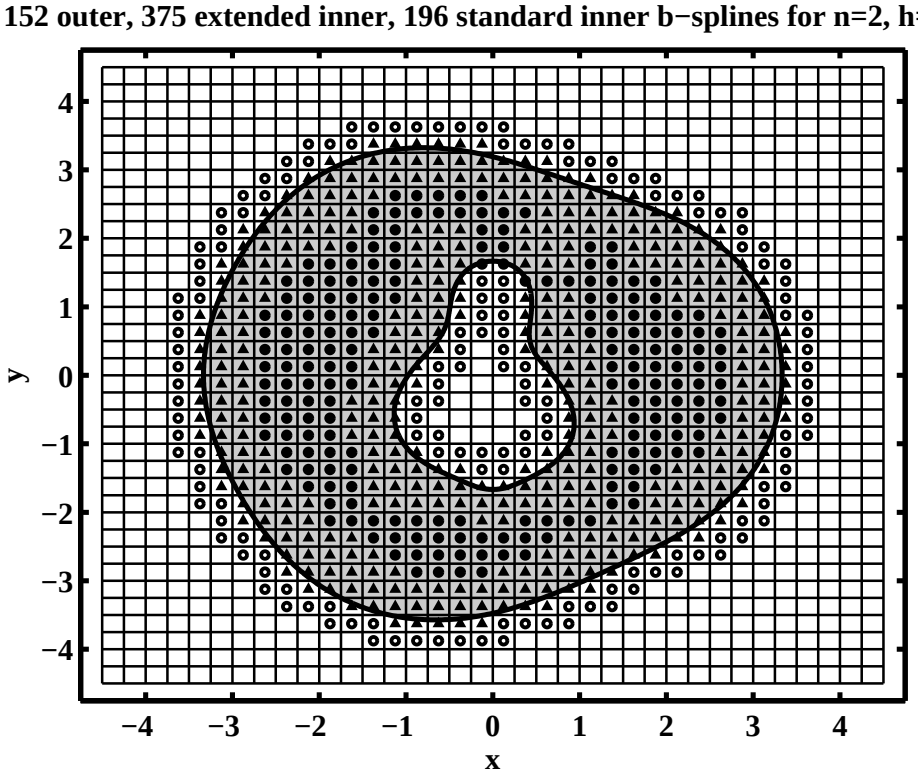

Figure 3.12. Outer (○), extended (▲), and standard (●) quadratic b-splines for $h = 0.25$

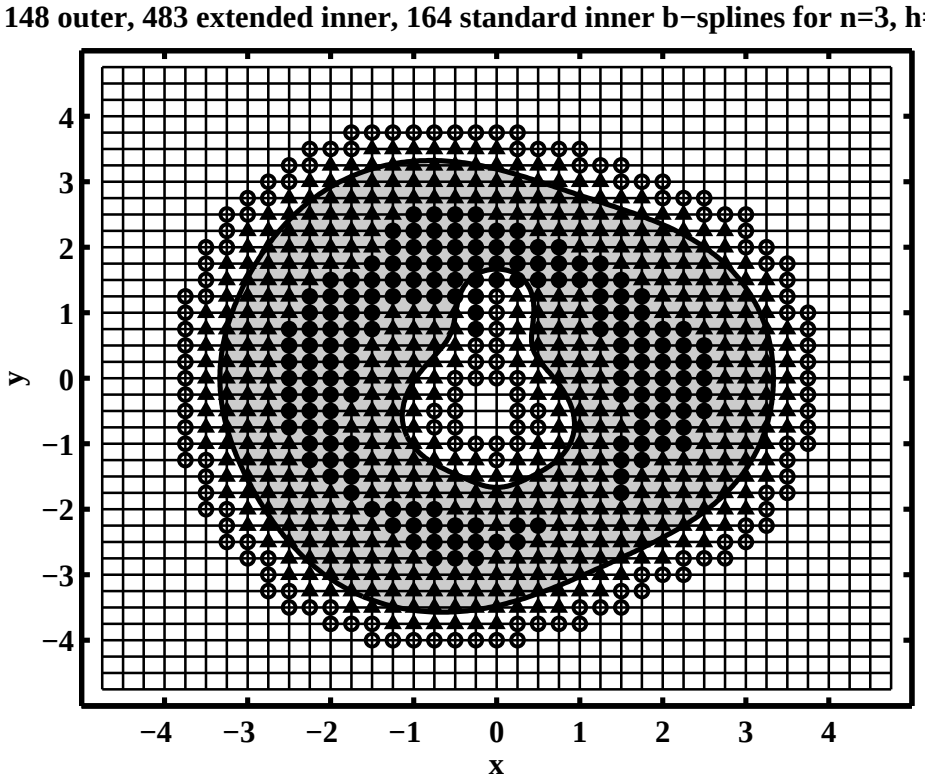

Figure 3.13. Outer (○), extended (▲), and standard (●) cubic b-splines for $h = 0.25$

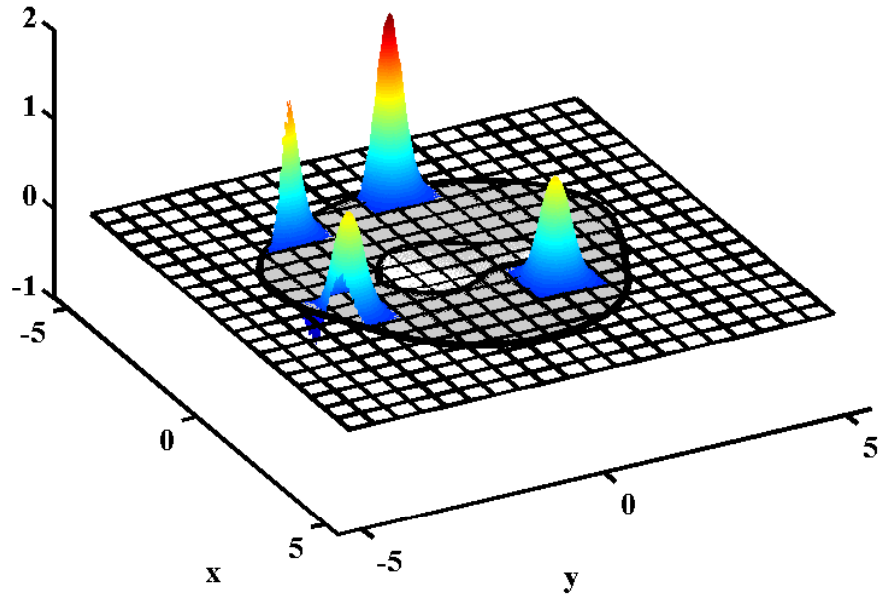

Figure 3.14. Extended quadratic b-splines

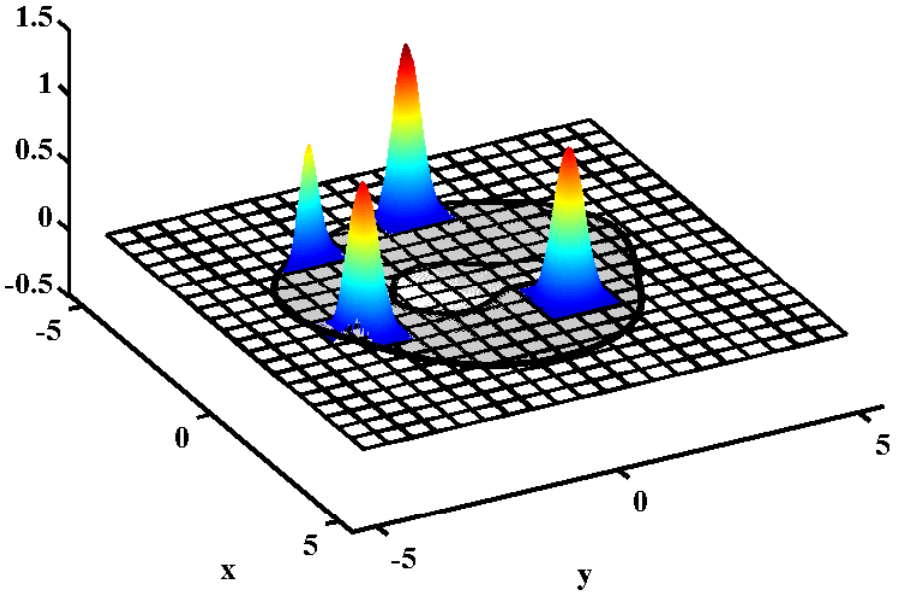

Figure 3.15. Weighted extended quadratic b-splines

3.6. The Assembly

To assemble the matrices, the convolution and the scalar products of b-splines are considered. Using Equations (2.43), (2.44), and (2.45), the integrals are calculated.

Figure 3.16 shows the value of stiffness matrix $K_{i,k}$ for the cubic b-splines ($|k| \preceq n, h = 1$). These are the integral values of gradients where the scalar products of both are not zero. If k is taken as minus three, the intersections of their supports are in gray color, and the integral of their gradients is $-1/302400$, written in the middle of lower-left grid cell of k.

$-\frac{1}{302400}$	$-\frac{1}{4200}$	$-\frac{67}{33600}$	$-\frac{73}{18900}$	$-\frac{67}{33600}$	$-\frac{1}{4200}$	$-\frac{1}{302400}$
$-\frac{1}{4200}$	$-\frac{1}{105}$	$-\frac{211}{4200}$	$-\frac{2}{25}$	$-\frac{211}{4200}$	$-\frac{1}{105}$	$-\frac{1}{4200}$
$-\frac{67}{33600}$	$-\frac{211}{4200}$	$-\frac{397}{6720}$	$\frac{41}{420}$	$-\frac{397}{6720}$	$-\frac{211}{4200}$	$-\frac{67}{33600}$
$-\frac{73}{18900}$	$-\frac{2}{25}$	$\frac{41}{420}$	$\frac{604}{945}$ i	$\frac{41}{420}$	$-\frac{2}{25}$	$-\frac{73}{18900}$
$-\frac{67}{33600}$	$-\frac{211}{4200}$	$-\frac{397}{6720}$	$\frac{41}{420}$	$-\frac{397}{6720}$	$-\frac{211}{4200}$	$-\frac{67}{33600}$
$-\frac{1}{4200}$	$-\frac{1}{105}$	$-\frac{211}{4200}$	$-\frac{2}{25}$	$-\frac{211}{4200}$	$-\frac{1}{105}$	$-\frac{1}{4200}$
$-\frac{1}{302400}$ k	$-\frac{1}{4200}$	$-\frac{67}{33600}$	$-\frac{73}{18900}$	$-\frac{67}{33600}$	$-\frac{1}{4200}$	$-\frac{1}{302400}$

Figure 3.16. The integral values of gradients for two cubic b-splines

The integrals for the standard b-splines are easy to compute, however the effects of boundaries are taken into consideration for the integrals of other splines. For the boundary cells, they are divided into sub cells. The subdivision requires cuts by straight lines. References [39] and [40] explain the integration procedure for numerical computation. The integration process is based on Gauss quadrature rules. According to Gauss quadrature, the polynomials of degree n can be integrated by using $(n+1)/2$

integration points. Table 3.2 shows the Gauss parameters. Using two, three, and four points; Gauss quadrature rule can be used to find the integral of equations up to $n = 3$, $n = 5$, and $n = 7$ respectively. For the inner cells, it is easy to find the integral with tensor product Gauss formulas, and for the boundary cells, subdivision is used.

Using linear combinations of web-splines, the linear system equations are assembled and solved easily. The Galerkin system is solved iteratively with bi-conjugate gradients method [41, 42]. After finding the coefficients of unknown function, the solution is shown graphically.

Table 3.2. Gauss parameters between $[0, 1]$

Degree	Points	Weight
2	$\frac{3\mp\sqrt{3}}{6}$	$\frac{1}{2}$
3	$\frac{1}{2}$ $\frac{5\mp\sqrt{15}}{10}$	$\frac{4}{9}$ $\frac{5}{18}$
4	$\frac{35\mp\sqrt{525-70\sqrt{30}}}{70}$ $\frac{35\mp\sqrt{525+70\sqrt{30}}}{70}$	$\frac{18+\sqrt{30}}{72}$ $\frac{18-\sqrt{30}}{72}$
5	$\frac{1}{2}$ $\frac{21\mp\sqrt{245-14\sqrt{70}}}{42}$ $\frac{21\mp\sqrt{245+14\sqrt{70}}}{42}$	$\frac{64}{225}$ $\frac{332+13\sqrt{70}}{1800}$ $\frac{332-13\sqrt{70}}{1800}$

4. WEB-SPLINE APPLICATIONS FOR ONE DIMENSION

This section considers the web-splines as basis function for FEM in electromagnetics with respect to the standard FEM applied to the two-point boundary value problems with different boundary conditions. This new approach, which provides more accurate results than standard FEM, is presented with respect to the other numerical techniques and applied to one-dimensional electromagnetic problems. Computed results are compared with the other numerical results in literature.

Some examples, compared web-spline method with the previous studies, are shown. First study shows the comparison of finite difference, finite element, finite volume, and cubic b-spline interpolation with the web-spline method [43, 44]. Other examples are electromagnetic problems. The web-spline method is applied to reflection and electromagnetic wave problems in literature [12, 16, 17].

4.1. Comparison of Some Numerical Techniques with Web-spline

Consider the PDE for one dimension as:

$$-\frac{d}{dx}\left(p(x)\frac{du}{dx}\right)+q(x)u=f(x),\ x\in[x_1,x_2] \tag{4.1}$$

with Dirichlet and/or Cauchy boundary conditions at x_1 and x_2 where $p(x),\ q(x)\in C^1[x_1,x_2],\ f(x)\in C[x_1,x_2]$.

For the given $p(x)=e^{1-x}$, $q(x)=0$, $f(x)=1+e^{1-x}$ using Equation (4.1) for the homogeneous boundary conditions on $[0,1]$, the exact solution is $u(x)=x(1-e^{x-1})$. The boundary condition is essential and modeled with a weight function.

Web-spline method has a better numerical approximation as shown in Table 4.1 compared with several numerical solution methods [44].

For FEM analysis; using quadratic, cubic Lagrange polynomials is not always easy to implement. Selection of grid width is important for higher older polynomials. However, using web-splines with higher orders is easy to implement compared to the standard FEM analysis.

Figure 4.1 shows the L_2 error norm of computation for various basis functions which are linear Lagrange polynomial (solid line), linear (dashed line), quadratic (dotted line), and cubic (dashed-dotted line) web-splines. As seen in Figure 4.2, the convergence rate is equal to one more of order n.

Table 4.1. The max-norm of errors with respect to exact solution of Section 4.1.

Methods	h	Max-norm/h^2
Finite Difference Method	0.1	$8.240e-3$
	0.01	$8.306e-3$
Finite Element Method (linear)	0.1	$6.351e-3$
	0.01	$6.364e-3$
Finite Element Method (quadratic)	0.1	$1.987e-3$
	0.01	$2.223e-5$
Finite Volume Method	0.1	$3.177e-3$
	0.01	$3.182e-3$
Cubic b-spline interpolation	0.1	$2.900e-4$
	0.01	$2.896e-6$
Finite Element Method (linear web-splines)	0.1	$5.365e-3$
	0.01	$5.776e-3$
Finite Element Method (quadratic web-splines)	0.1	$2.055e-6$
	0.01	$4.910e-8$
Finite Element Method (cubic web-splines)	0.1	$4.771e-7$
	0.01	$4.823e-9$

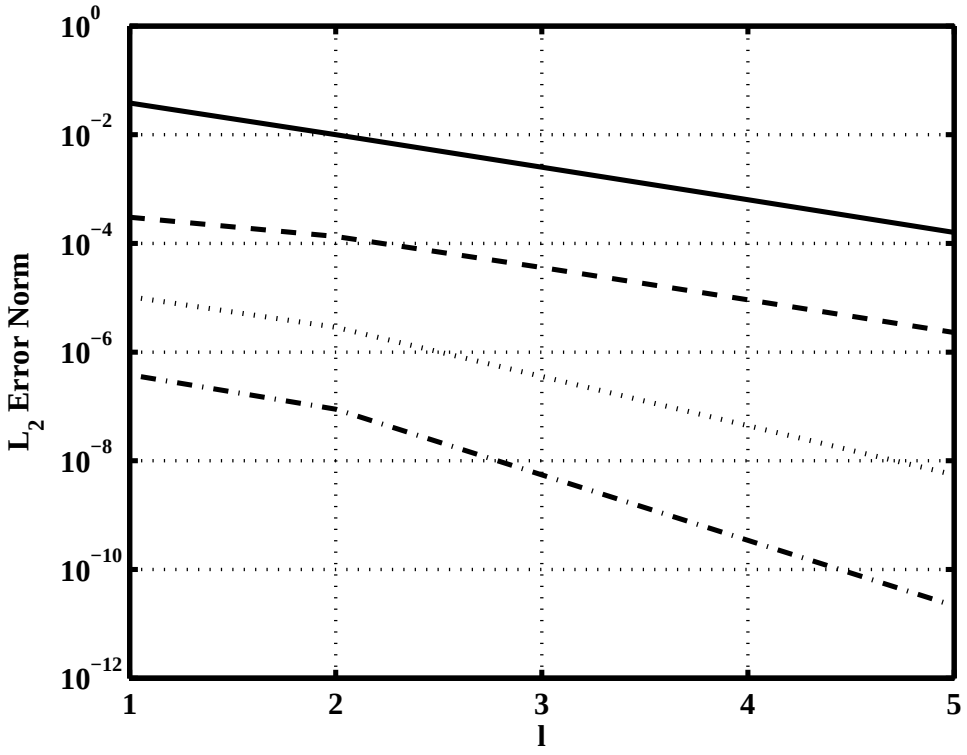

Figure 4.1. L_2 error norm of FEM using Lagrange (solid), linear (dash), quadratic (dot), and cubic (dash-dot) web-spline

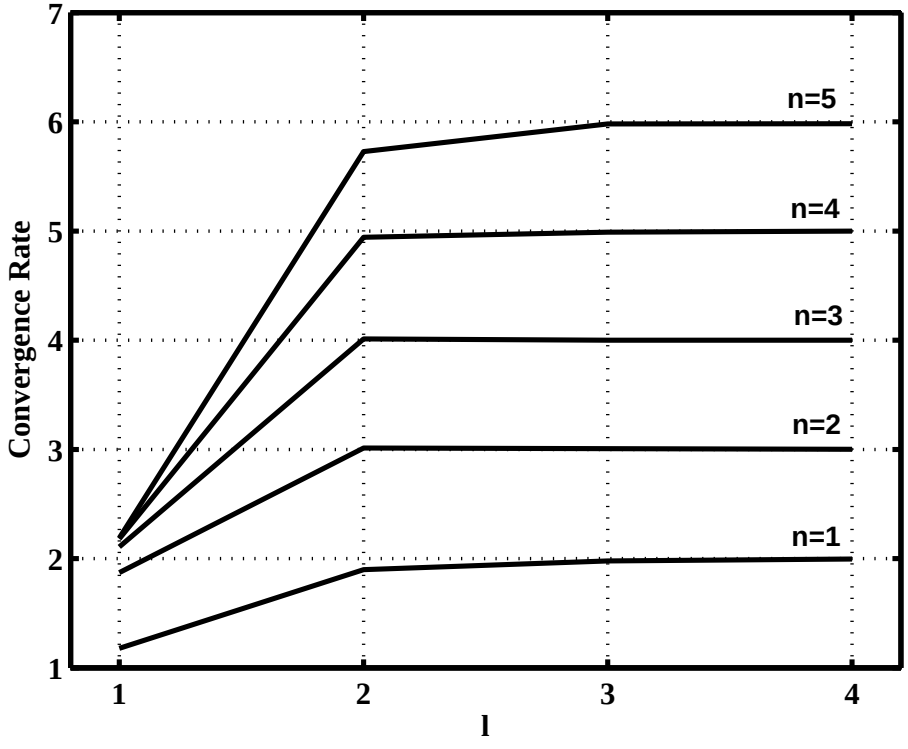

Figure 4.2. Convergence rate of web-splines by increasing degree

4.2. Reflection from a Metal Dielectric Slab

Consider a uniform plane wave which is incident upon a dielectric slab shown in Figure 4.3 with thickness T, relative permittivity ε_r, relative permeability μ_r; the reflection coefficient of the slab (R) is to be calculated.

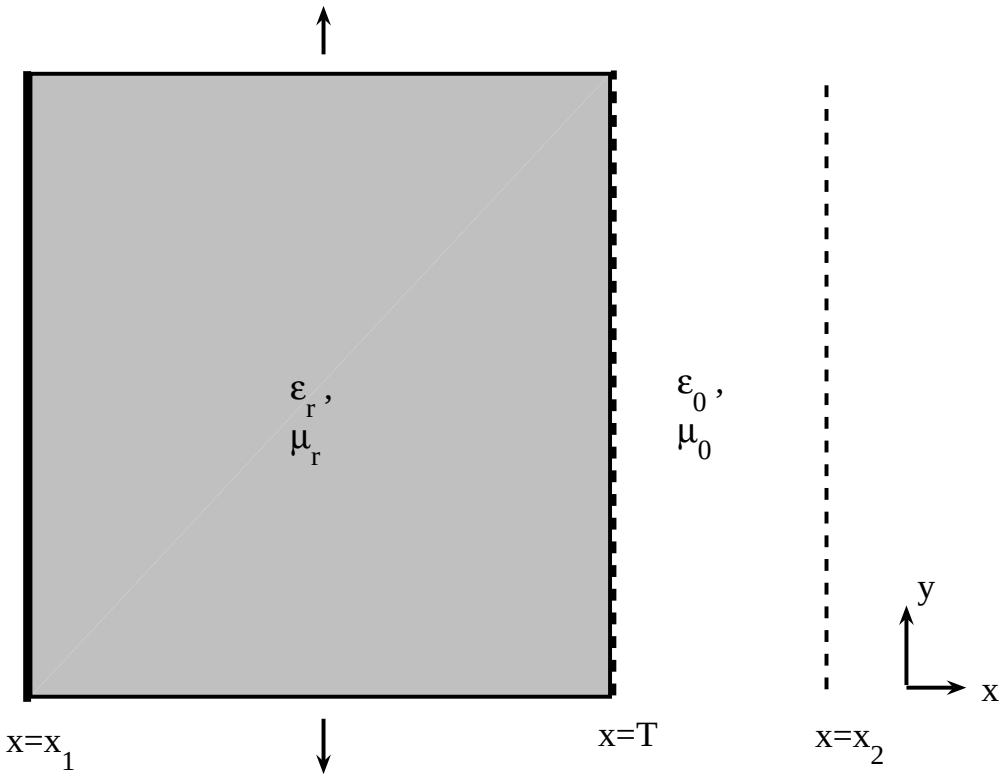

Figure 4.3. The metal dielectric slab

The electric field (perpendicular polarization) reflected from a metal dielectric slab is found by using Equation (2.14) as:

$$\frac{d}{dx}\left(\frac{1}{\mu_r}\frac{d}{dx}E_z\right) + \widetilde{k}_0^2\varepsilon_r E_z = 0 \tag{4.2}$$

with Dirichlet and Cauchy boundary conditions on $[x_1, x_2]$

$$E_z(x_1) = 0 \tag{4.3}$$

$$\frac{d}{dx}E_z(x_2) + j\widetilde{k}_0 E_z(x_2) = 2j\widetilde{k}_0 e^{j\widetilde{k}_0 x_2} \tag{4.4}$$

The incident and reflected fields at normal incidence are represented as:

$$E_z^{in} = e^{j\widetilde{k}_0 x} \tag{4.5}$$

$$E_z^{r} = R \cdot e^{-j\widetilde{k}_0 x} \tag{4.6}$$

where R is the reflection coefficient. The analytical reflection coefficient is found as:

$$R = -\frac{\sqrt{\varepsilon_r} - j\sqrt{\mu_r}\tan(\widetilde{k}_0 T\sqrt{\mu_r\varepsilon_r})}{\sqrt{\varepsilon_r} + j\sqrt{\mu_r}\tan(\widetilde{k}_0 T\sqrt{\mu_r\varepsilon_r})} \tag{4.7}$$

According to FEM analysis, the sum of incident and reflected wave is found. It is noted that the grid width should be selected as small compared to the wavelength. In order to find the reflection coefficient, the electric field at x_2 is used. The reflection coefficient by the help of FEM is obtained by using

$$R^{FEM} = \frac{E_z(x_2) - E_z^{in}(x_2)}{E_z^{in}(x_2)} \tag{4.8}$$

The reflection coefficient is obtained by using thickness, permittivity, frequency (f), x_2, and grid width which are tabulated in Table 4.2. Figure 4.4 shows the exact and computed reflection coefficients at normal incidence while changing the loss parameter (β) of the material using linear web-splines. The results give good agreement with the exact solution.

The error analysis, which agrees with the previous application, shows better approximation when web-splines are used as basis functions. Figure 4.5 shows the comparison of maximum error analysis with the standard FEM and the linear, quadratic, cubic web-splines. As seen in Figure 4.5 the error increases for high loss parameter. So, high order polynomials like cubic web-splines are suitable.

Table 4.2. The parameters for the reflection from dielectric slab

Parameter	Value
T	0.25
ε_r	$4 - j\beta$
μ_r	1
f	$300\ MHz$
x_2	0.3
h	0.05

While doing some simulations for $\varepsilon_r = 4 - 0.5j$, and frequencies 200 MHz, 2 GHz, 20 GHz; the relative maximum errors are obtained in the fourth decimal place if $k_0 h$ is taken between 0.2 and 0.5. Therefore; the grid width and the domain must be small for high frequencies in order to obtain fast calculation.

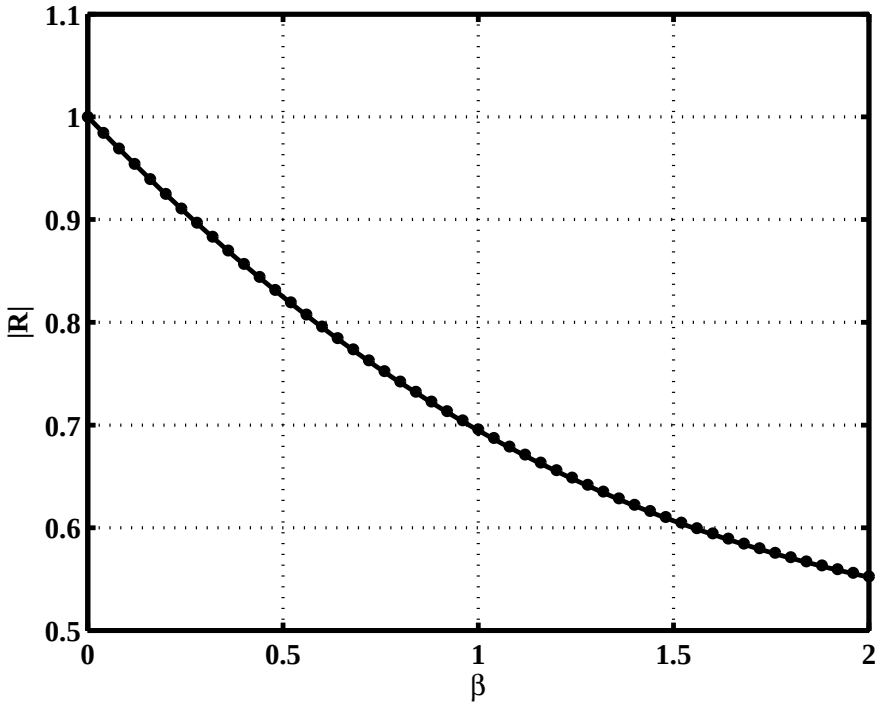

Figure 4.4. Exact (solid) and computed (points) reflection coefficient versus loss parameter for FEM using linear web-splines

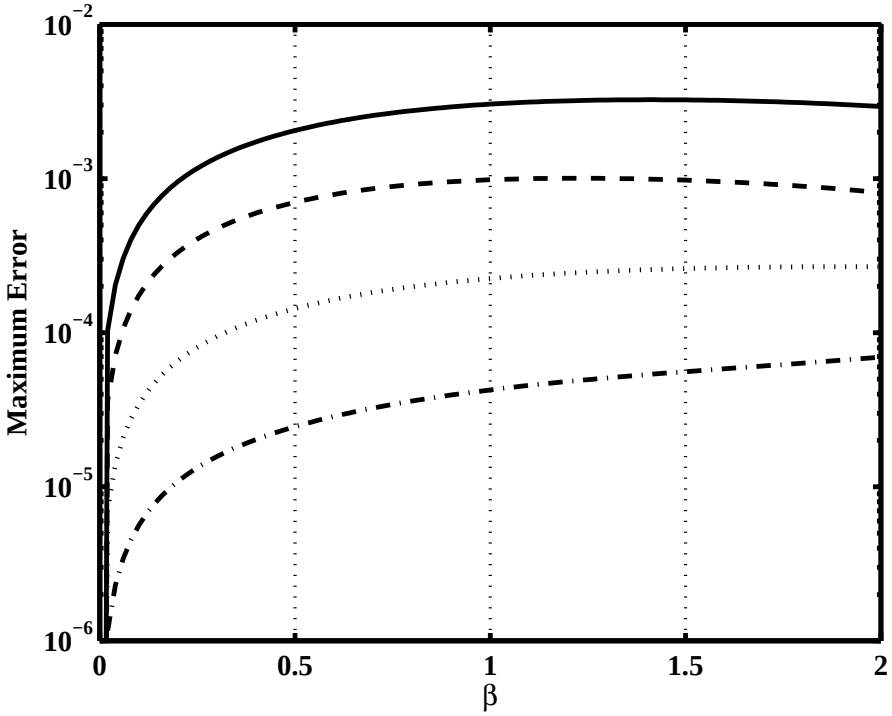

Figure 4.5. Maximum error analysis using Lagrange (solid), linear (dash), quadratic (dot), and cubic (dash-dot) web-splines

4.3. Electromagnetic Waves Between Parallel Plates

One of the other examples of electromagnetic problems in one dimension is to find the electromagnetic waves between parallel plates, shown in Figure 4.6.

Consider the parallel plate waveguide; the general differential equation is given as [16]:

$$\frac{d}{dx}\left(\frac{1}{\mu_r}\frac{d}{dx}E_y\right) + \widetilde{k}_0^2\varepsilon_r E_y = f(x) \tag{4.9}$$

where E_y is the electric field between plates, $f(x)$ is the source, and other parameters are defined in previous example.

The first application uses the parameters; $\mu_r = 1$, $\widetilde{k}_0^2\varepsilon_r = \pi^2$, $f(x) = 2\pi^2\sin(\pi x)$ with the homogeneous Dirichlet boundary conditions $E_y(0) = E_y(1) = 0$ in order to obtain the results using FEM with web-splines. The exact solution is found as

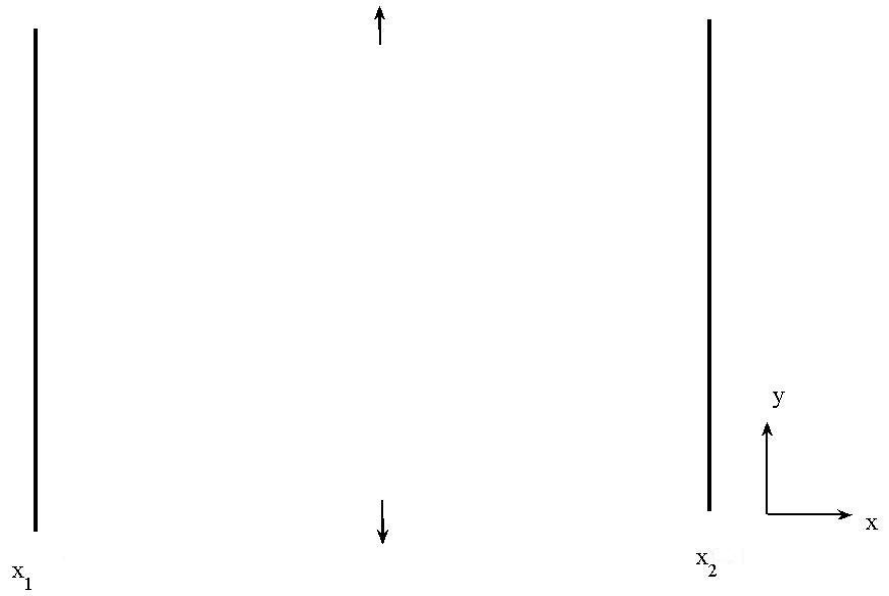

Figure 4.6. Parallel plates

$E_y(x) = \sin(\pi x)$.

Solving the system using eleven web-splines shown in Figure 4.7, more accurate results are obtained with respect to the standard FEM [16]. Figure 4.7 shows the quadratic b-splines between zero and one. The grid width is taken as 0.1 in simulations. Figure 4.8 shows the exact analytical results and simulated results using linear web-splines with solid line and points respectively. The maximum error is in the third, sixth, and seventh decimal place for the linear, quadratic, and cubic b-splines respectively.

The simulations are compared with the standard FEM, which uses linear Lagrange polynomial basis functions. As seen in Figure 4.9, by using web-splines basis functions, more accurate results are obtained with respect to the standard FEM analysis.

Figure 4.10 shows the relative L_2 error norm of computation for various basis functions which are linear Lagrange polynomial (solid), linear (dash), quadratic (dot), and cubic (dash-dot) web-splines.

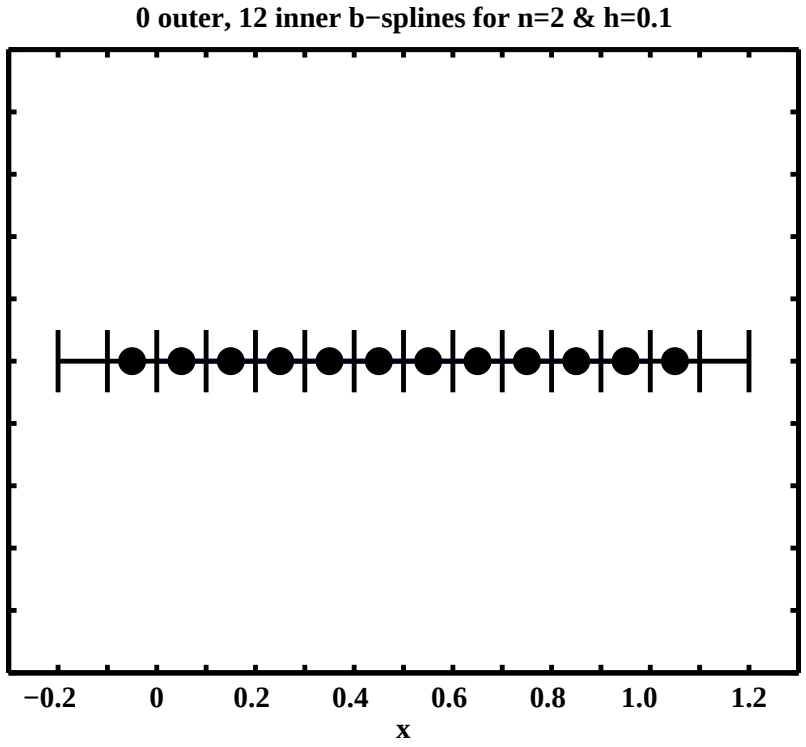

Figure 4.7. Weighted quadratic inner (•) b-splines for parallel plates between 0 and 1

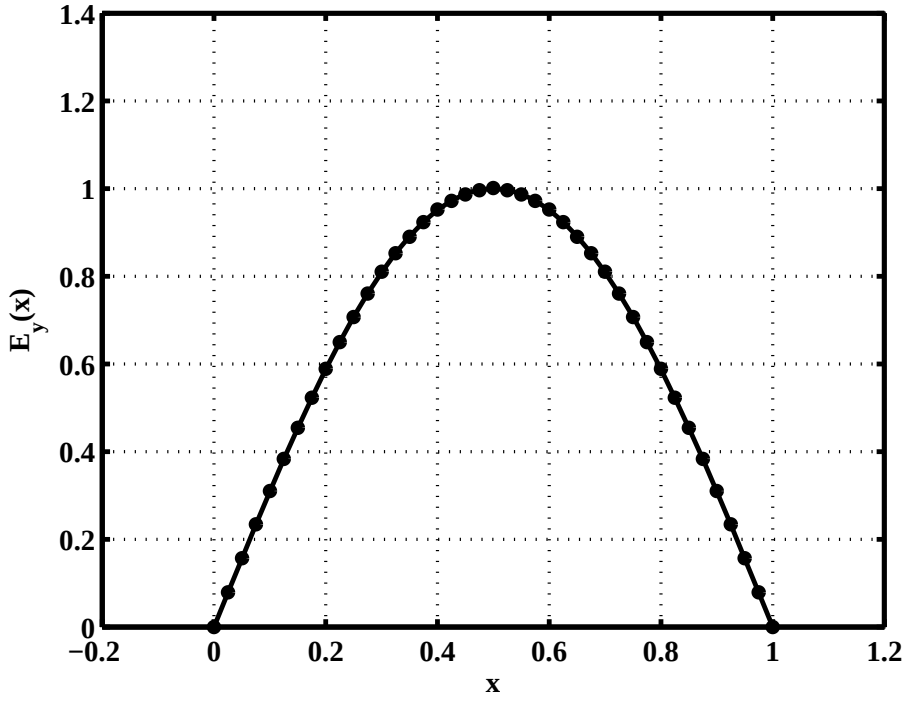

Figure 4.8. Exact (solid) and computed (points) electric fields of parallel plates using linear web-splines

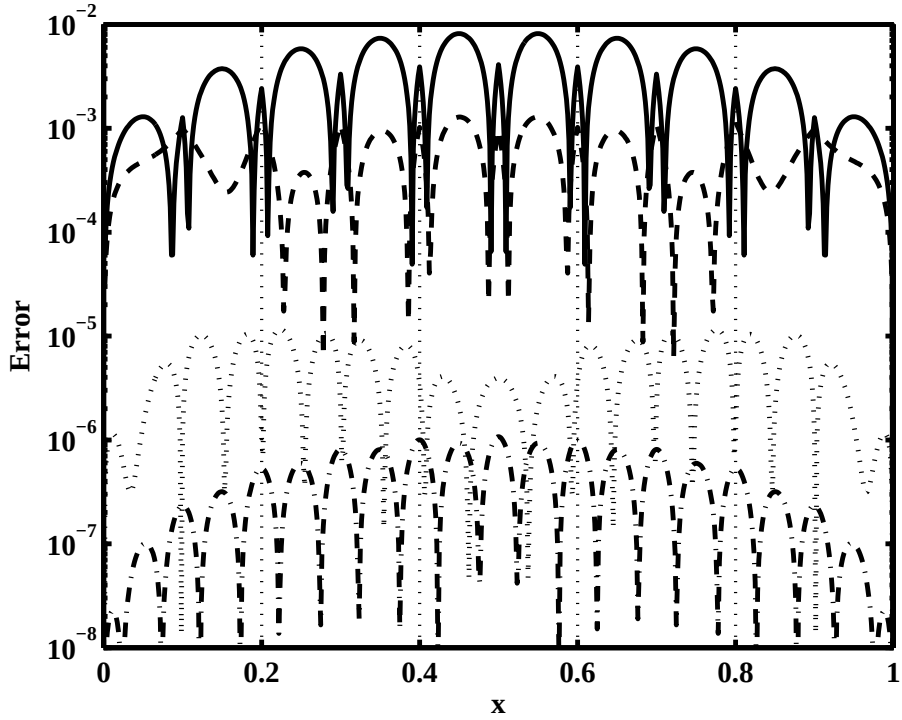

Figure 4.9. Error analysis of parallel plates using standard FEM (solid) and linear (dash), quadratic (dot), and cubic (dash-dot) web-splines

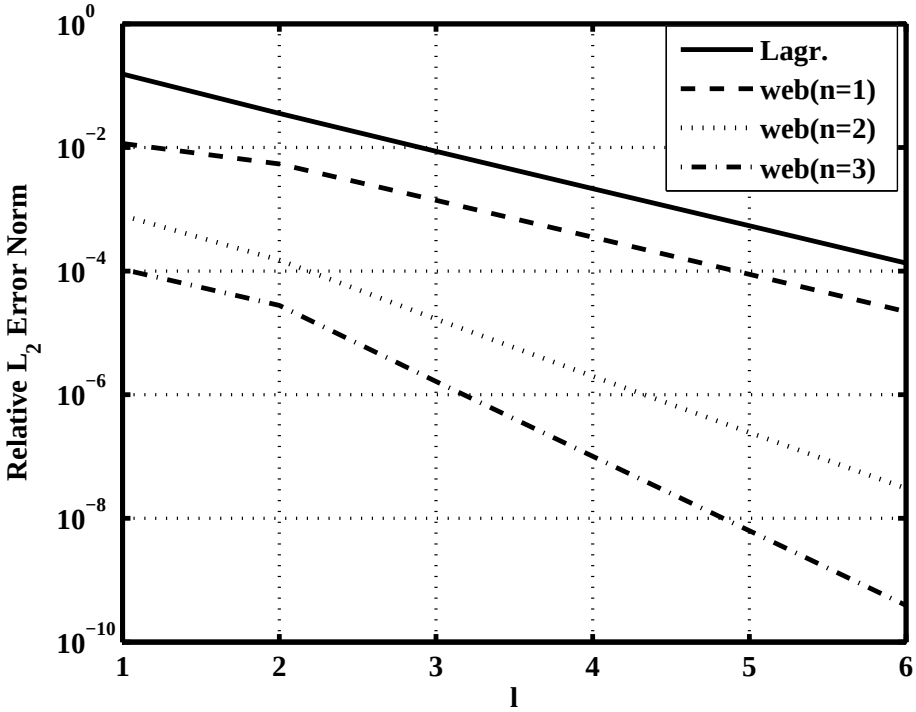

Figure 4.10. The relative L_2 error norm of parallel plates between 0 and 1 for various basis functions versus the number of nodes

The second application uses the parameters; $\mu_r = 1$, $\widetilde{k}_0^2 \varepsilon_r = \pi^2$, and $f(x) = 2\pi^2 \sin(\pi(x - 0.2))$ with the homogeneous Dirichlet boundary conditions $E_y(0.2) = E_y(1.2) = 0$ in order to obtain the results using FEM with web-splines. The exact solution is found as $E_y(x) = \sin(\pi(x - 0.2))$. Figure 4.11 shows the quadratic b-splines taking the grid width 0.125.

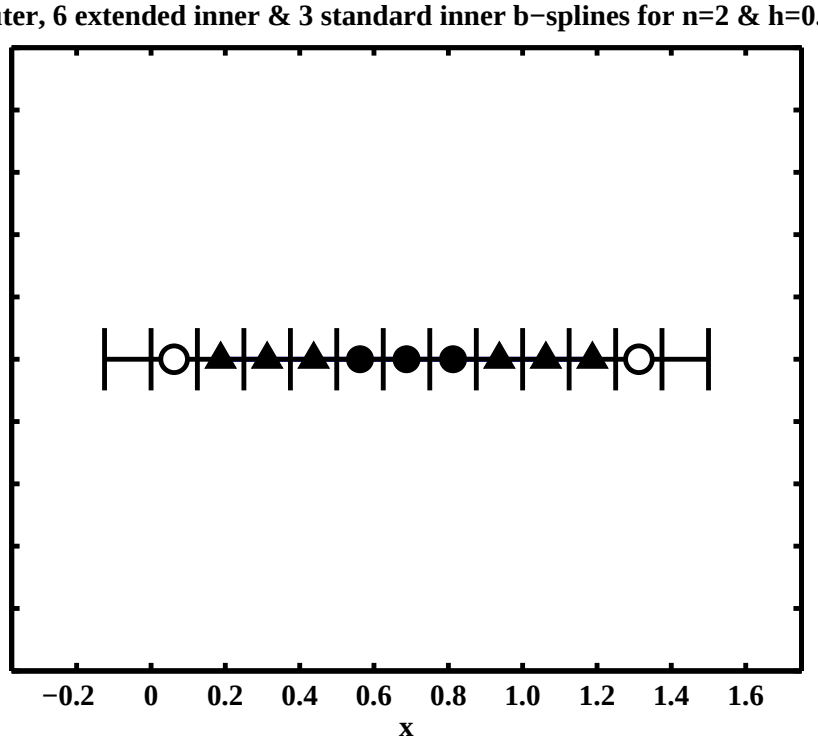

Figure 4.11. Weighted extended quadratic b-splines for parallel plates between 0.2 and 1.2 (outer (○), extended inner (▲), and standard inner (●) b-splines)

In all simulations, the standard FEM uses linear Lagrange polynomial basis functions. By using web-splines as basis functions, more accurate results are obtained as compared with standard FEM analysis. Figure 4.12 shows the L_2 error norm of computation for various basis functions which are linear Lagrange polynomial, linear, quadratic, and cubic web-splines.

The condition number is a measure of stability of linear system to the numerical operations. It is defined as the product of the norm of the matrix and the norm of the inverse of matrix. If the condition number is low, it is said to be well-conditioned which

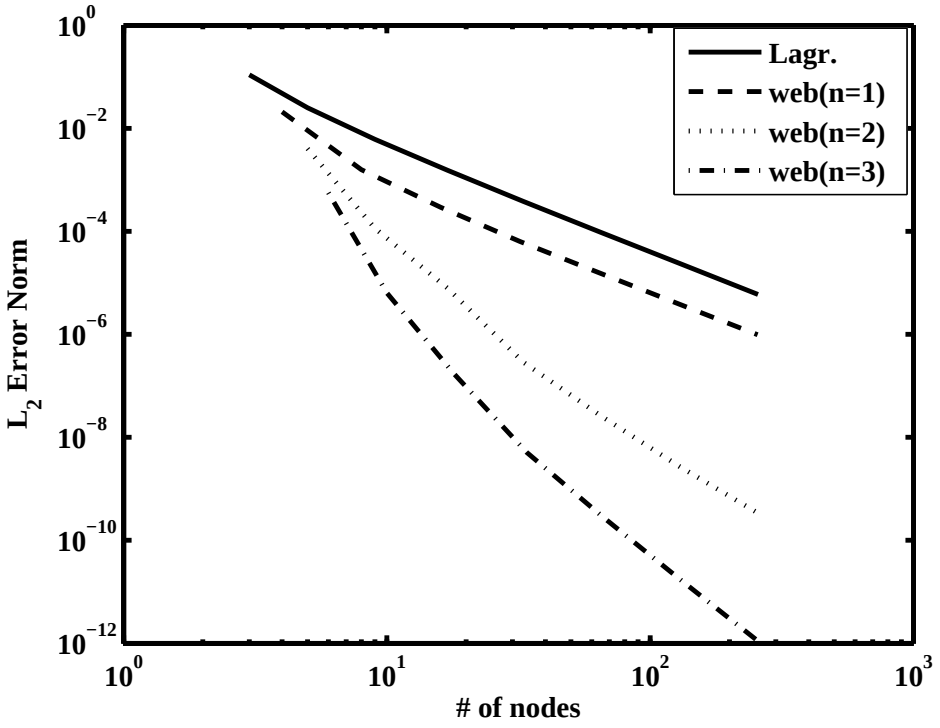

Figure 4.12. The L_2 error norm of parallel plates between 0.2 and 1.2 for various basis functions versus the number of nodes

means its inverse can be computed with good accuracy. If the condition number is high, it is said to be ill-conditioned. Using web-splines instead of weighted b-splines, the condition number decreases, which means the instability problem is solved. Secondly, more accurate maximum errors and L_2 errors are obtained.

5. WEB-SPLINE APPLICATIONS FOR TWO DIMENSIONS

In this section, the web-spline method is applied to electromagnetic wave problems and waveguides illustrated in literature [16, 17, 45, 46, 47, 48, 49]. For the wave equation analysis, the square and circular domains are chosen in order to compare with the exact results by using error analysis. Then, the method is used for two dimensional waveguides and compared with the previous studies. These studies show that using web-splines in electromagnetic applications gets more accurate results with fewer nodes, higher stability than standard FEM analysis.

5.1. Wave Equation Analysis For Square Domain

The wave equation obeys the Helmholtz equation shown at Equation (2.14). First application is to study the Helmholtz equation for the square boundary shown in Figure 5.1 using boundary conditions given at Equation (2.23) for $s = 1$, $r = j\widetilde{k}$ and $g(x, y)$ as:

$$g(x,y) = \begin{cases} j\widetilde{k}(1-\sin\theta)e^{j\widetilde{k}(\cos\theta x+\sin\theta y_1)} & \text{on } \Gamma_1 \\ j\widetilde{k}(1+\cos\theta)e^{j\widetilde{k}(\cos\theta x_2+\sin\theta y)} & \text{on } \Gamma_2 \\ j\widetilde{k}(1+\sin\theta)e^{j\widetilde{k}(\cos\theta x+\sin\theta y_2)} & \text{on } \Gamma_3 \\ j\widetilde{k}(1-\cos\theta)e^{j\widetilde{k}(\cos\theta x_1+\sin\theta y)} & \text{on } \Gamma_4 \end{cases} \tag{5.1}$$

where θ shows the direction angle of wave. The exact solution of wave equation for the above conditions is obtained as [46]:

$$u(x,y) = e^{j\widetilde{k}(\cos\theta x+\sin\theta y)} \tag{5.2}$$

According to the wave equation for square domain, web-spline method is compared with the standard FEM by using the exact solution. The square domain has 2×2 m side lengths. Figure 5.2 shows triangulation for the square domain using 665 nodes

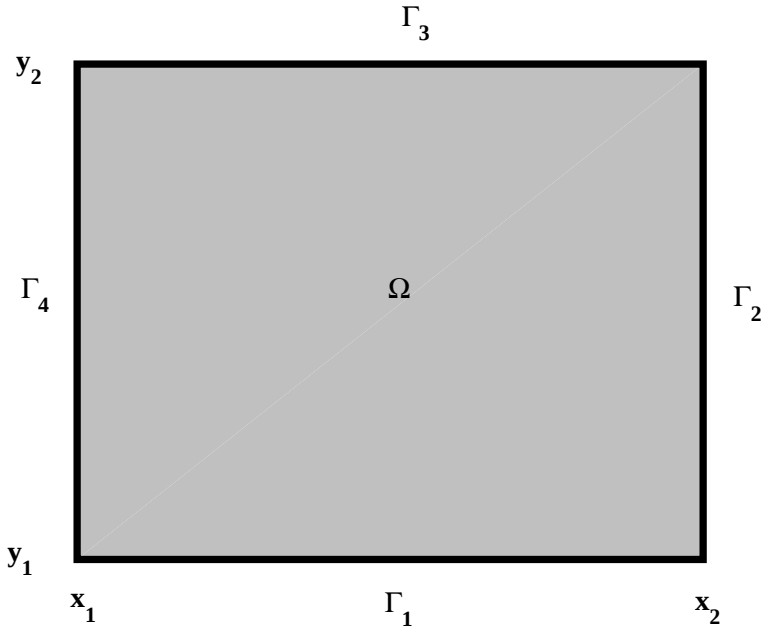

Figure 5.1. Square domain

and 1248 triangles. Figure 5.3 shows the b-spline basis of the same domain using 100 inner b-splines. Since the square domain is regular, there are no outer b-splines. The simulations can be studied by changing the direction of wave, wave number, and the grid width.

Figure 5.4 shows the computational results of wave equation (5.2) using standard FEM with 665 nodes. Then, the web-spline method is tested with the same parameters for the comparison as seen in Figure 5.5 for the direction angle $\pi/4$, wave number π, and grid width 0.25 m. Both results are reconciled with the exact solution. However, the web-spline method only uses 100 b-splines to compute.

The relative L_2 error norm with the number of nodes is used to compare the methods. Figure 5.6 shows the relative L_2 error norm versus number of nodes for square domain. Although the linear b-splines are same as the hat functions, regular grid generation works better than triangulation for square domain.

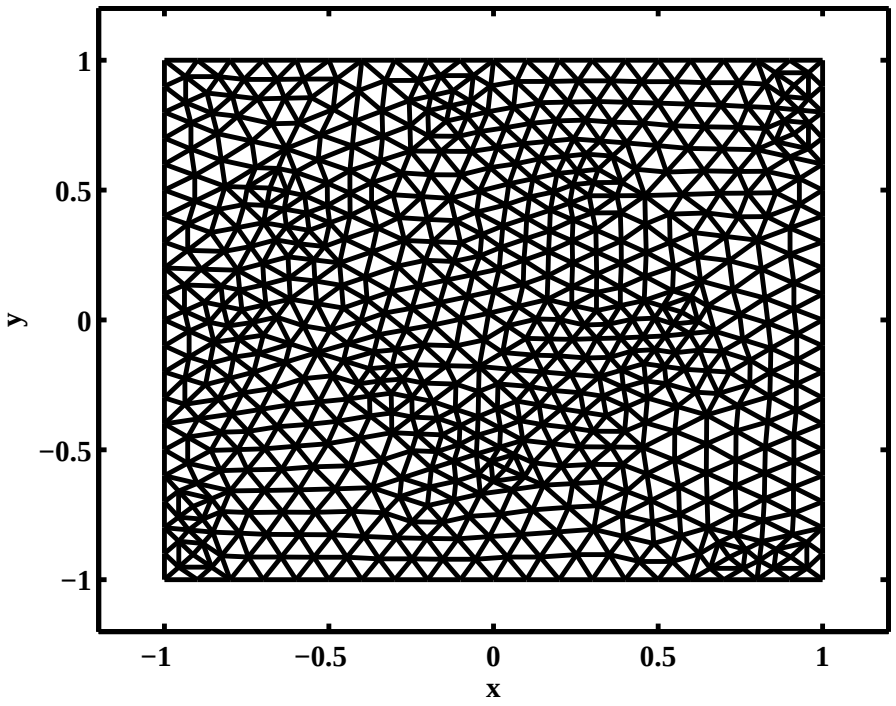

Figure 5.2. Triangulation for square domain

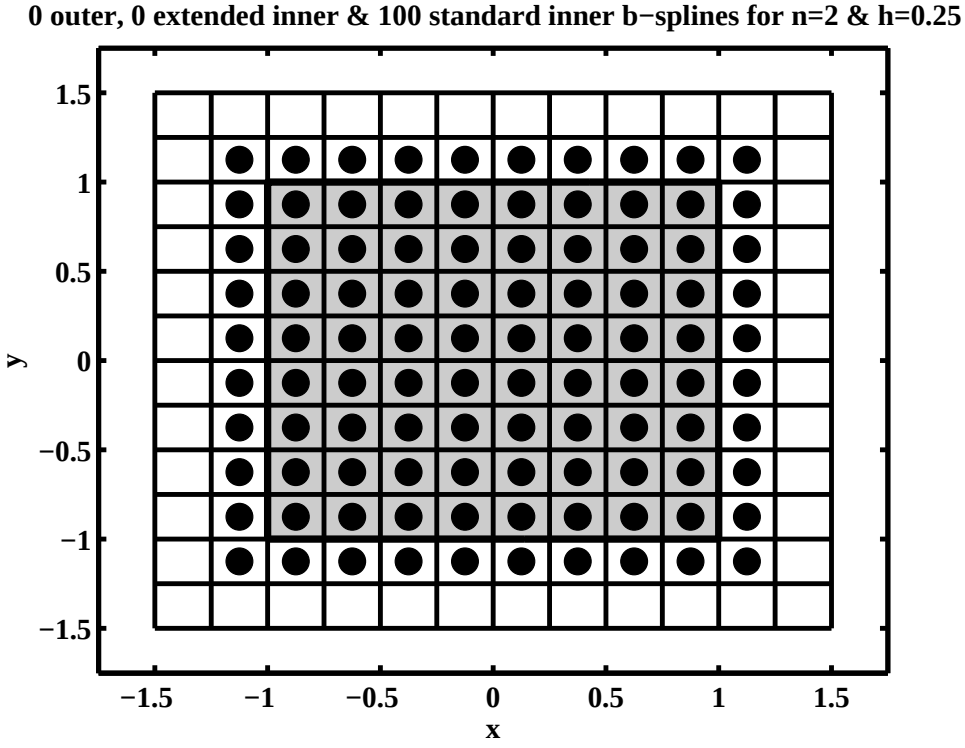

Figure 5.3. Quadratic b-spline basis for square domain (standard inner (•) b-splines)

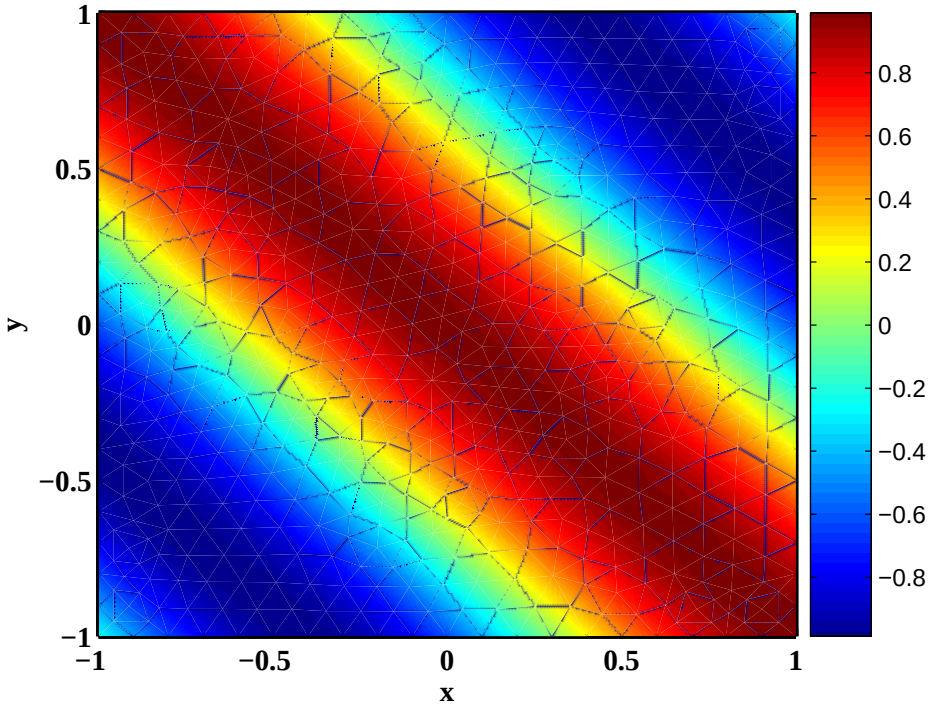

Figure 5.4. The computational results of electric field using standard FEM for square domain

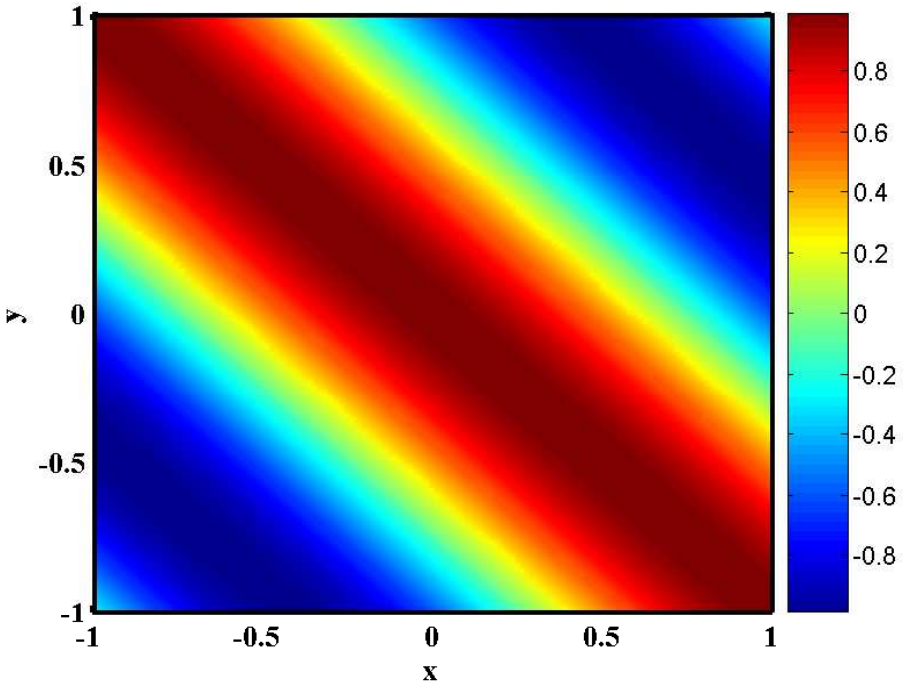

Figure 5.5. The computational results of electric field using web-spline method for square domain

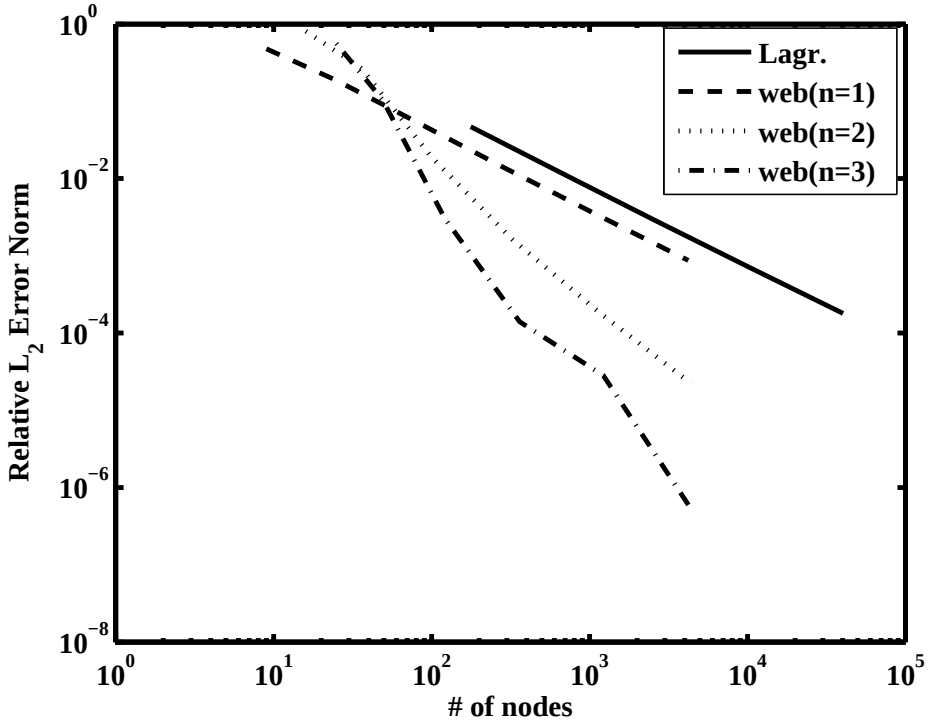

Figure 5.6. The relative L_2 error norm for various basis functions versus the number of nodes for square domain

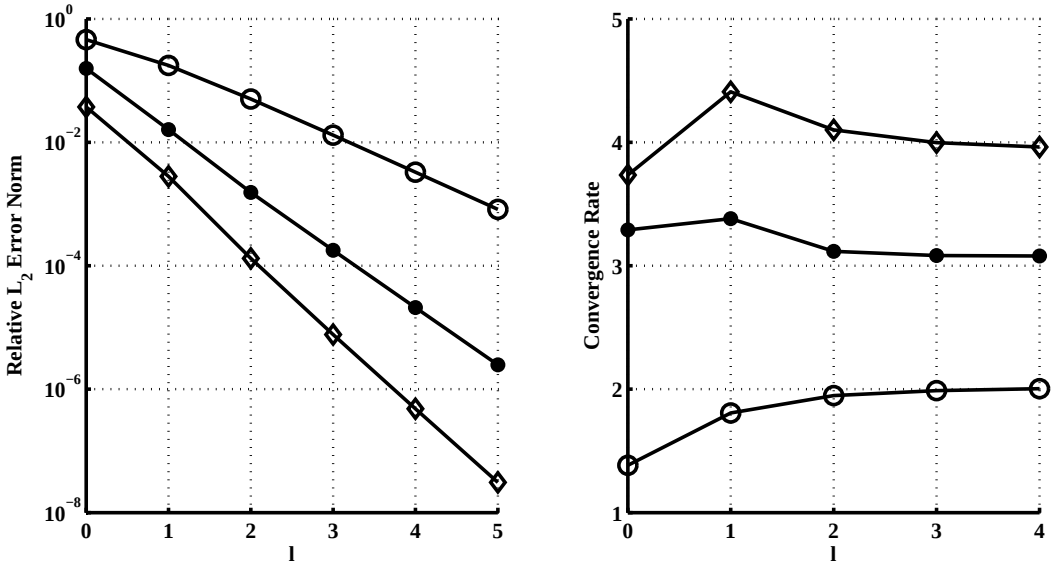

Figure 5.7. The relative L_2 error norm and convergence rate for linear ($\circ$), quadratic ($\bullet$), and cubic b-splines ($\diamond$) for square domain

Figure 5.7 shows the relative L_2 error norm and convergence rate for the grid width $h = 2^{-l}$, $l = 0, 1, ..., 5$. As seen in Figure 5.7, the convergence rate equals one more of degree n for the relative L_2 error norm for square domain.

5.2. Wave Equation Analysis For Circular Domain

Considering the wave equation with Cauchy boundary conditions, the solution of the wave equation for circular domain is obtained by using linear, quadratic, and cubic extended b-splines.

According to the wave equation for circular domain, the web-spline method is compared with the standard FEM by using the exact solution given in Equation (5.2). Figure 5.8 shows triangulation for the circular domain using 549 nodes and 1032 triangles. Figure 5.9 shows the b-spline basis of the same domain using 68 outer, 148 extended inner, and 76 standard inner quadratic b-splines. Figure 5.10 shows the computational results of wave equation using standard FEM with 549 nodes. Then, the web-spline method is tested for comparison seen in Figure 5.11 for the direction angle $0°$, wave number $\pi/2$, grid width 0.125. Both results are in line with the exact solution. Although the relative L_2 error norm for the standard FEM with 549 nodes is $1.8 \cdot 10^{-3}$, the web-spline method uses 224 b-splines with a relative L_2 error norm $1.27 \cdot 10^{-4}$.

The error analysis shows better approximation when web-splines are used as basis functions. Figure 5.12 shows the relative L_2 error norm versus number of nodes with the standard FEM and the linear, quadratic, and cubic extended b-splines. According to figure, more accurate results are obtained by using web-splines with fewer basis functions instead of standard finite elements.

According to Table 5.1, the efficiency of using web-splines instead of weighted splines is tabulated for various grid width and degree values. For example, 59 nodes are used for $n = 1, h = 1/4$ instead of 100 nodes or the necessary time to obtain the results is 10 seconds for $n = 2, h = 1/8$ instead of 100 seconds. The computational time improvement for two dimension is efficiently better. The reason is that the new

basis function is more stable and the condition number of stiffness and mass matrix is smaller than the standard weighted b-splines.

For $h = 0.25$ m and $\widetilde{k}^2 = 10$, the condition number is 78.06 instead of 216.89 with 41 per cent less nodes using linear web-splines instead of linear weighted b-splines. The condition number is 56.36 instead of $2.30e5$ with 38 per cent less nodes using quadratic web-splines instead of quadratic weighted b-splines. The condition number is 544.58 instead of $1.76e9$ with 34 per cent less nodes using cubic web-splines instead of cubic weighted b-splines. The condition number is $2.84e4$ instead of $5.44e13$ with 31 per cent less nodes using quantic web-splines instead of quantic weighted b-splines. The condition number is $9.06e6$ instead of $1.25e19$ with 29 per cent less nodes using quintic web-splines instead of quintic weighted b-splines.

In conclusion, web-splines are better basis functions with more stable and less computation time.

Table 5.1. The efficiency of web-spline method for circular domain (per cent)

n	h	Efficiency of nodes (per cent)	Efficiency of computation time (per cent)
1	1/4	41.56	90
	1/8	24.90	80
	1/16	13.90	70
2	1/4	37.50	90
	1/8	23.29	90
	1/16	13.36	90
3	1/4	34.19	90
	1/8	21.89	90
	1/16	12.87	90

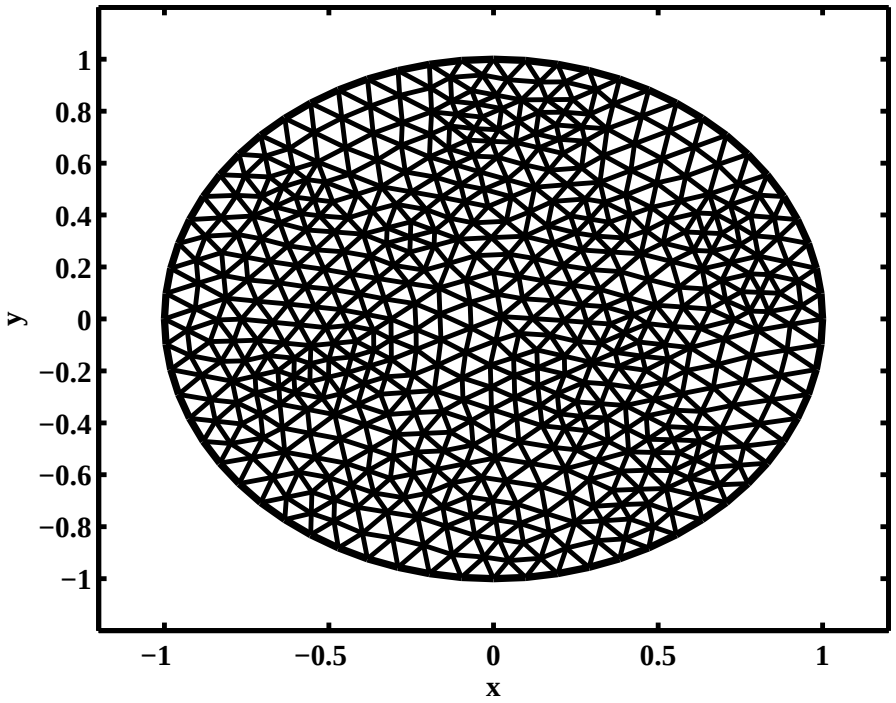

Figure 5.8. Triangulation for circular domain

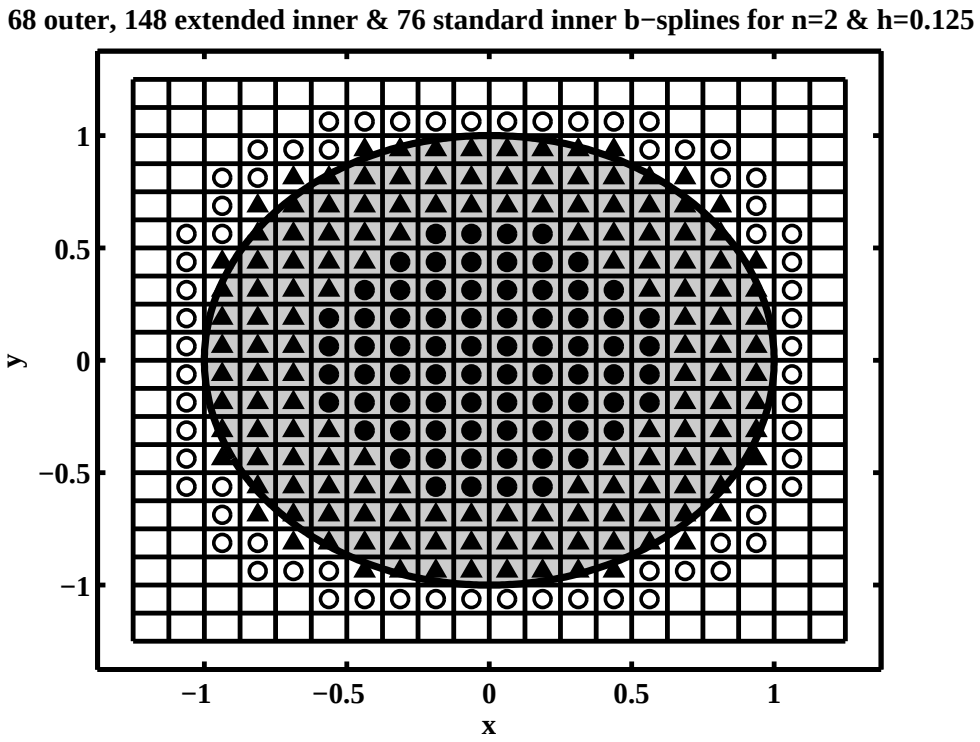

Figure 5.9. Quadratic extended b-splines for circular domain (outer (○), extended inner (▲), and standard (●) inner b-splines)

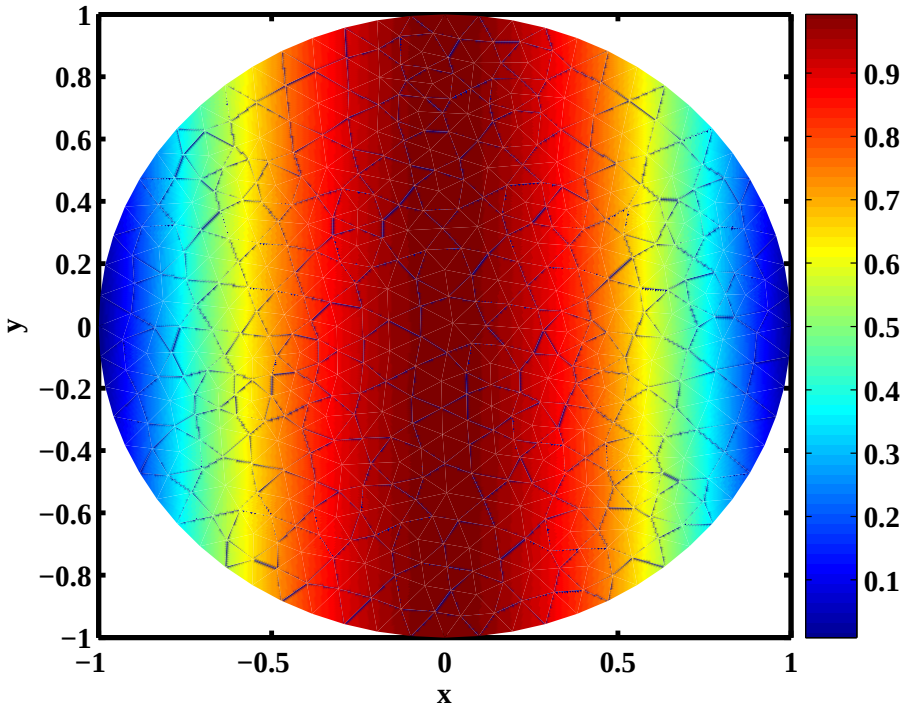

Figure 5.10. The computational electric field using standard FEM for circular domain

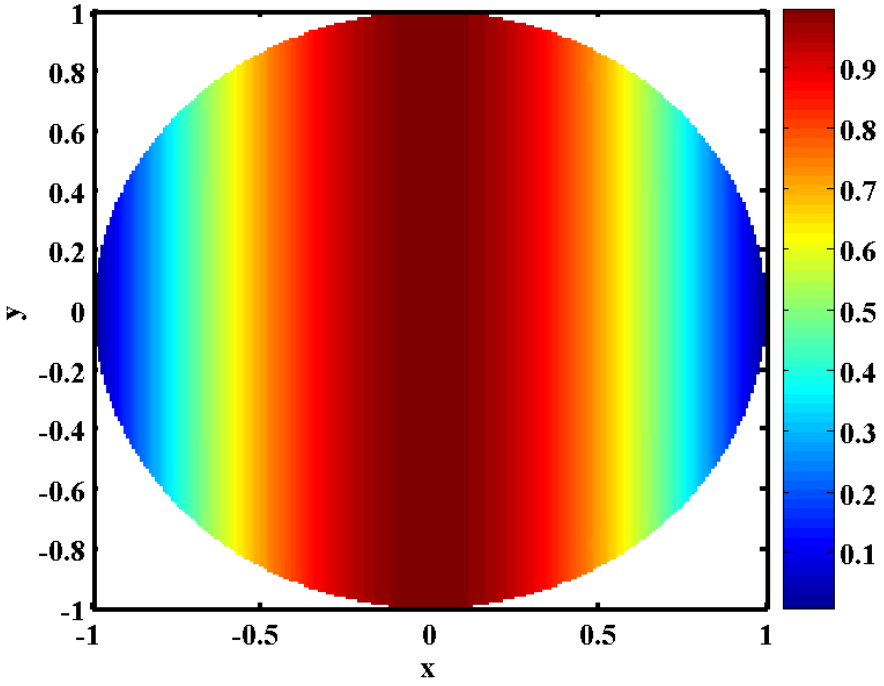

Figure 5.11. The computational electric field using web-spline method for circular domain

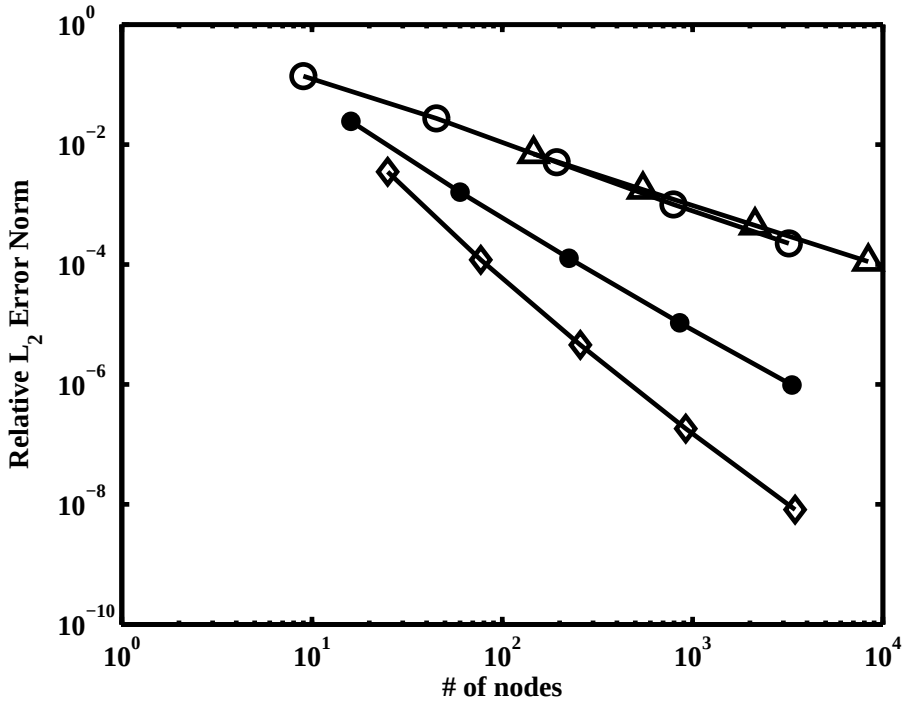

Figure 5.12. The relative L_2 error norm for various basis functions which are linear Lagrange polynomial (△), linear (○), quadratic (●), and cubic (◇) extended b-splines versus the number of nodes for circular domain

5.3. Waveguides

Waveguides are used to carry electromagnetic waves over a wide portion of the electromagnetic spectrum. However, they are useful in microwave and optical frequency ranges. Depending on the frequency, they can be constructed from either conductive or dielectric materials. Waveguides are used for transferring both power and communication signals.

Waveguides are usually used in a frequency range where only the lowest mode or few modes propagate.

This part studies two dimensional waveguide problems using FEM with triangulation and web-splines by using Equation (2.14) without source. These results are compared with the analytical results given by [16, 17, 47, 48, 49].

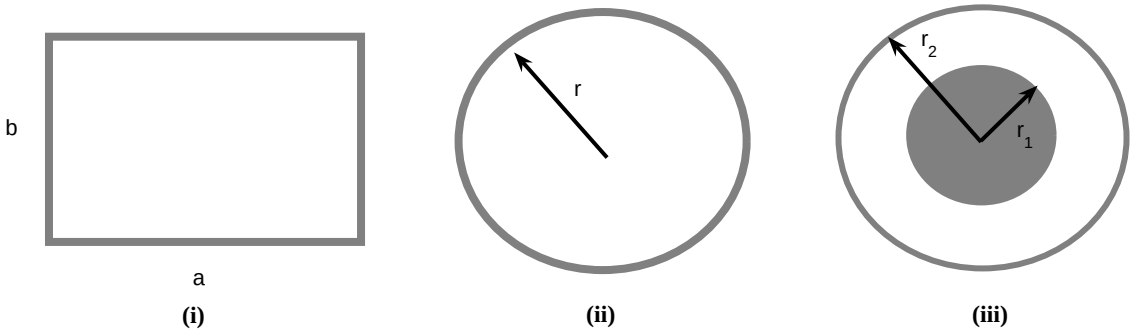

Figure 5.13. Cross section of (i) rectangular, (ii) circular, and (iii) coaxial waveguides

5.3.1. Rectangular Waveguides

Consider rectangular waveguide of sides a and b on x and y direction shown in Figure 5.13(i). The cutoff wave numbers $(\widetilde{k}_c)$ for Transverse Electric (TE) and Transverse Magnetic (TM) modes are obtained [48] as:

$$\left(\widetilde{k}_c\right)_{mn} = \sqrt{\left(\frac{m\pi}{a}\right)^2 + \left(\frac{n\pi}{b}\right)^2} \qquad \begin{cases} m = n \neq 0 \text{ (TE)} \begin{cases} m = 0, 1, 2, \dots \\ n = 0, 1, 2, \cdots \end{cases} \\ \text{(TM)} \begin{cases} m = 1, 2, 3, \dots \\ n = 1, 2, 3, \cdots \end{cases} \end{cases} \tag{5.3}$$

Tables 5.2 and 5.3 show some corrections about the ratio of analytical cutoff frequencies of TE and TM modes in bold for the given tables in [48].

FEM is used to obtain numerical solution of cutoff wave numbers for various TE, TM modes. Figures 5.14-5.25 show the relative errors of $\widetilde{k}_c a$ for TE and TM modes respectively using FEM with triangulation and web-spline method.

The web-spline method provides more accurate results with using the same num-

ber of nodes. Therefore, web-splines for Dirichlet conditions and extended splines for Neumann conditions are used to find the wave number of TM and TE modes respectively. As a result of Dirichlet and Neumann boundary condition, the relative errors for TM modes (Dirichlet boundary condition) are more accurate than the TE modes (Neumann boundary condition) according to the error analysis.

Table 5.2. The ratio cutoff frequency (R_{mn}) of TE_{mn} modes to that of TE_{10} mode

a/b	10	5	2.25	2	1
m,n	$1,0$	$1,0$	$1,0$	$1,0$	$1,0;\ 0,1$
R_{mn}	1	1	1	1	1
m,n	$2,0$	$2,0$	$2,0$	$2,0;\ 0,1$	$1,1$
R_{mn}	2	2	2	2	1.414
m,n	$3,0$	$3,0$	$0,1$	$1,1$	$2,0;\ \mathbf{0},\mathbf{2}$
R_{mn}	3	3	2.25	2.236	2
m,n	$4,0$	$4,0$	$1,1$	$2,1$	$2,1;\ 1,2$
R_{mn}	4	4	2.462	2.828	2.236
m,n	$5,0$	$5,0;\ 0,1$	$3,0$	$3,0$	$2,2$
R_{mn}	5	5	3	3	2.828
m,n	$6,0$	$1,1$	$2,1$	$3,1$	$3,0;\ 0,3$
R_{mn}	6	5.099	3.010	3.606	3
m,n	$7,0$	$2,1$	$3,1$	$4,0;\ 0,2$	$3,1;\ 1,3$
R_{mn}	7	5.385	3.75	4	3.162
m,n	$8,0$	$3,1$	$4,0$	$1,2$	$3,2;\ 2,3$
R_{mn}	8	5.831	4	4.123	3.606
m,n	$9,0$	$6,0$	$0,2$	$4,1;\ 2,2$	$4,0;\ 0,4$
R_{mn}	9	6	4.5	4.472	4
m,n	$10,0;\ 0,1$	$4,1$	$4,1$	$5,0;\ 3,2$	$4,1;\ 1,4$
R_{mn}	10	6.403	4.589	5	4.123

Table 5.3. The ratio cutoff frequency (T_{mn}) of TM_{mn} modes to that of TE_{10} mode

a/b	10	5	2.25	2	1
m,n	$1,1$	$1,1$	$1,1$	$1,1$	$1,1$
T_{mn}	10.050	5.099	2.462	**2.236**	1.414
m,n	$2,1$	$2,1$	$2,1$	$2,1$	$2,1;\ 1,2$
T_{mn}	**10.198**	**5.385**	3.010	2.828	2.236
m,n	$3,1$	$3,1$	$3,1$	$3,1$	$2,2$
T_{mn}	10.440	**5.831**	3.75	3.606	2.828
m,n	$4,1$	$4,1$	$4,1$	$1,2$	$3,1;\ 1,3$
T_{mn}	10.770	6.403	4.589	4.123	3.162
m,n	$5,1$	$5,1$	$1,2$	$4,1;\ 2,2$	$3,2;\ 2,3$
T_{mn}	11.180	7.071	**4.610**	4.472	3.606
m,n	$6,1$	$6,1$	$2,2$	$3,2$	$4,1;\ 1,4$
T_{mn}	11.662	7.810	**4.924**	5	4.123
m,n	$7,1$	$7,1$	$\mathbf{3,2}$	$5,1$	$3,3$
T_{mn}	12.207	8.602	**5.408**	5.385	4.243
m,n	$8,1$	$8,1$	$\mathbf{5,1}$	$4,2$	$4,2;\ 2,4$
T_{mn}	12.806	9.434	**5.483**	5.657	4.472
m,n	$9,1$	$1,2$	$4,2$	$1,3$	$4,3;\ 3,4$
T_{mn}	**13.454**	**10.050**	**6.021**	6.083	5
m,n	$10,1$	$2,2$	$6,1$	$2,3$	$5,1;\ 1,5$
T_{mn}	14.142	10.198	6.408	**6.325**	**5.099**

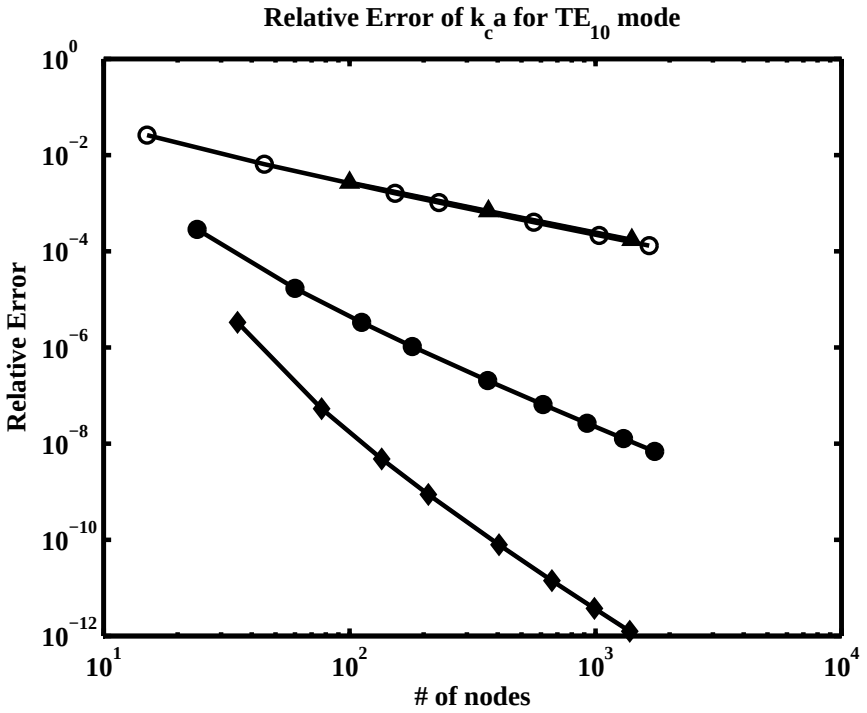

Figure 5.14. The relative errors of $\widetilde{k}_c a$ (TE_{10} mode) using basis functions which are linear Lagrange polynomial (▲), linear (○), quadratic (●), and cubic (⧫) web-splines versus the number of nodes for rectangular waveguide ($a/b = 2$)

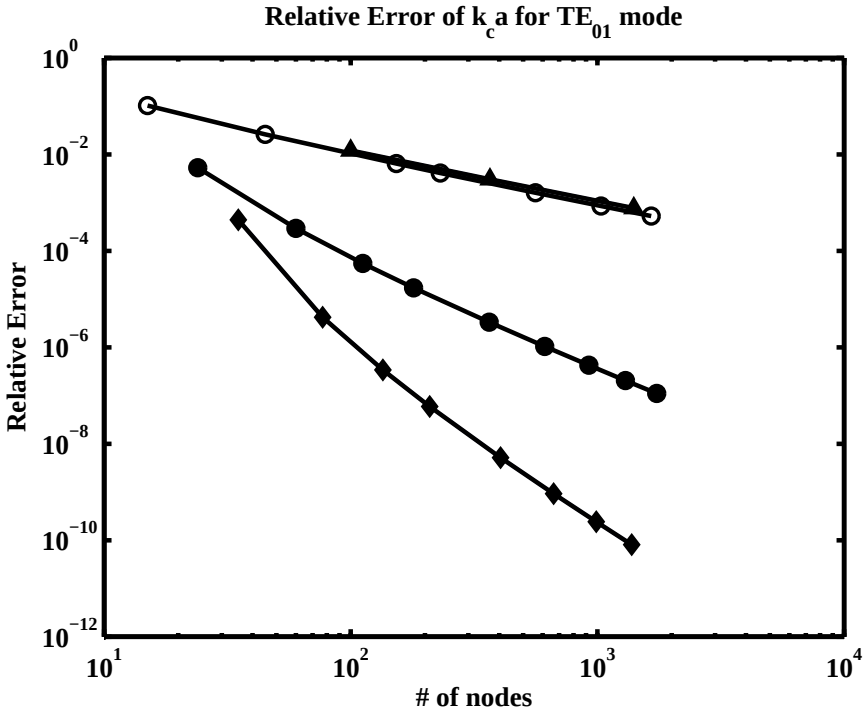

Figure 5.15. The relative errors of $\widetilde{k}_c a$ (TE_{01} mode) using basis functions which are linear Lagrange polynomial (▲), linear (○), quadratic (●), and cubic (⧫) web-splines versus the number of nodes for rectangular waveguide ($a/b = 2$)

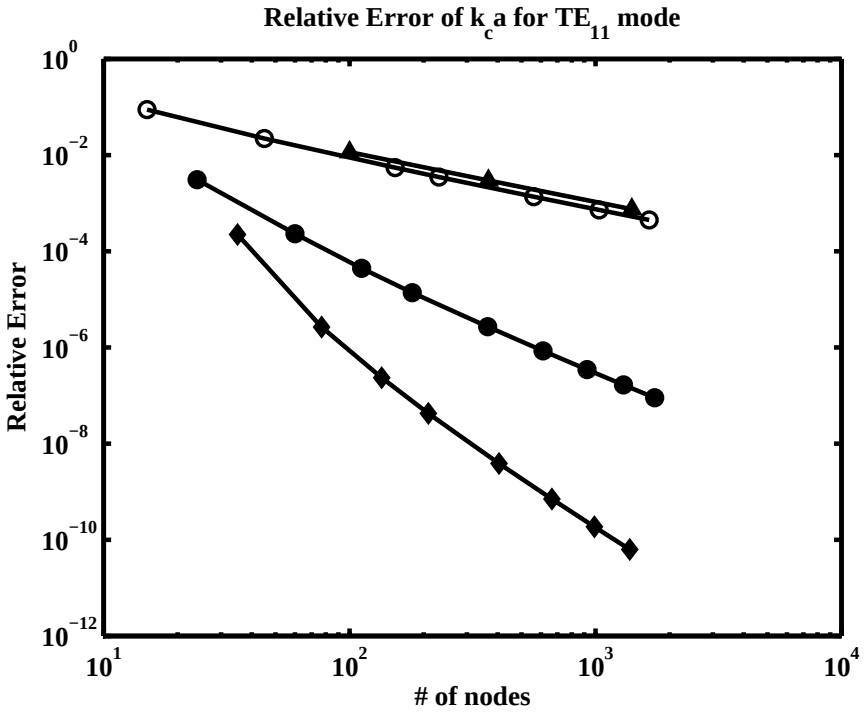

Figure 5.16. The relative errors of $\widetilde{k}_c a$ (TE_{11} mode) using basis functions which are linear Lagrange polynomial (▲), linear (○), quadratic (●), and cubic (⧫) web-splines versus the number of nodes for rectangular waveguide ($a/b = 2$)

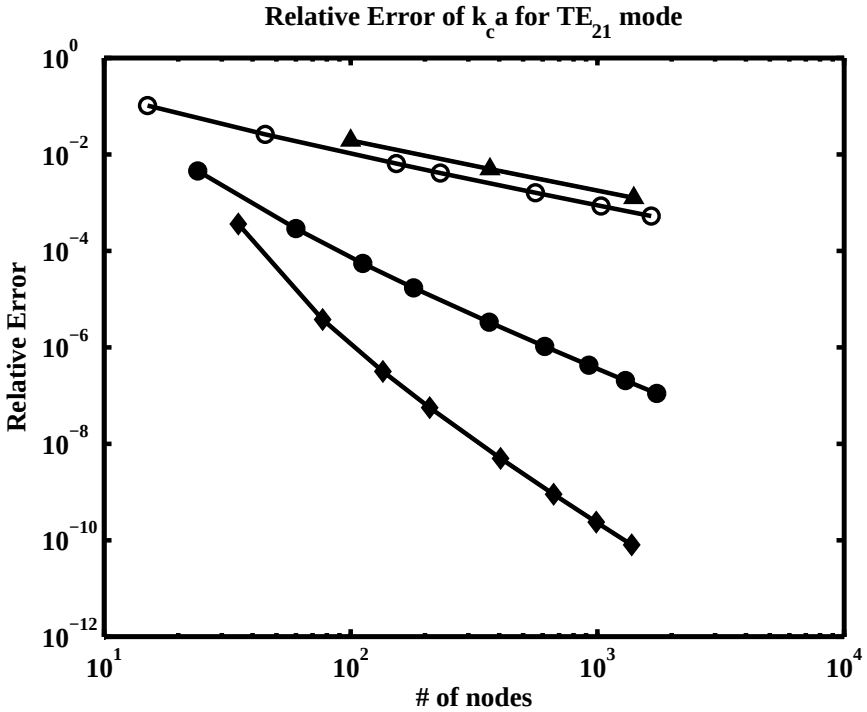

Figure 5.17. The relative errors of $\widetilde{k}_c a$ (TE_{21} mode) using basis functions which are linear Lagrange polynomial (▲), linear (○), quadratic (●), and cubic (⧫) web-splines versus the number of nodes for rectangular waveguide ($a/b = 2$)

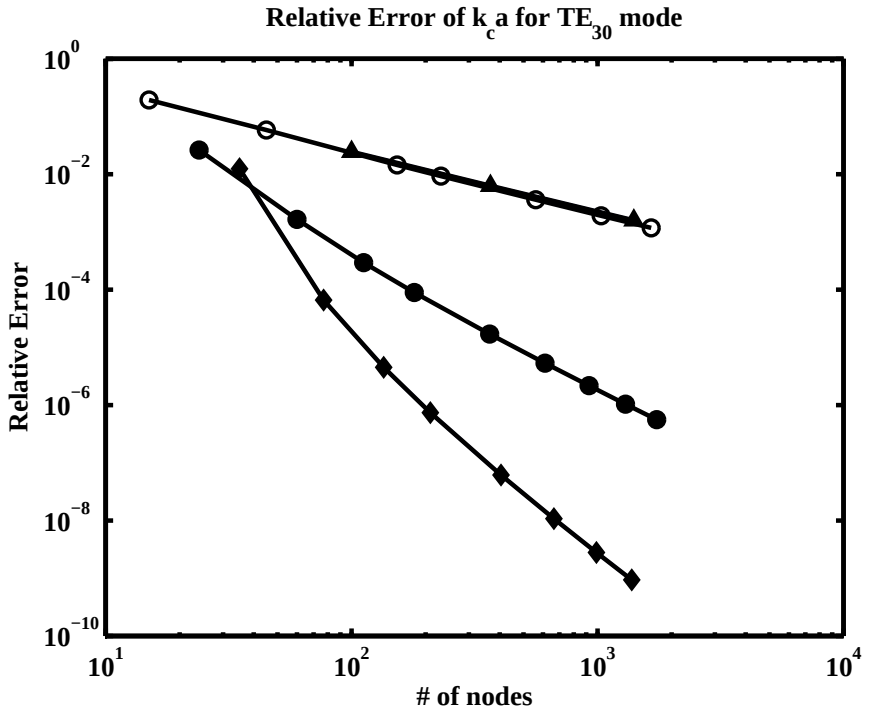

Figure 5.18. The relative errors of $\widetilde{k}_c a$ (TE_{30} mode) using basis functions which are linear Lagrange polynomial (▲), linear (○), quadratic (●), and cubic (⧫) web-splines versus the number of nodes for rectangular waveguide ($a/b = 2$)

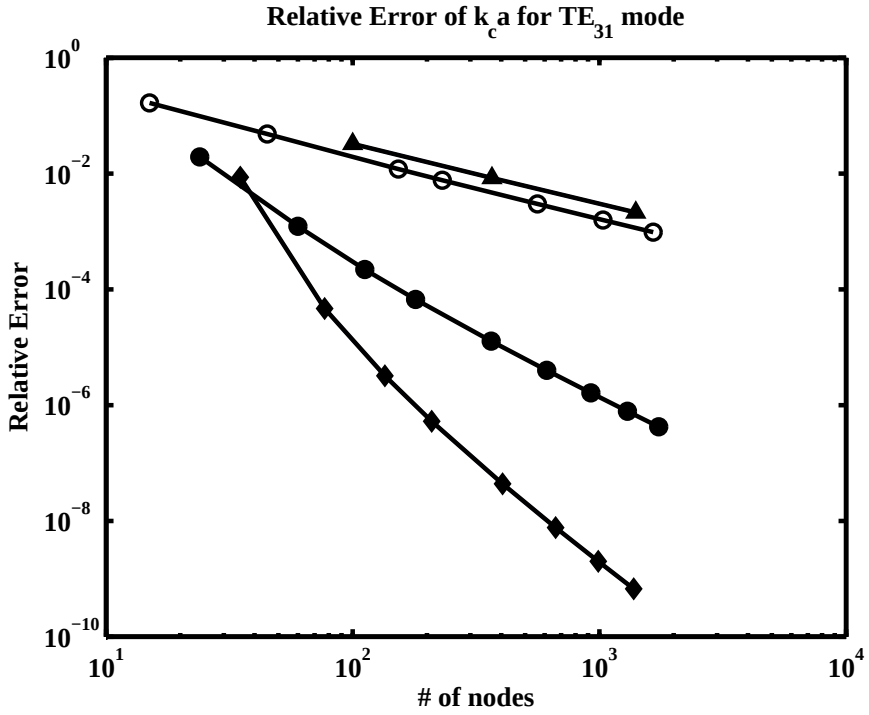

Figure 5.19. The relative errors of $\widetilde{k}_c a$ (TE_{31} mode) using basis functions which are linear Lagrange polynomial(▲), linear(○), quadratic(●), and cubic(⧫) web-splines versus the number of nodes for rectangular waveguide ($a/b = 2$)

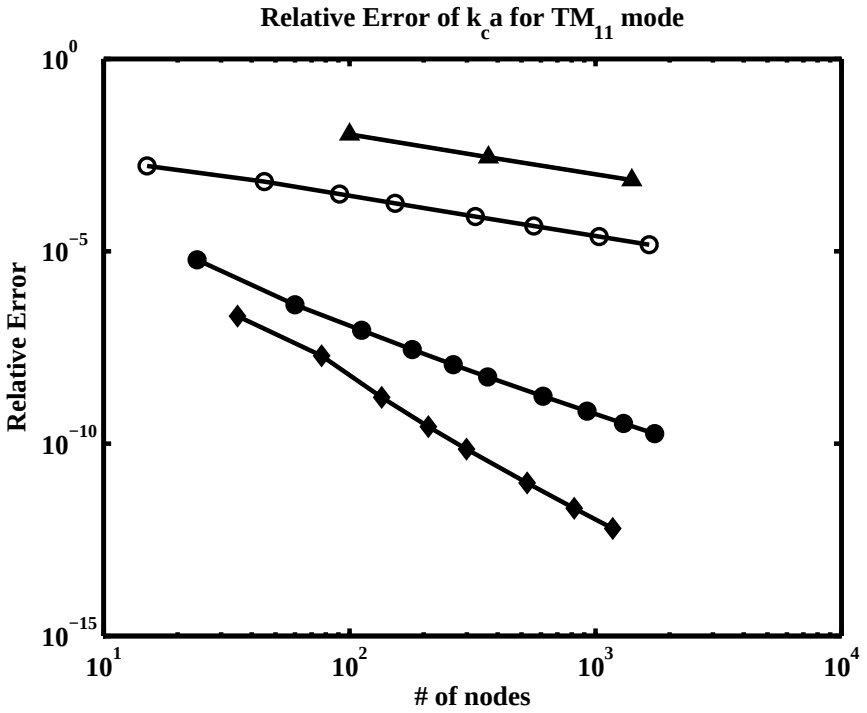

Figure 5.20. The relative errors of $\widetilde{k}_c a$ (TM_{11} mode) using basis functions which are linear Lagrange polynomial (▲), linear (○), quadratic (●), and cubic (⧫) web-splines versus the number of nodes for rectangular waveguide ($a/b = 2$)

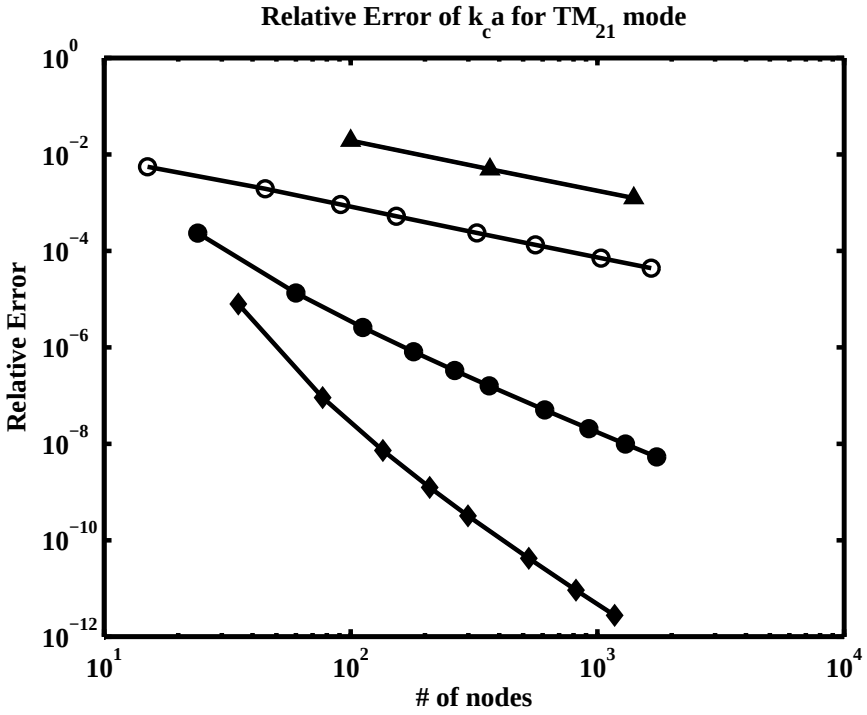

Figure 5.21. The relative errors of $\widetilde{k}_c a$ (TM_{21} mode) using basis functions which are linear Lagrange polynomial (▲), linear (○), quadratic (●), and cubic (⧫) web-splines versus the number of nodes for rectangular waveguide ($a/b = 2$)

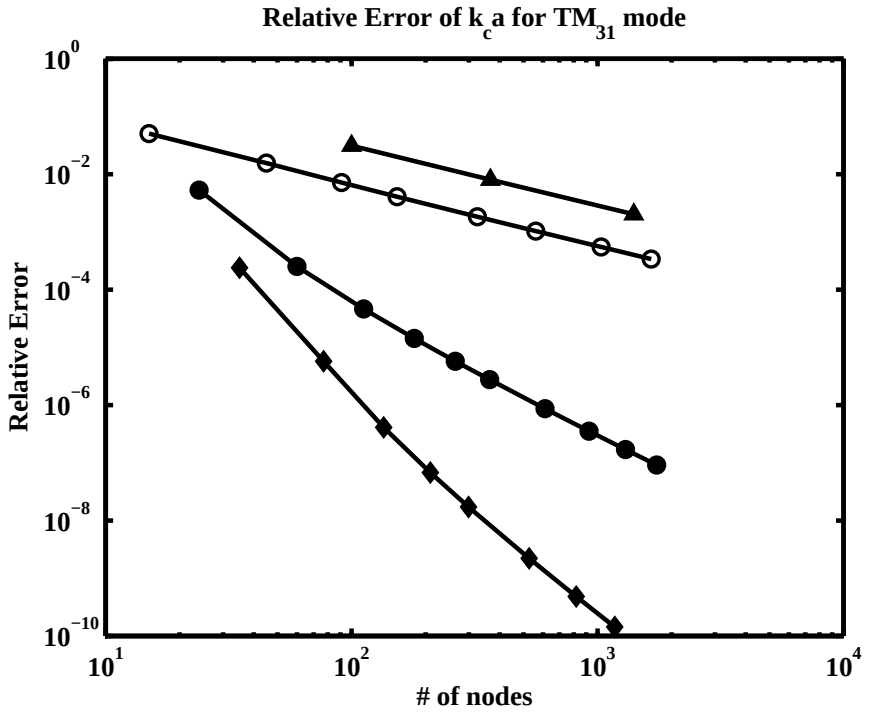

Figure 5.22. The relative errors of $\widetilde{k}_c a$ (TM_{31} mode) using basis functions which are linear Lagrange polynomial (▲), linear (○), quadratic (●), and cubic (⧫) web-splines versus the number of nodes for rectangular waveguide ($a/b = 2$)

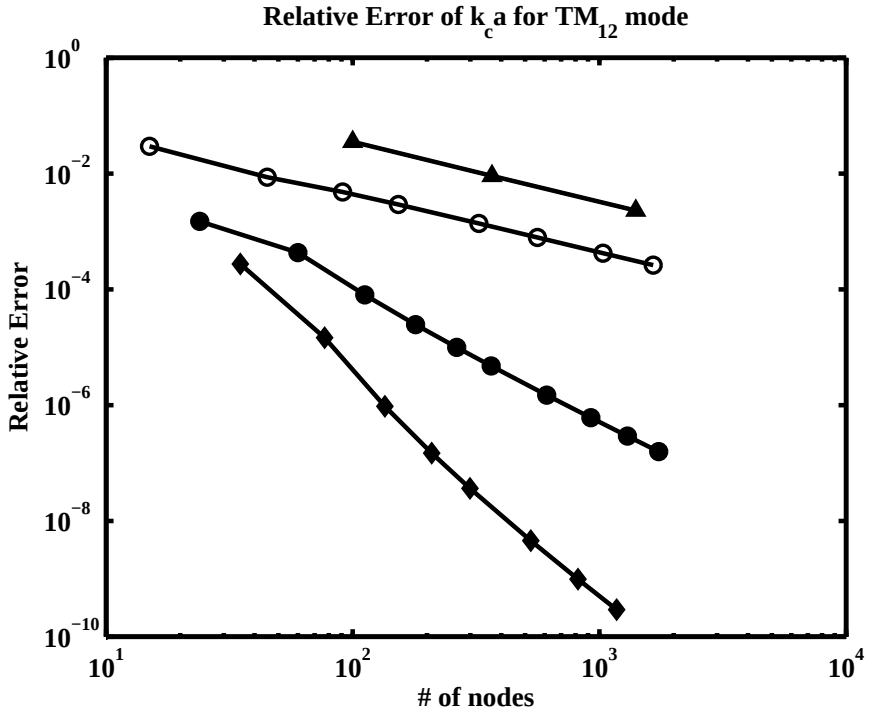

Figure 5.23. The relative errors of $\widetilde{k}_c a$ (TM_{12} mode) using basis functions which are linear Lagrange polynomial (▲), linear (○), quadratic (●), and cubic (⧫) web-splines versus the number of nodes for rectangular waveguide ($a/b = 2$)

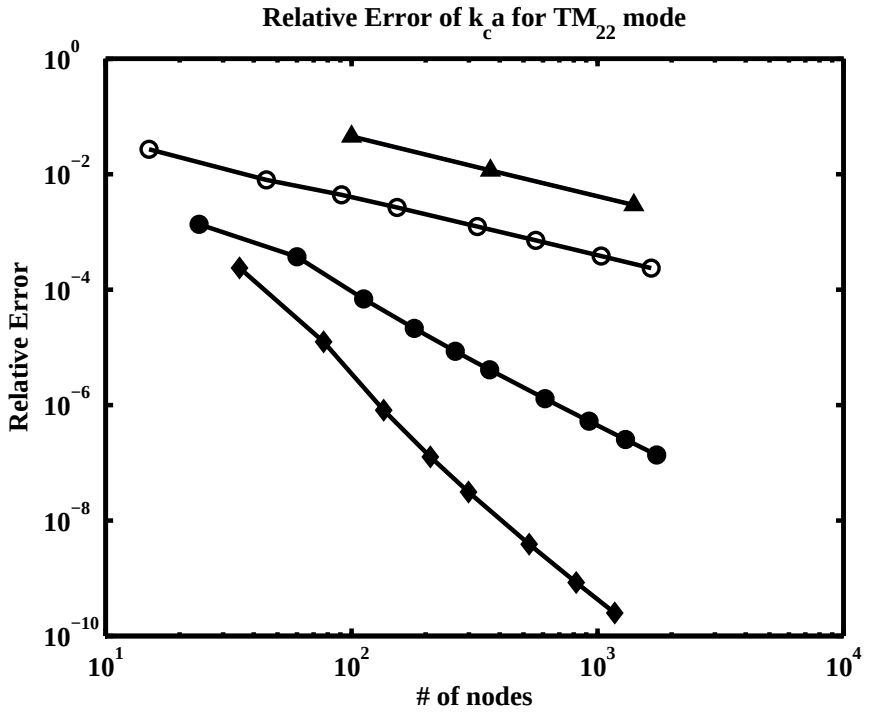

Figure 5.24. The relative errors of $\widetilde{k}_c a$ (TM_{22} mode) using basis functions which are linear Lagrange polynomial (▲), linear (○), quadratic (●), and cubic (⧫) web-splines versus the number of nodes for rectangular waveguide ($a/b = 2$)

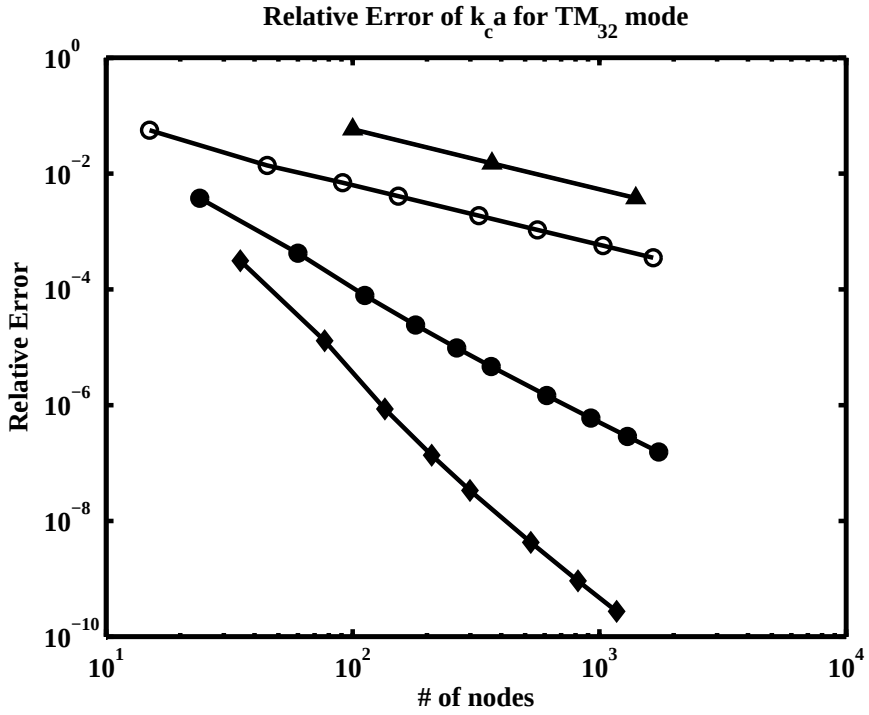

Figure 5.25. The relative errors of $\widetilde{k}_c a$ (TM_{32} mode) using basis functions which are linear Lagrange polynomial (▲), linear (○), quadratic (●), and cubic (⧫) web-splines versus the number of nodes for rectangular waveguide ($a/b = 2$)

5.3.2. Circular Waveguides

The cutoff wave numbers for circular waveguide shown in Figure 5.13(ii) are obtained by using FEM analysis and compared with the analytical results, which are tabulated in Table 5.4.

20 per cent less nodes are used to obtain relative errors $1.4e-3$, $4.8e-7$, and $1.3e-9$ for the linear, quadratic, and cubic web-spline analysis of TE_{11} mode. Figures 5.26-5.37 show the relative errors of $\widetilde{k}_c r$ for various TE and TM modes using FEM with triangulation and web-spline method. As seen in figures, the web-spline method provides more accurate results with using the same number of nodes than standard FEM. Same as the previous study, the relative errors for the TM modes are more accurate than the TE modes too, since TM and TE modes use Dirichlet and Neumann boundary conditions respectively.

Table 5.4. $\widetilde{k}_c r$ for a circular waveguide

mode	$\widetilde{k}_c r$
TE_{11}	1.84118378134066
TM_{01}	2.40482555769577
TE_{21}	3.05423692822714
TM_{11}; TE_{01}	3.83170597020751
TE_{31}	4.20118894121053
TM_{21}	5.13562230184068
TE_{41}	5.31755312608400
TE_{12}	5.33144277352503
TM_{02}	5.52007811028631
TM_{31}	6.38016189592398
TE_{51}	6.41561637570024
TE_{22}	6.70613319415846
TE_{02}	7.01558666981562
TE_{61}	7.50126614468415

Table 5.5. The efficiency of web-spline method for circular waveguides (per cent)

n	h	Efficiency of nodes (per cent)	Efficiency of computation time (per cent)
1	1/4	41.56	50
	1/8	24.90	30
	1/16	13.90	20
2	1/4	37.50	70
	1/8	23.29	50
	1/16	13.36	30
3	1/4	34.19	80
	1/8	21.89	40
	1/16	12.87	40

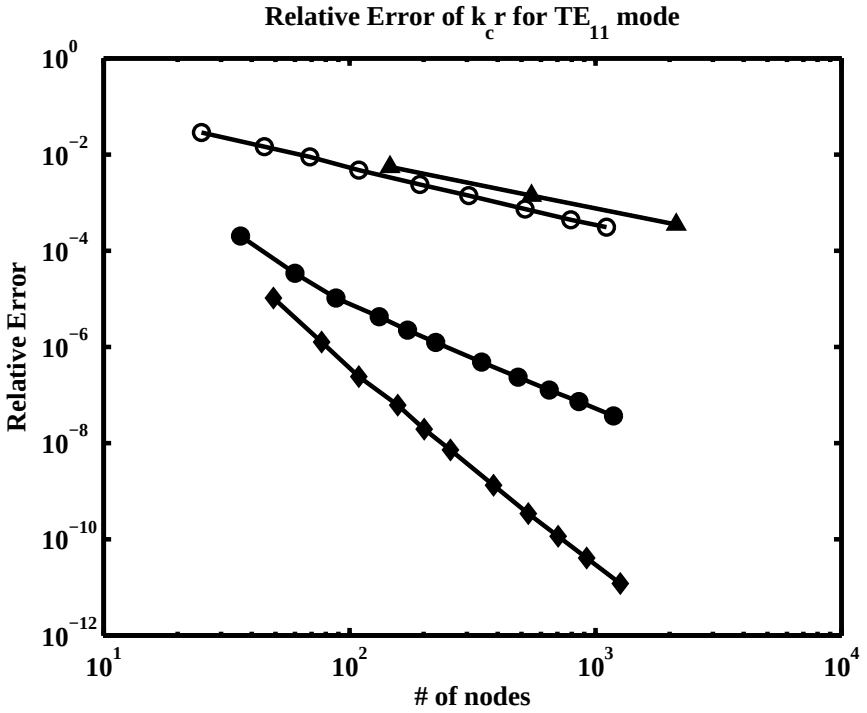

Figure 5.26. The relative errors of $\widetilde{k}_c r$ (TE_{11} mode) using basis functions which are linear Lagrange polynomial (▲), linear (○), quadratic (●), and cubic (⧫) web-splines versus the number of nodes for circular waveguide

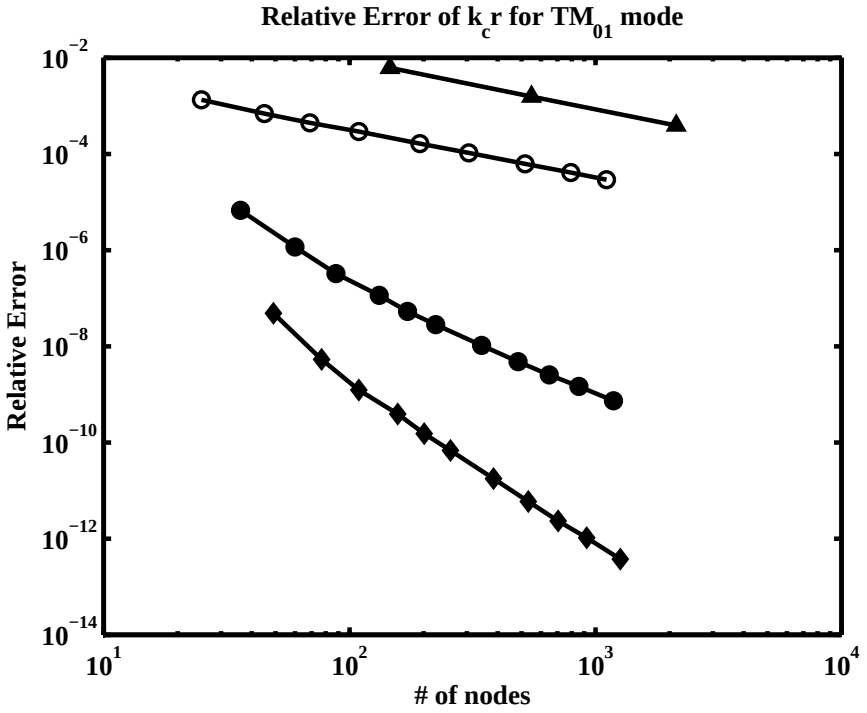

Figure 5.27. The relative errors of $\widetilde{k}_c r$ (TM_{01} mode) using basis functions which are linear Lagrange polynomial (▲), linear (○), quadratic (●), and cubic (⧫) web-splines versus the number of nodes for circular waveguide

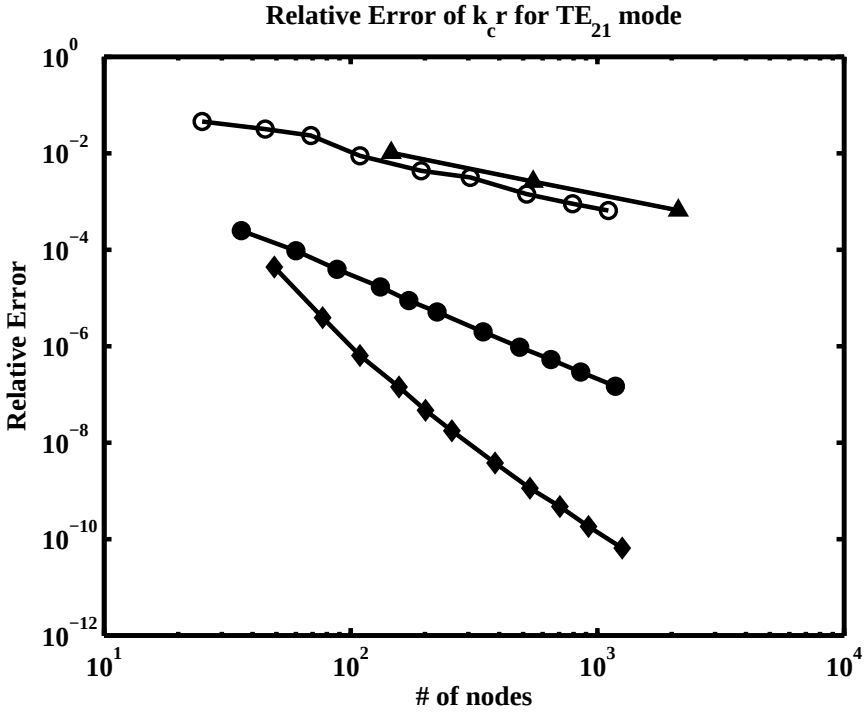

Figure 5.28. The relative errors of $\widetilde{k}_c r$ (TE_{21} mode) using basis functions which are linear Lagrange polynomial (▲), linear (○), quadratic (●), and cubic (⧫) web-splines versus the number of nodes for circular waveguide

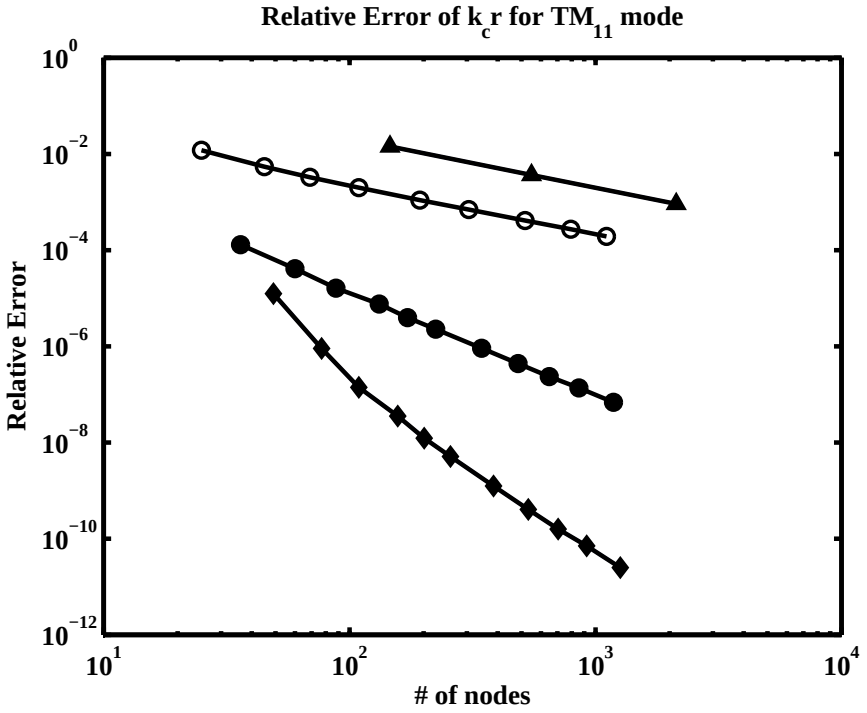

Figure 5.29. The relative errors of $\widetilde{k}_c r$ (TM_{11} mode) using basis functions which are linear Lagrange polynomial (▲), linear (○), quadratic (●), and cubic (⧫) web-splines versus the number of nodes for circular waveguide

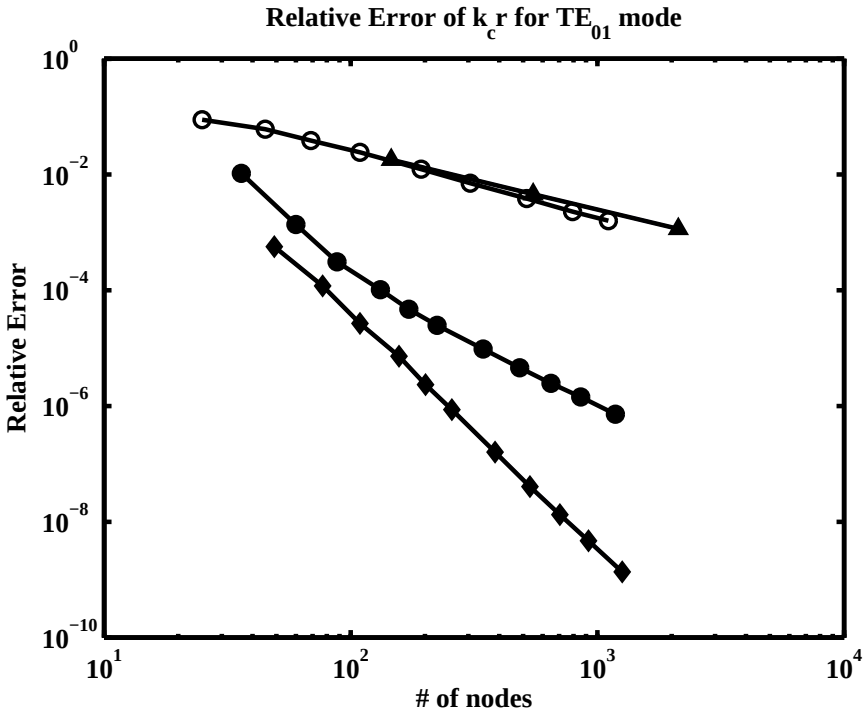

Figure 5.30. The relative errors of $\widetilde{k}_c r$ (TE_{01} mode) using basis functions which are linear Lagrange polynomial (▲), linear (○), quadratic (●), and cubic (⧫) web-splines versus the number of nodes for circular waveguide

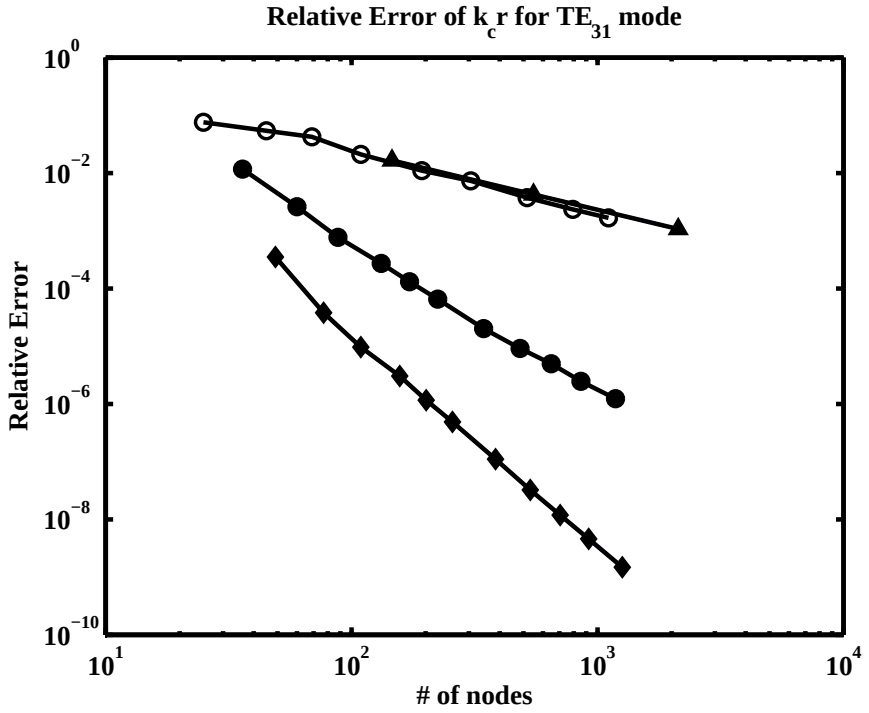

Figure 5.31. The relative errors of $\widetilde{k}_c r$ (TE_{31} mode) using basis functions which are linear Lagrange polynomial (▲), linear (○), quadratic (●), and cubic (⧫) web-splines versus the number of nodes for circular waveguide

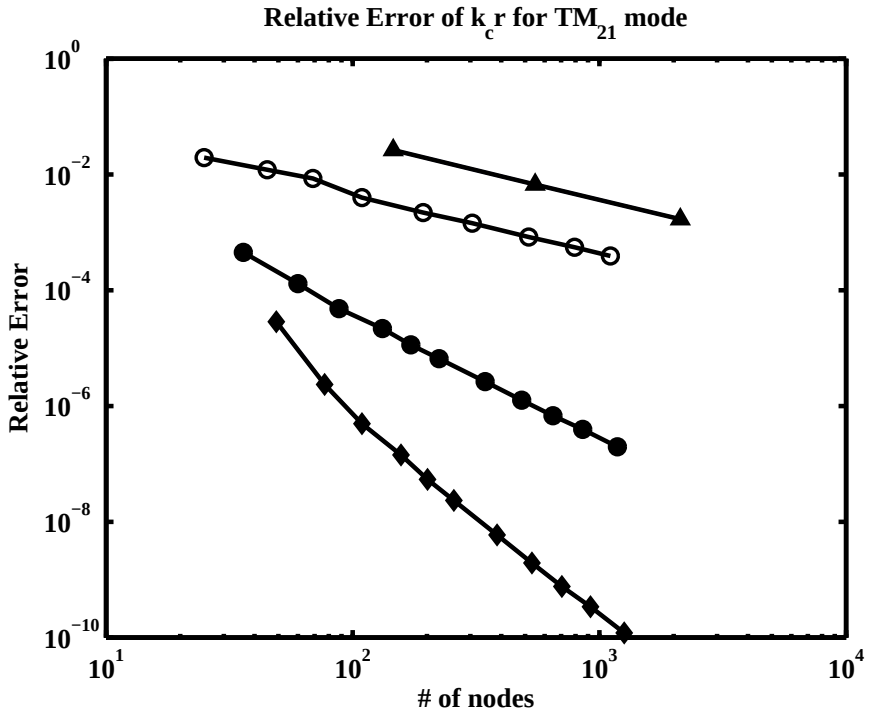

Figure 5.32. The relative errors of $\widetilde{k}_c r$ (TM_{21} mode) using basis functions which are linear Lagrange polynomial (▲), linear (○), quadratic (●), and cubic (⧫) web-splines versus the number of nodes for circular waveguide

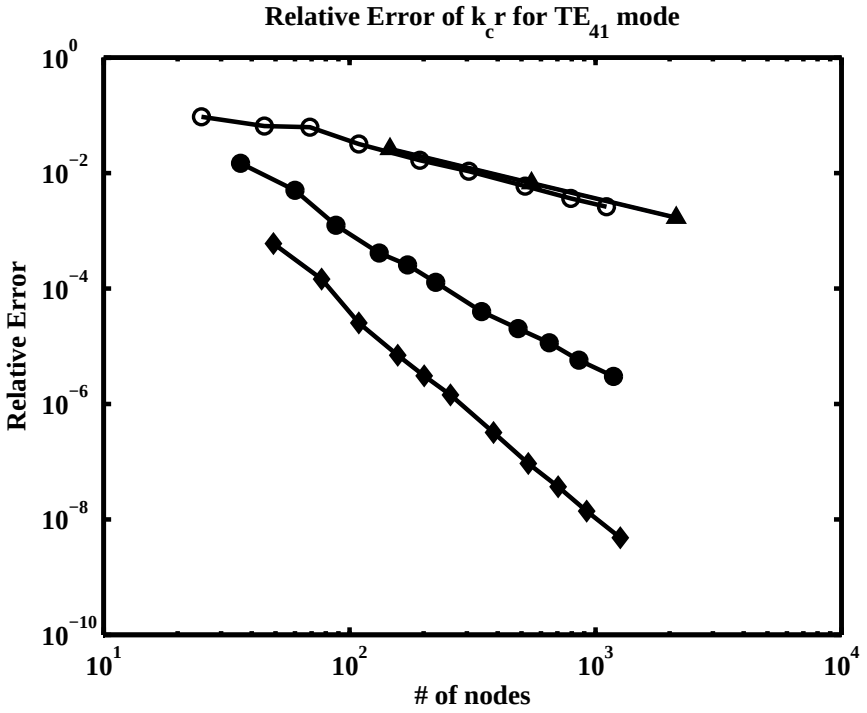

Figure 5.33. The relative errors of $\widetilde{k}_c r$ (TE_{41} mode) using basis functions which are linear Lagrange polynomial (▲), linear (○), quadratic (●), and cubic (⧫) web-splines versus the number of nodes for circular waveguide

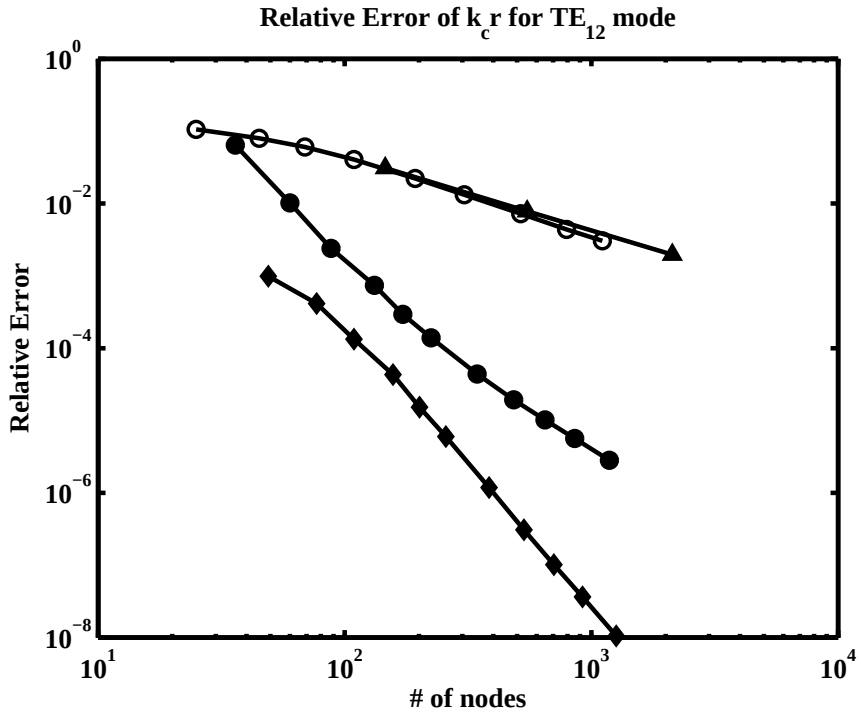

Figure 5.34. The relative errors of $\widetilde{k}_c r$ (TE_{12} mode) using basis functions which are linear Lagrange polynomial (▲), linear (○), quadratic (●), and cubic (⧫) web-splines versus the number of nodes for circular waveguide

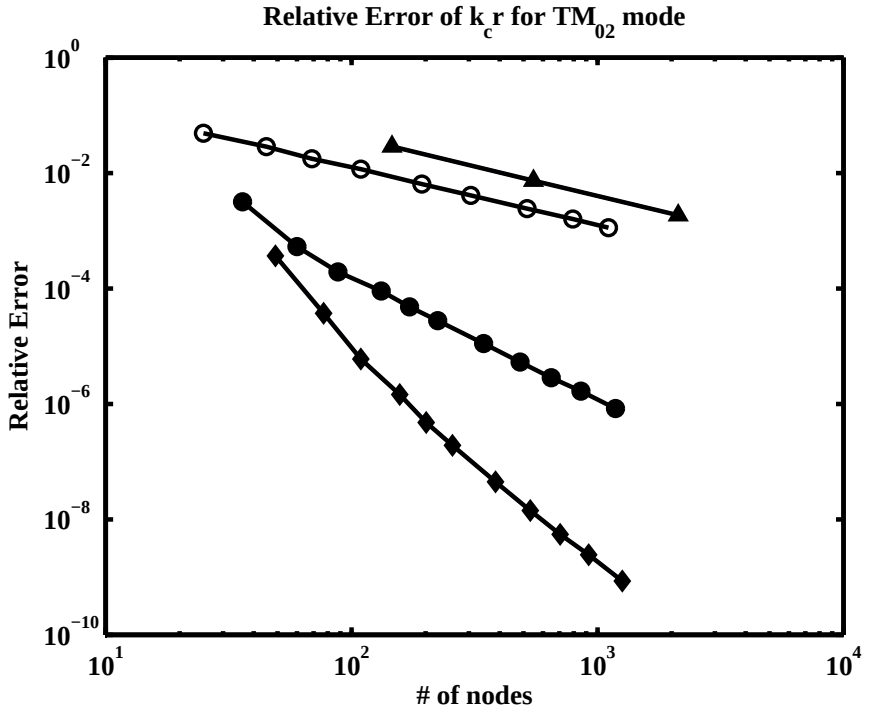

Figure 5.35. The relative errors of $\widetilde{k}_c r$ (TM_{02} mode) using basis functions which are linear Lagrange polynomial (▲), linear (○), quadratic (●), and cubic (⧫) web-splines versus the number of nodes for circular waveguide

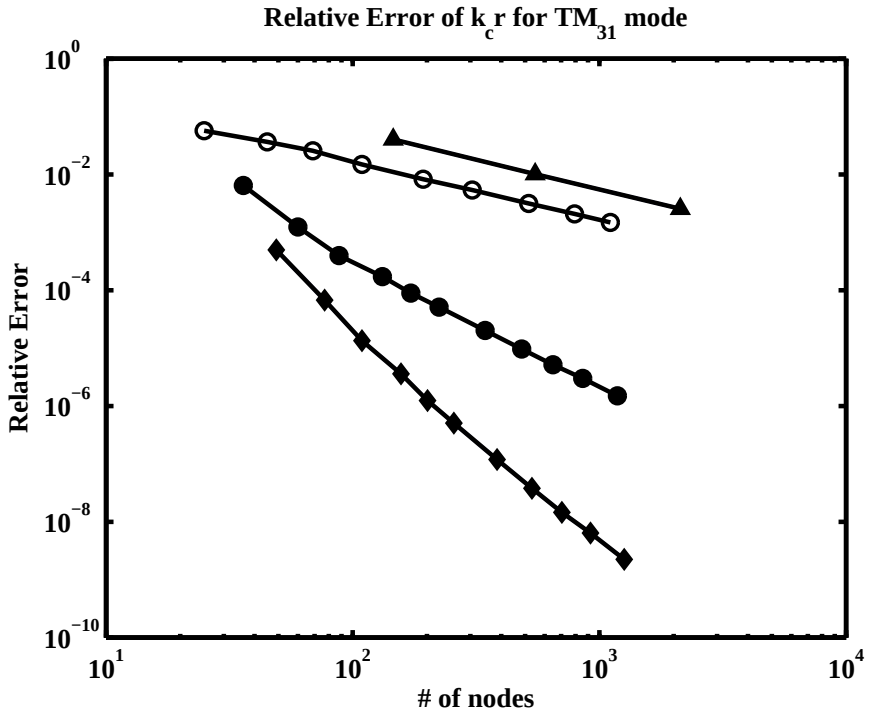

Figure 5.36. The relative errors of $\widetilde{k}_c r$ (TM_{31} mode) using basis functions which are linear Lagrange polynomial (▲), linear (○), quadratic (●), and cubic (⧫) web-splines versus the number of nodes for circular waveguide

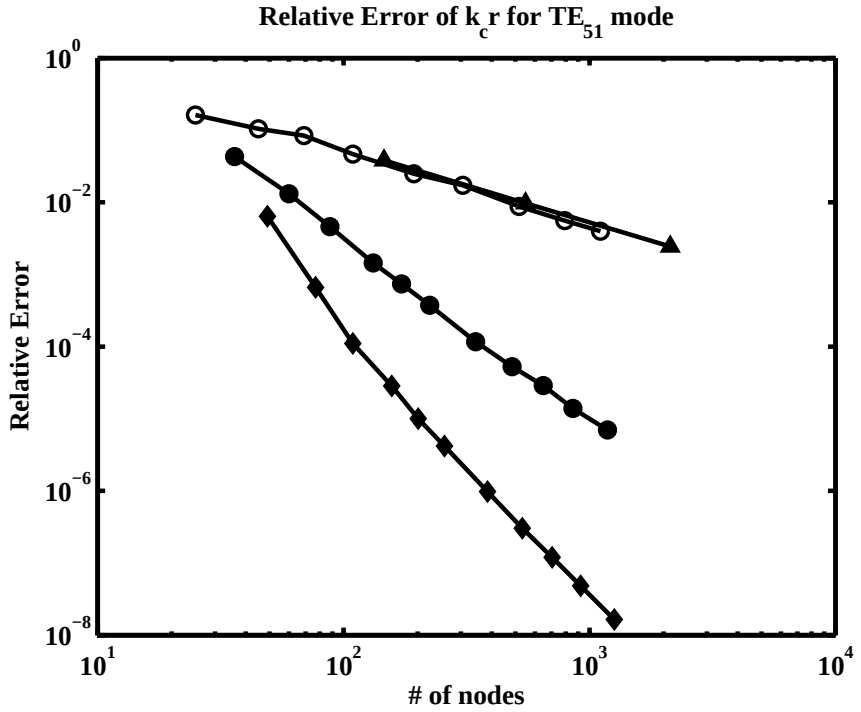

Figure 5.37. The relative errors of $\widetilde{k}_c r$ (TE_{51} mode) using basis functions which are linear Lagrange polynomial (▲), linear (○), quadratic (●), and cubic (⧫) web-splines versus the number of nodes for circular waveguide

5.3.3. Coaxial Waveguides

Figure 5.13(iii) shows the cross section of coaxial waveguide. The analytical values of cutoff wave numbers of TE and TM modes, which are tabulated in Table 5.6, are obtained with the n^{th} roots of the Bessel-Neumann and its derivative combination respectively given in [49] and compared with FEM results.

20-30 per cent less nodes are used to obtain relative errors $1.04e-4$, $6.3e-7$, and $1.4e-9$ for the linear, quadratic, and cubic web-spline analysis of TM_{01} mode. Table 5.7 shows the efficiency of web-spline method for coaxial waveguides.

Figures 5.38-5.43 show the relative errors of $\widetilde{k}_c r_1$ for some TE and TM modes by using FEM with triangulation and web-spline method for $r_2/r_1 = 2$. More accurate results are obtained by using fewer nodes for linear, quadratic and cubic web-splines.

Table 5.6. $\widetilde{k}_c r_1$ for a coaxial waveguide ($r_2/r_1 = 2$)

mode	$\widetilde{k}_c r_1$
TE_{11}	0.67733600513658
TE_{21}	1.34060214333442
TE_{31}	1.97887709391199
TM_{01}	3.12303091959569
TM_{11}	3.19657838081063
TM_{21}	3.40692142656753

Table 5.7. The efficiency of web-spline method for coaxial waveguides (per cent)

n	h	Efficiency of nodes (per cent)	Efficiency of computation time (per cent)
1	1/4	52.63	90
	1/8	37.29	70
	1/16	23.47	60
2	1/4	41.67	90
	1/8	31.43	60
	1/16	21.01	40
3	1/4	35.04	80
	1/8	27.16	60
	1/16	19.01	40

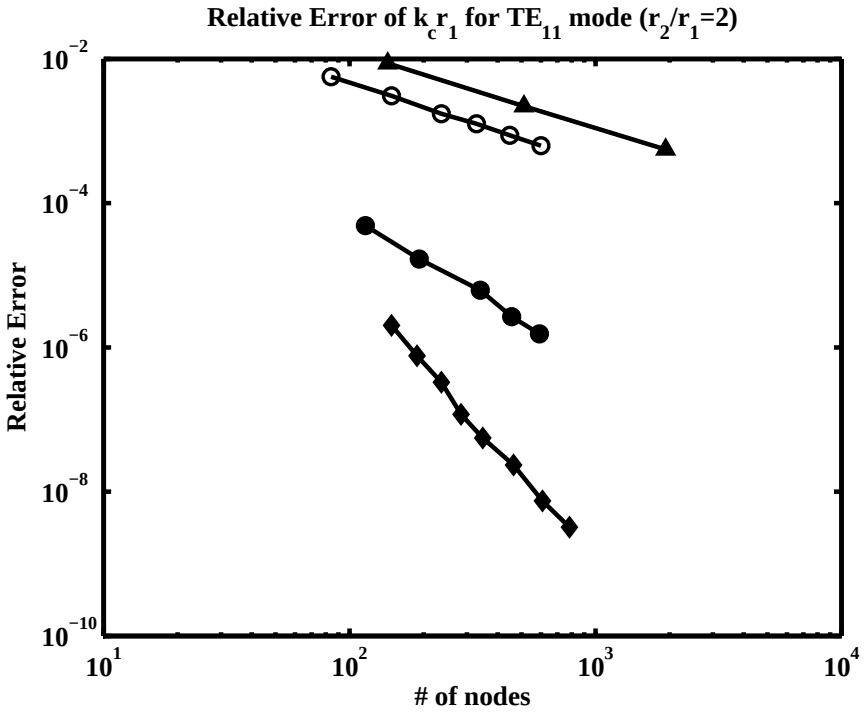

Figure 5.38. The relative errors of $\widetilde{k}_c r_1$ (TE_{11} mode) using basis functions which are linear Lagrange polynomial (▲), linear (○), quadratic (●), and cubic (⧫) web-splines versus the number of nodes for coaxial waveguide ($r_2/r_1 = 2$)

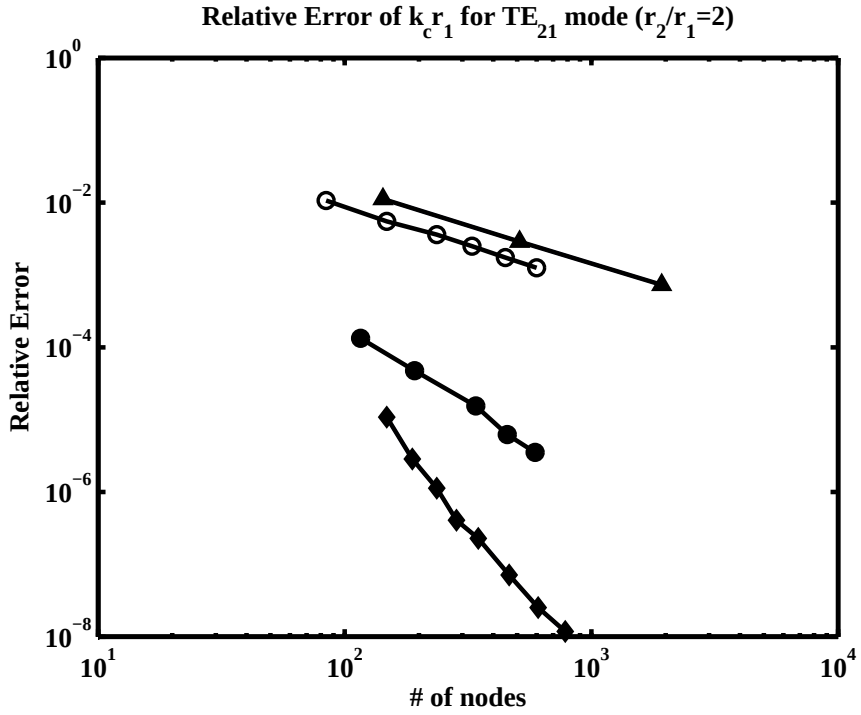

Figure 5.39. The relative errors of $\widetilde{k}_c r_1$ (TE_{21} mode) using basis functions which are linear Lagrange polynomial (▲), linear (○), quadratic (●), and cubic (⧫) web-splines versus the number of nodes for coaxial waveguide ($r_2/r_1 = 2$)

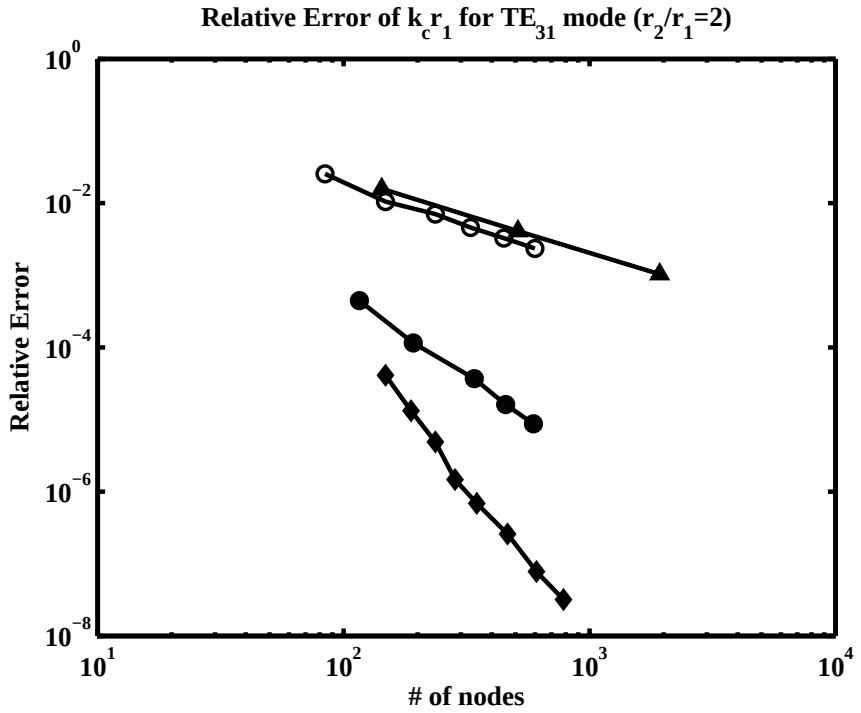

Figure 5.40. The relative errors of $\widetilde{k}_c r_1$ (TE_{31} mode) using basis functions which are linear Lagrange polynomial (▲), linear (○), quadratic (●), and cubic (⧫) web-splines versus the number of nodes for coaxial waveguide ($r_2/r_1 = 2$)

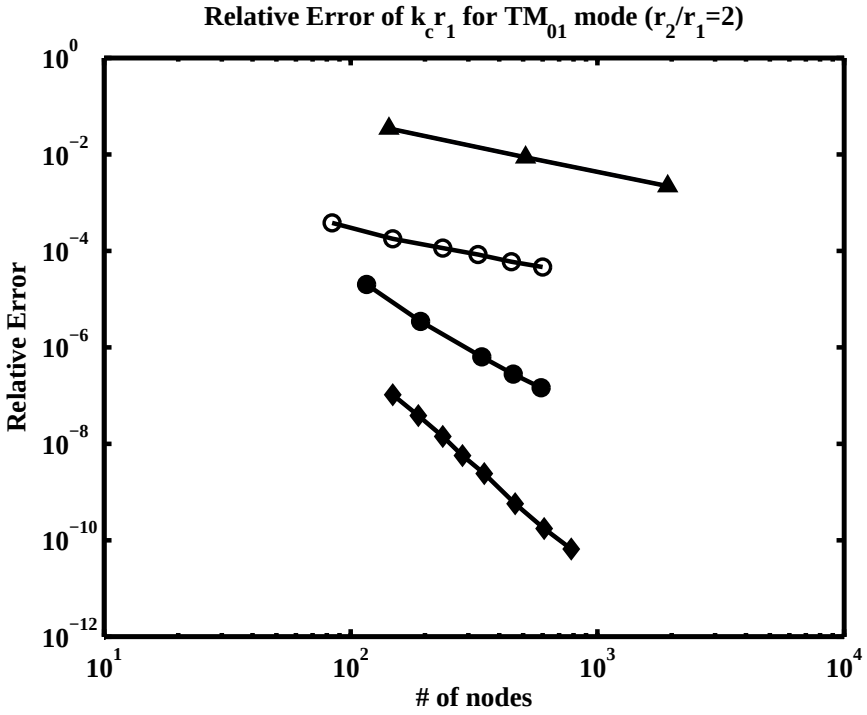

Figure 5.41. The relative errors of $\widetilde{k}_c r_1$ (TM_{01} mode) using basis functions which are linear Lagrange polynomial (▲), linear (○), quadratic (●), and cubic (⧫) web-splines versus the number of nodes for coaxial waveguide ($r_2/r_1 = 2$)

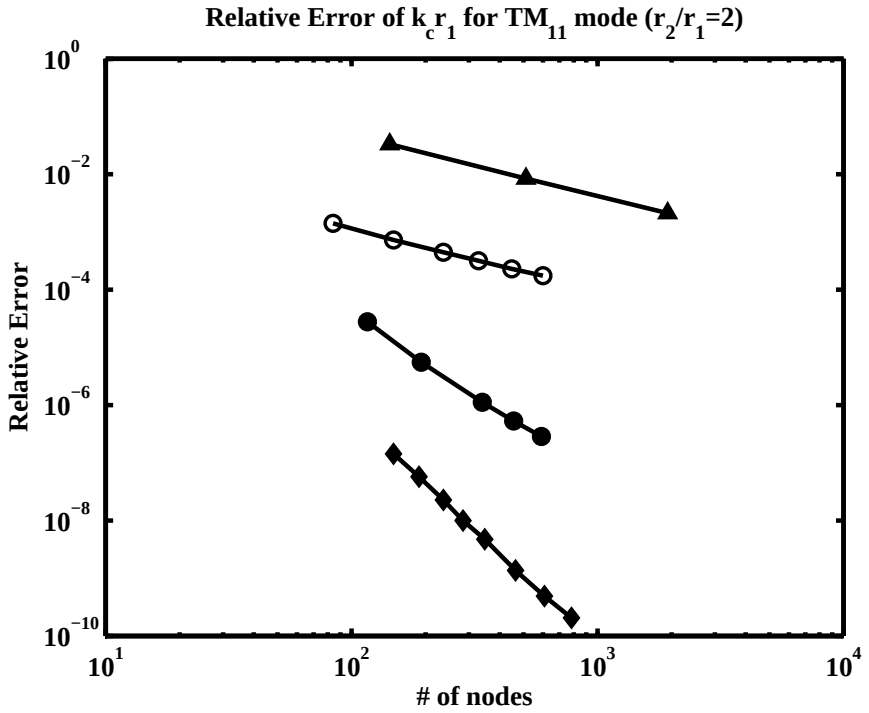

Figure 5.42. The relative errors of $\widetilde{k}_c r_1$ (TM_{11} mode) using basis functions which are linear Lagrange polynomial (▲), linear (○), quadratic (●), and cubic (⧫) web-splines versus the number of nodes for coaxial waveguide ($r_2/r_1 = 2$)

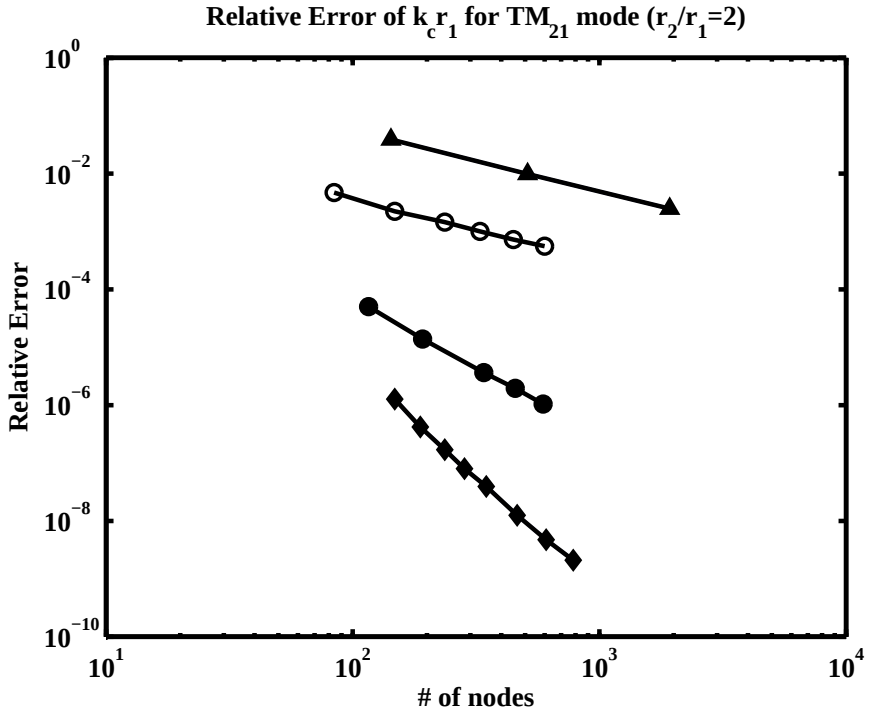

Figure 5.43. The relative errors of $\widetilde{k}_c r_1$ (TM_{21} mode) using basis functions which are linear Lagrange polynomial (▲), linear (○), quadratic (●), and cubic (⧫) web-splines versus the number of nodes for coaxial waveguide ($r_2/r_1 = 2$)

Figure 5.44 shows the analytical weight function for coaxial waveguides

$$w_A(x,y) = (r_2^2 - x^2 - y^2) \cdot (x^2 + y^2 - r_1^2) \tag{5.4}$$

and Figure 5.45 shows the Rvachev's weight function

$$w_R(x,y) = (r_2^2 - x^2 - y^2) + (x^2 + y^2 - r_1^2) - \sqrt{(r_2^2 - x^2 - y^2)^2 + (x^2 + y^2 - r_1^2)^2} \tag{5.5}$$

in order to find the cutoff wave numbers of TM modes.

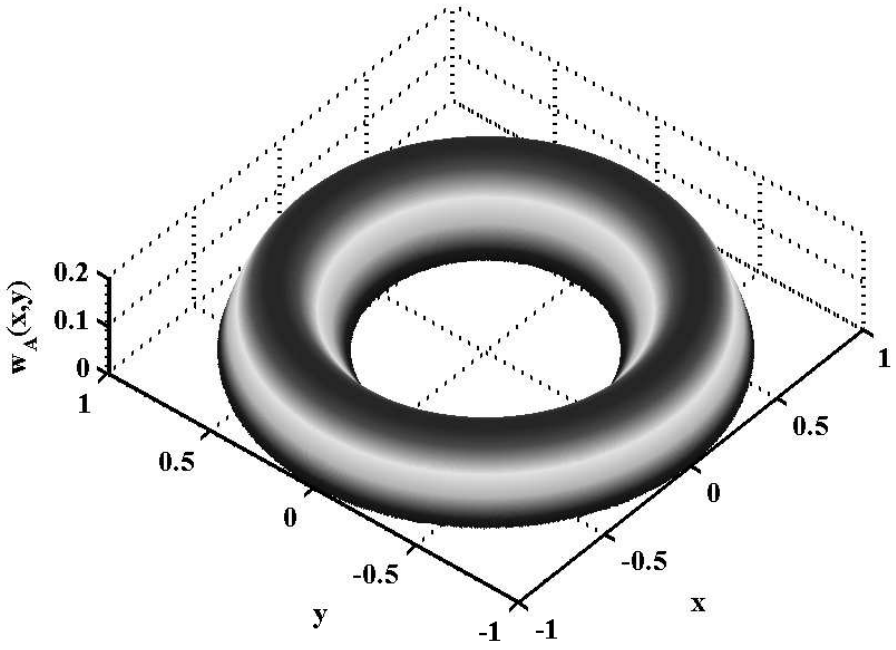

Figure 5.44. Analytical weight function for coaxial waveguides

The supported b-splines for the coaxial waveguide are shown in Figure 5.46.

Table 5.8 shows the analytical values of $\widetilde{k}_c r_1$ for various r_2/r_1 in order to compare with the numerical solution for the given coaxial waveguide in Figure 5.46.

Figures 5.47 and 5.48 show the relative errors of $\widetilde{k}_c r_1$ for TM_{01} and TE_{11} modes using FEM with quadratic and cubic web-splines, while changing r_2/r_1 from 2 to 4 for $h = 0.1$. The web-spline method is implemented easily and provides accurate results.

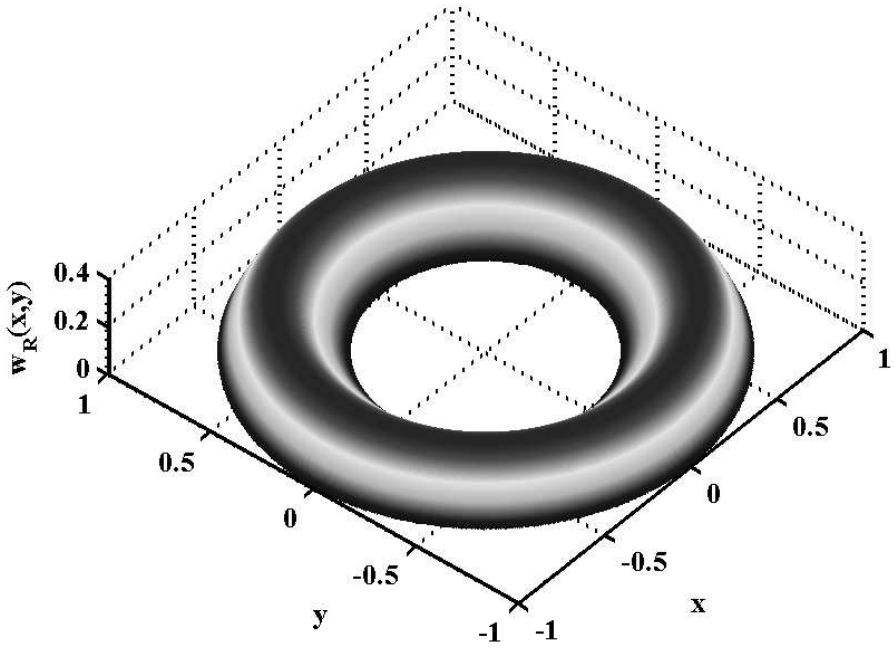

Figure 5.45. Rvachev's weight function for coaxial waveguides

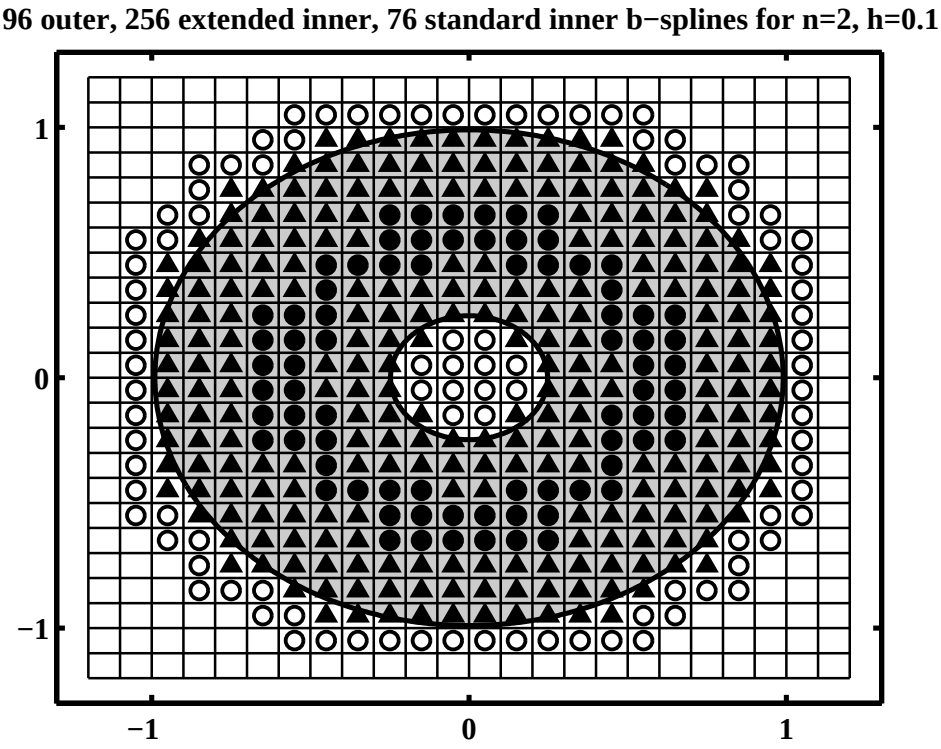

Figure 5.46. The standard (•), extended inner (▲) and outer (○) web-splines for coaxial waveguide

Table 5.8. $\widetilde{k}_c r_1$ for a coaxial waveguide ($r_2/r_1 \in [2,4]$)

r_2/r_1	TM_{01}	TE_{11}
2.0	3.12303091959569	0.67733600513658
2.2	2.59814845372033	0.63705643879578
2.4	2.22320266075340	0.60121330544258
2.6	1.94200987592583	0.56905474087215
2.8	1.72334328339505	0.54000687063417
3.0	1.54845877828945	0.51362117246967
3.2	1.40542346707625	0.48953964470270
3.4	1.28627912101119	0.46747120951993
3.6	1.18551434706994	0.44717537336804
3.8	1.09919127148333	0.42845067387739
4.0	1.02442138481921	0.41112634431194

The condition numbers for the weighted b-splines and weighted extended b-splines are shown in Figures 5.49 and 5.50. Web-splines use $20-25$ per cent less nodes and they are more stable than the weighted b-splines.

5.4. Waveguides For Arbitrary Domain

The last application studies the web-spline method for finding cutoff wave numbers of an arbitrary domain, shown in Figure 3.2.

The eigenvalue analysis is used to compare web-spline method with the standard FEM. Figure 5.51 shows triangulation for an arbitrary domain using 8863 nodes and 15928 triangles. For web-spline FEM analysis, Figure 5.52 shows the relevant cubic b-splines of the same domain using 62 outer, 172 extended inner, and 26 standard inner web-splines. The distance weight function is used for TM mode analysis as shown in Figure 3.6.

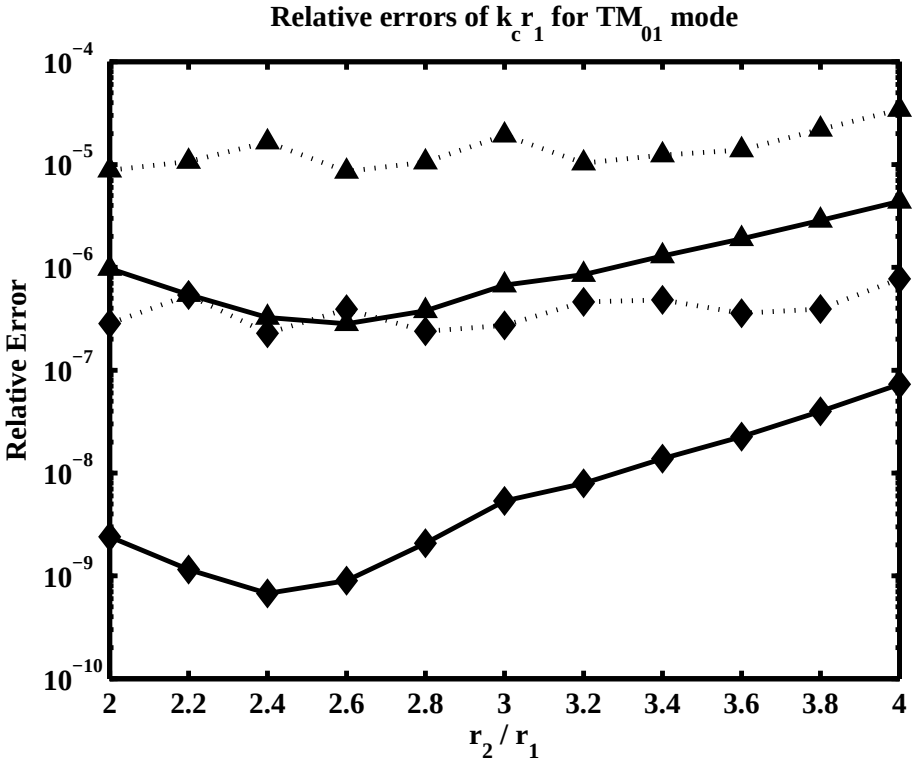

Figure 5.47. The relative errors of $\widetilde{k}_c r_1$ for coaxial waveguide using quadratic (▲) and cubic (♦) web-splines with w_A (solid) and w_R (dashed) weight functions versus r_2/r_1.

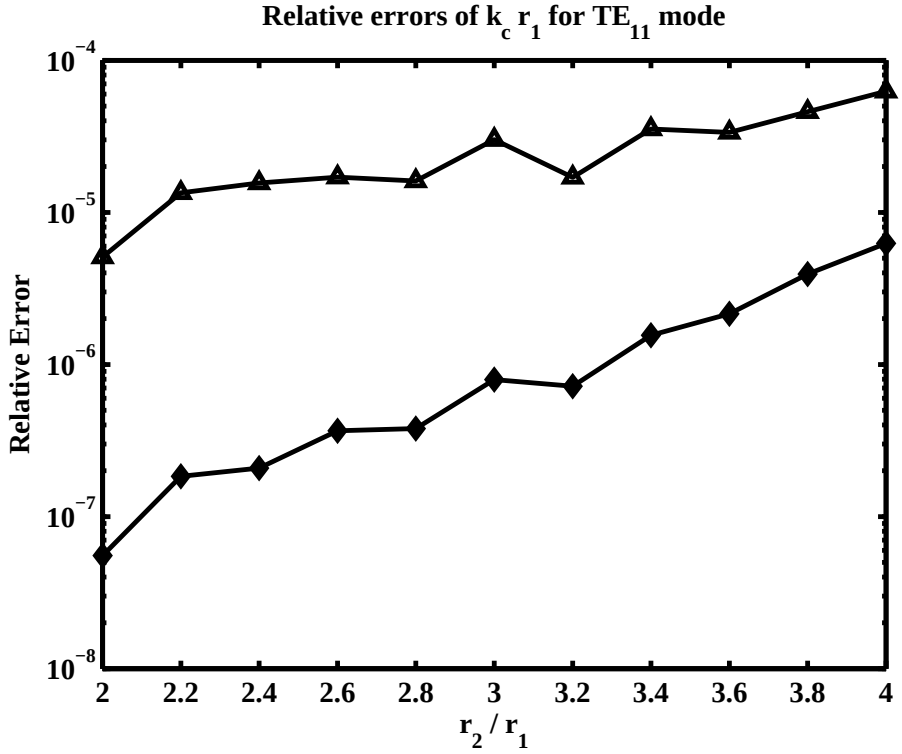

Figure 5.48. The relative errors of $\widetilde{k}_c r_1$ for coaxial waveguide using quadratic (▲) and cubic (♦) web-splines versus r_2/r_1.

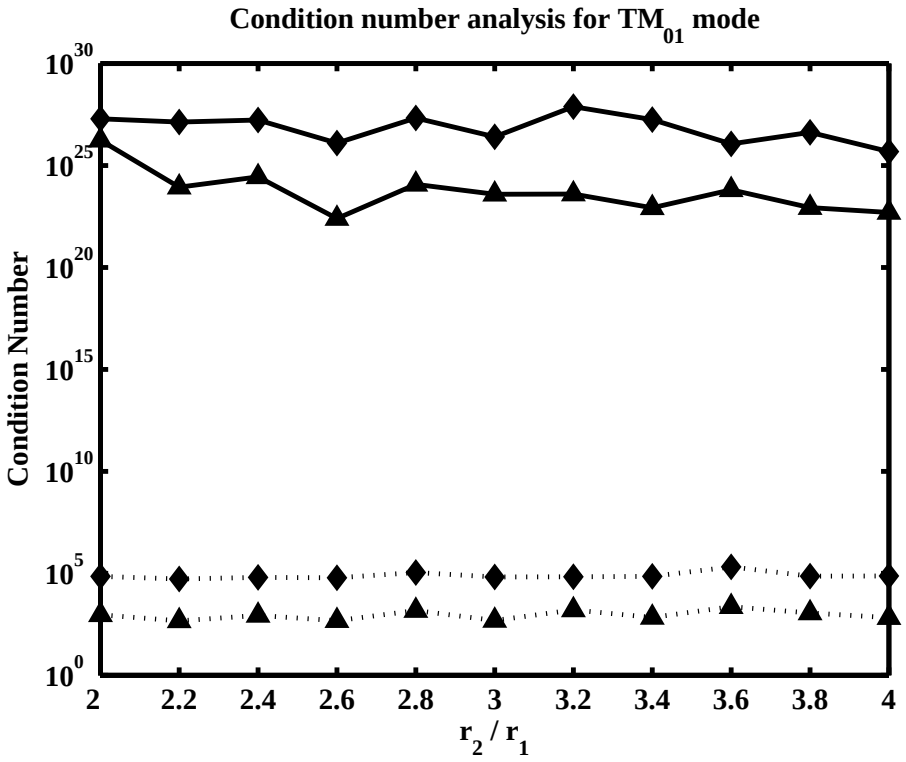

Figure 5.49. The condition numbers for weighted b-splines (solid) and web-splines (dashed) using quadratic (▲) and cubic (♦) b-splines versus r_2/r_1.

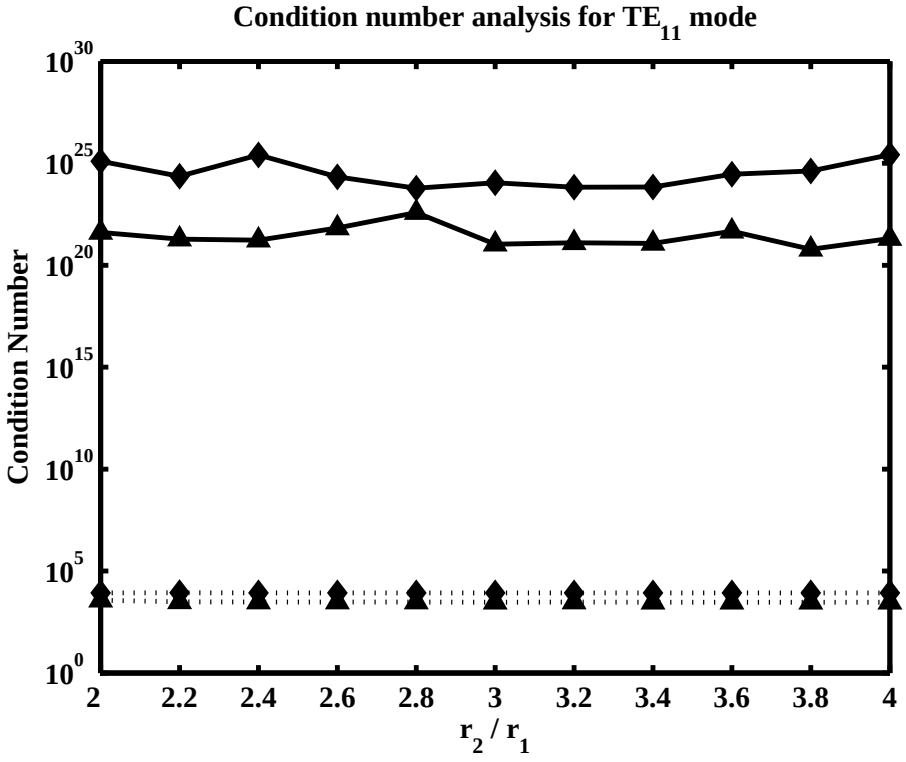

Figure 5.50. The condition numbers for b-splines (solid) and eb-splines (dashed) using quadratic (▲) and cubic (♦) b-splines versus r_2/r_1.

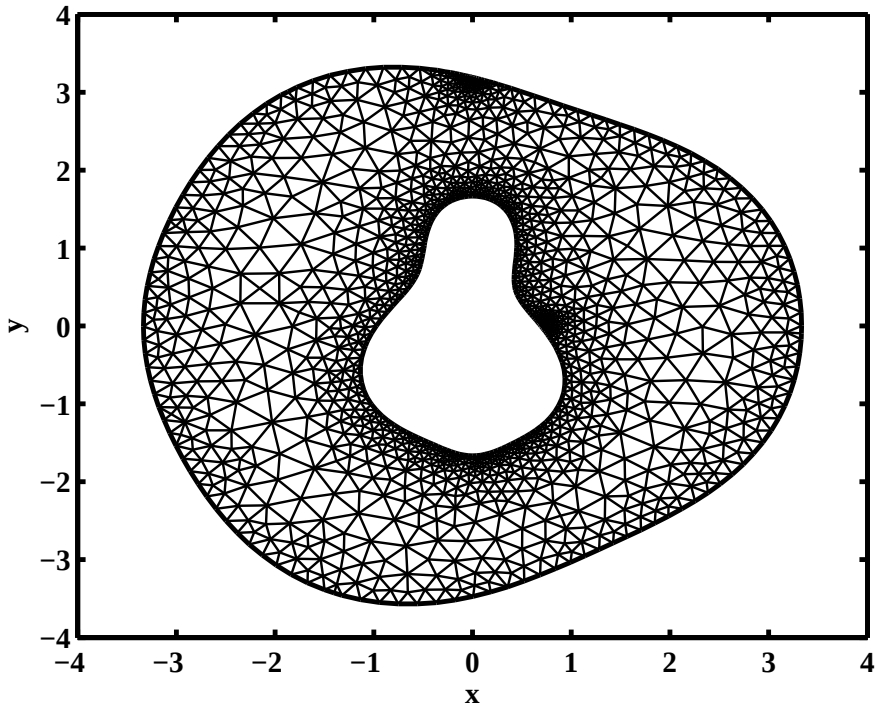

Figure 5.51. Triangulation for an arbitrary domain

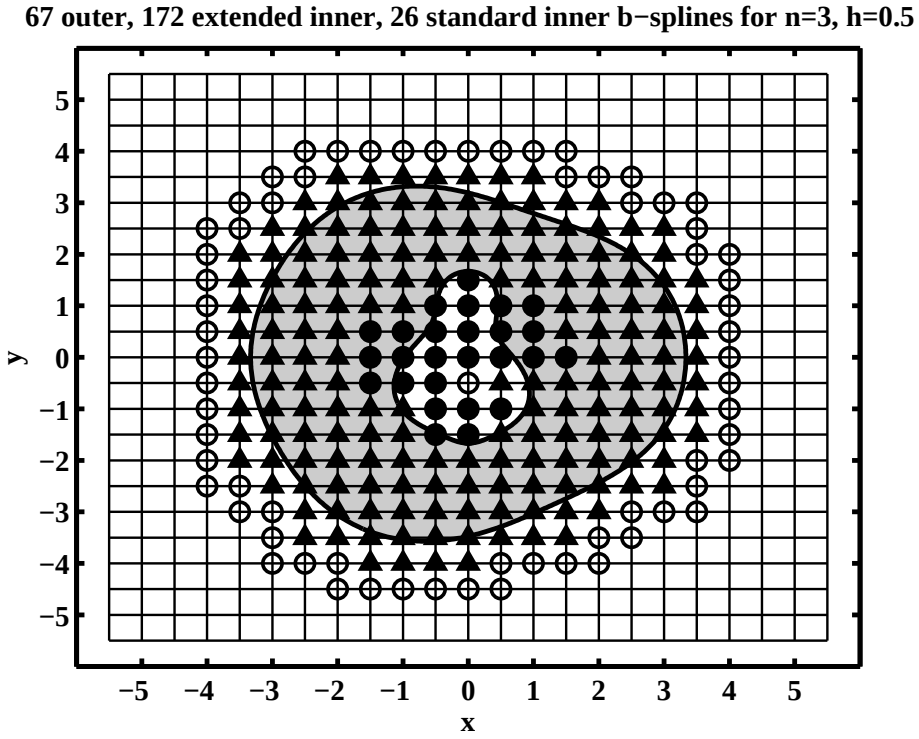

Figure 5.52. Web-spline method for an arbitrary domain (outer (○), extended inner (▲), and standard inner (●) b-splines)

The first three cutoff wave numbers of TM and TE modes are obtained as {1.41, 1.42, 1.61} and {0.40, 0.47, 0.86} respectively.

Table 5.9. The efficiency of web-spline method for an arbitrary domain (per cent)

n	Efficiency of nodes (per cent)	Efficiency of computation time (per cent)
1	36.87	70
2	29.44	60
3	25.28	50

According to Table 5.9, the efficiency of using web-splines instead of weighted splines for an arbitrary domain is shown. Secondly, Table 5.10 shows the number of nodes used for triangulation and web-splines in order to get same results. The web-spline method for an arbitrary domain provides accurate results with less computation time.

Table 5.10. The results of FEM analysis for an arbitrary domain

number of nodes	FEM method	mode	first three cutoff wave numbers			time(sec)
8663	standard	TE	0.40	0.47	0.86	2.9
125	linear web-spline	TE	0.41	0.47	0.87	0.1
163	quadratic web-spline	TE	0.40	0.47	0.86	0.2
198	cubic web-spline	TE	0.40	0.47	0.86	0.3
10061	standard	TM	1.41	1.42	1.62	4.9
125	linear web-spline	TM	1.43	1.45	1.66	0.1
163	quadratic web-spline	TM	1.41	1.42	1.62	0.2
198	cubic web-spline	TM	1.41	1.42	1.61	0.3

6. GUI TOOLBOX

6.1. B-splines and Their Derivatives

Graphical User Interfaces (GUI) are used to analyze b-splines and their derivatives in one, two, and three dimensions. All plots are based on the integer degree n and grid witdh h.

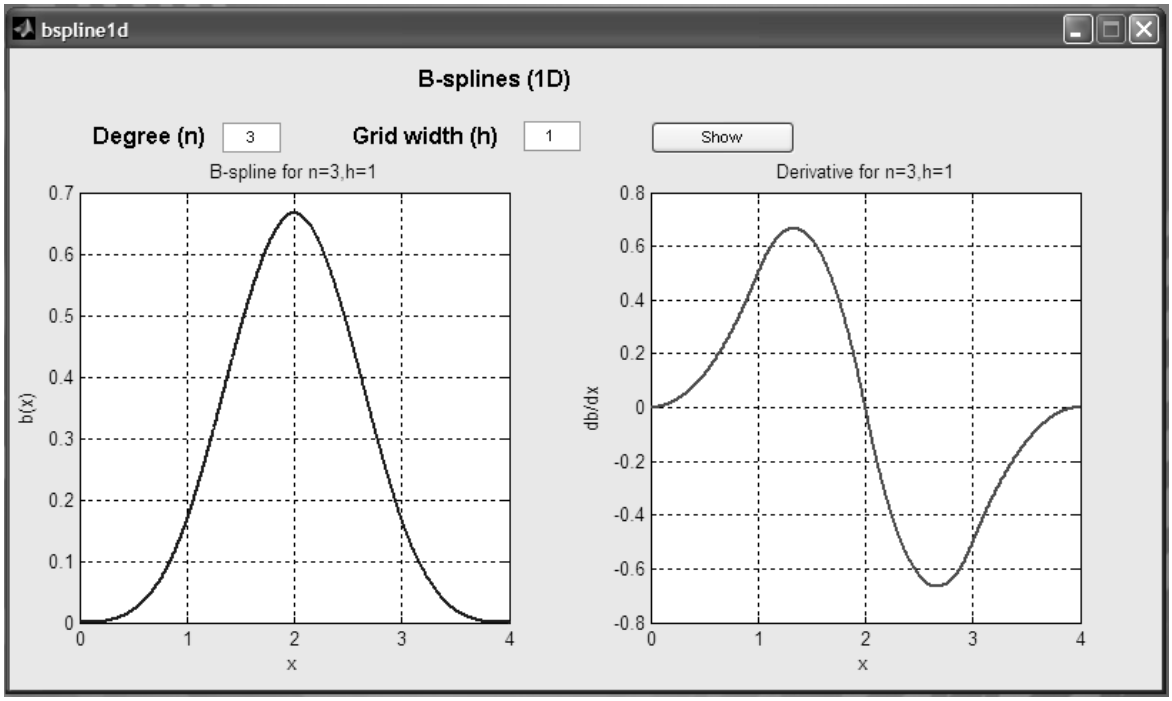

Figure 6.1. 1D b-spline and its derivative by changing n and h

Figure 6.2 shows the first order derivatives of n^{th} degree b-spline with respect to x and y. Then, Figure 6.3 shows the derivatives according to x, y, and z. These graphical interfaces are easy to use.

6.2. The Classification of B-splines for Web-splines

This section shows the classification of b-splines. According to Figure 6.4, while changing the degree and grid width, the user can see how to determine b-splines in one dimension. Moreover, the number of outer, extended inner, and standard inner b-splines are shown.

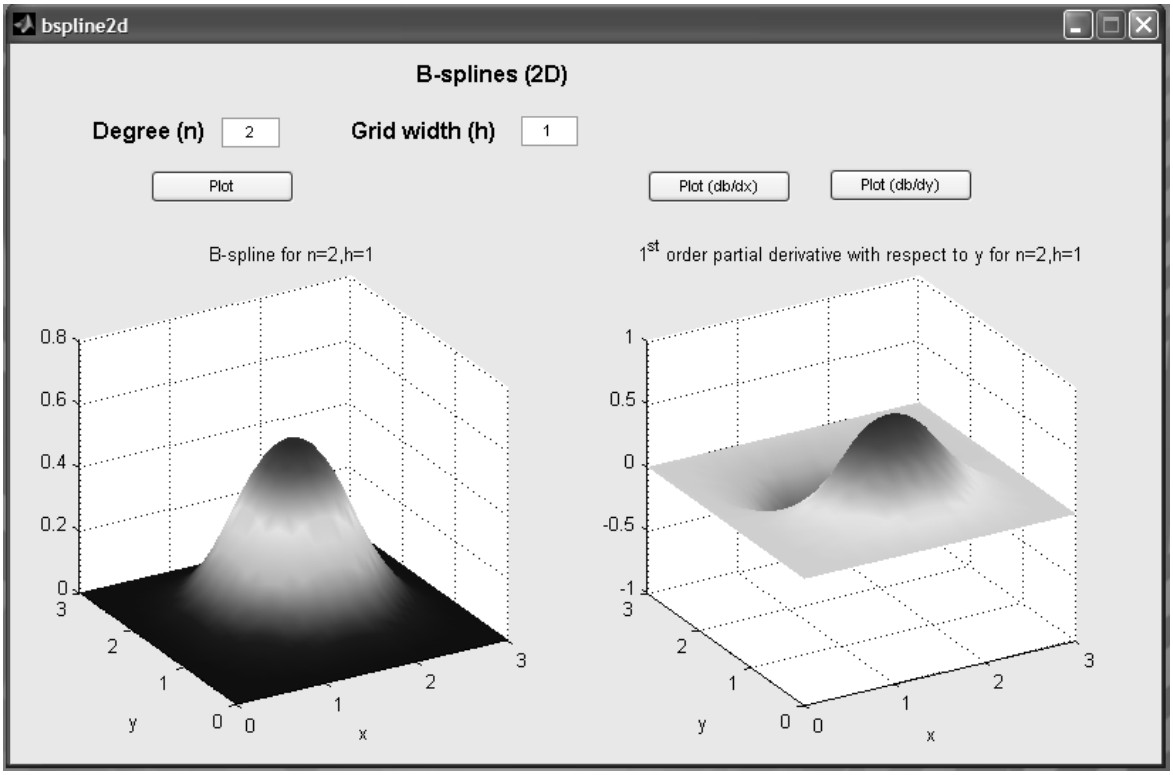

Figure 6.2. 2D b-spline and its derivative with respect to x and y

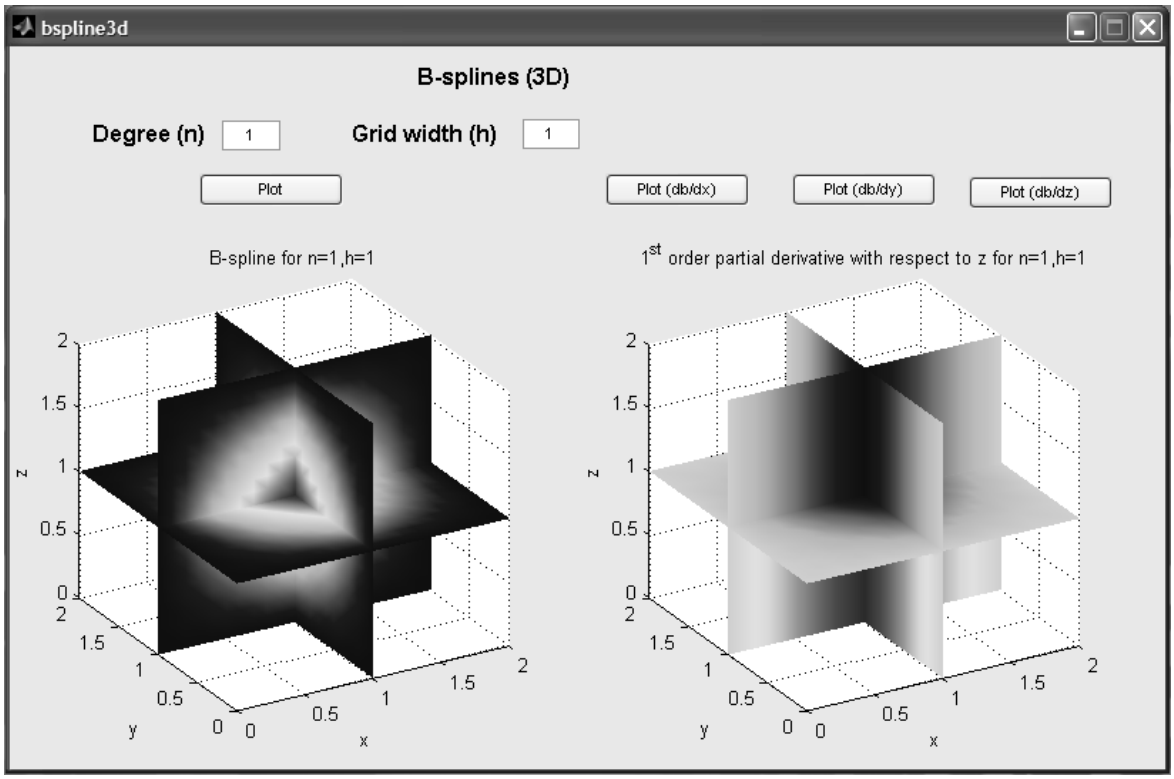

Figure 6.3. 3D b-spline and its derivative with respect to x, y, and z

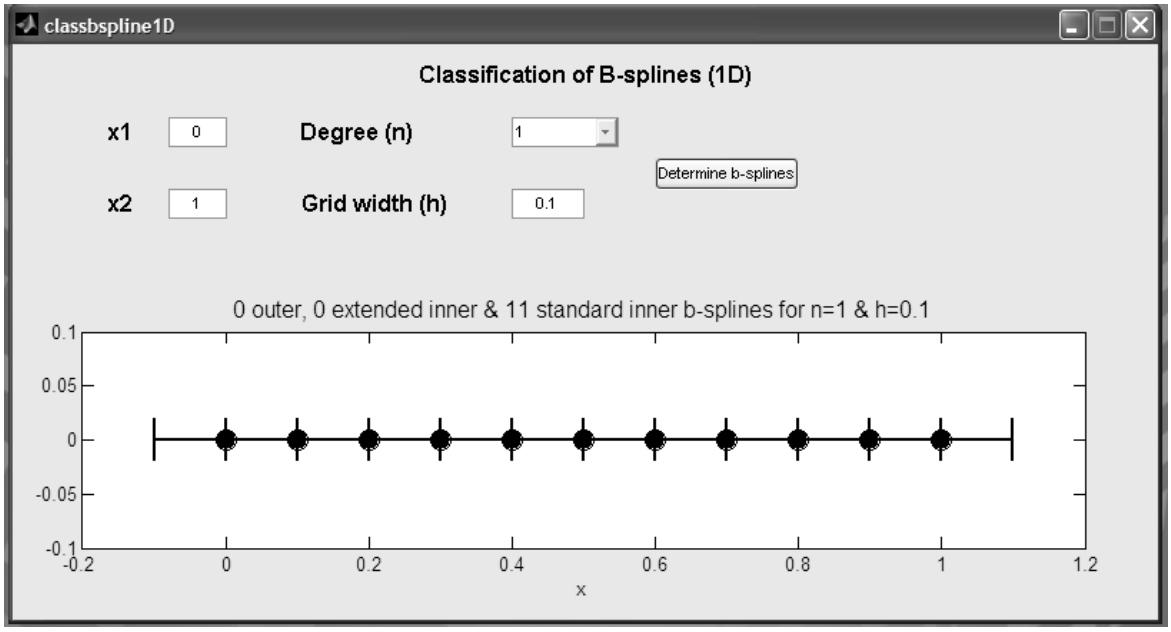

Figure 6.4. 1D classification of b-splines (inner (•) b-splines)

Figure 6.6 shows the classification of b-splines in two dimensions according to the given domain. The degree and grid width are changed easily. Input file as text file shown in Figure 6.5 is written for the following rule:

First line can be 'rect', 'ellipse' or 'arbit'. For rectangle, the second and third line gives the lower left corner of domain and side lengths on x and y respectively. For ellipse, the second line must be semi minor and major axis values. The third line must be center points of ellipse. For arbitrary domain, each line shows the points which passes on the boundary. If there are more than one boundary, same procedure is written for the given rule. The number of outer, extended inner, and standard inner b-splines are shown.

6.3. Calculation of Extension Coefficients

The extension coefficients are used to adjoin outer b-splines to inner b-splines. One dimension and two dimensions extension coefficients are obtained by using Equation (3.2). This section shows how to find extension coefficients for the given degree of b-splines. The one dimension extension coefficients for $n = 1, 2, 3, 4, 5$ are tabulated in Table 6.1.

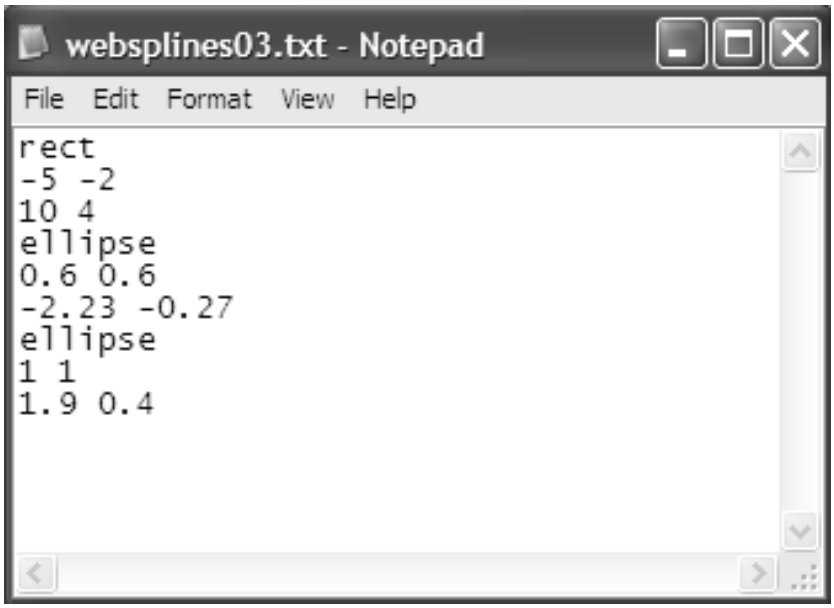

Figure 6.5. Input file for 2D web-splines

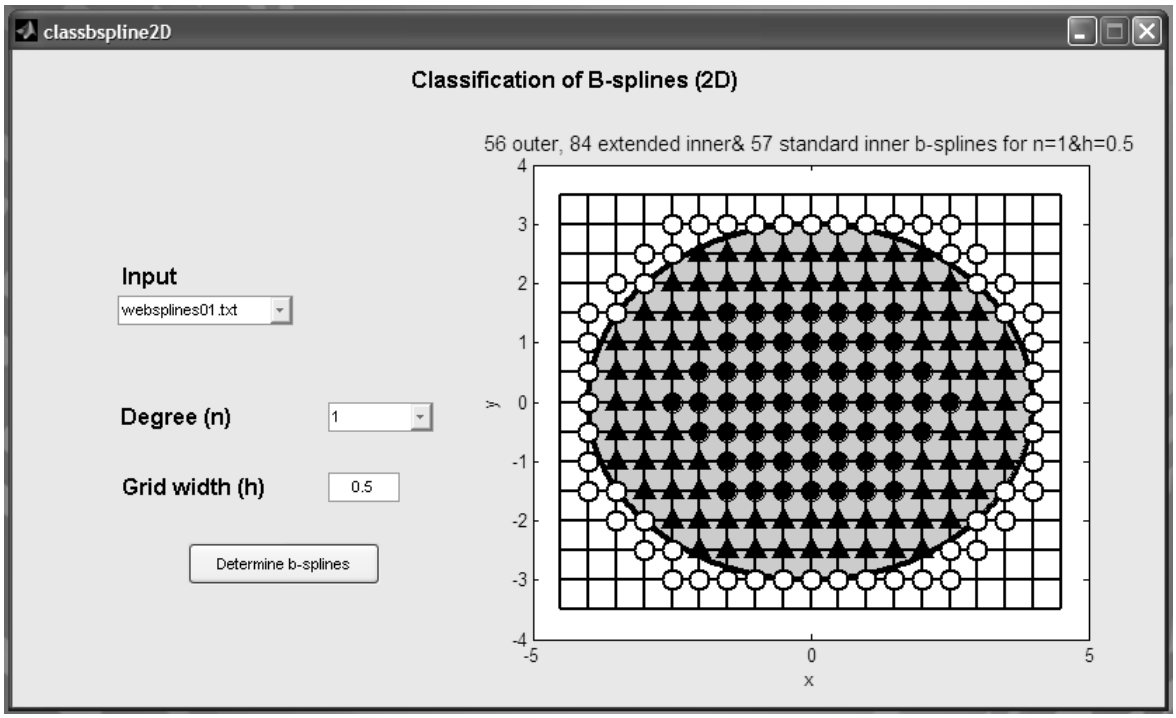

Figure 6.6. 2D classification of b-splines (the outer (○), extended inner (▲), and standard inner (●) b-splines)

Table 6.1. Extension coefficients for 1D

degree(n)	Extension coefficients
1	$(2, -1)$
2	$(3, -3, 1)$
3	$(4, -6, 4, -1)$
4	$(5, -10, 10, -5, 1)$
5	$(6, -15, 20, -15, 6, -1)$

Table 6.2. Extension coefficients for 2D

degree(n)	Corner Extension coefficients
1	$\begin{matrix} -2 & 1 \\ 4 & -2 \end{matrix}$
2	$\begin{matrix} 3 & -3 & 1 \\ -9 & 9 & -3 \\ 9 & -9 & 3 \end{matrix}$
3	$\begin{matrix} -4 & 6 & -4 & 1 \\ 16 & -24 & 16 & -4 \\ -24 & 36 & -24 & 6 \\ 16 & -24 & 16 & -4 \end{matrix}$

Figure 6.8 shows the extension coefficients in two dimensions. The extended inner b-splines for the outer b-splines are identified according to the boundary curve. The shortest distance from the centers of outer b-splines to the boundary determines which inner b-splines are affected. $(n+1)$ or $(n+1)^2$ inner b-splines are affected.

Four gray regions show the extension coefficients for the corner conditions. The two dimensions extension coefficients for $n = 1, 2, 3$ are tabulated in Table 6.2.

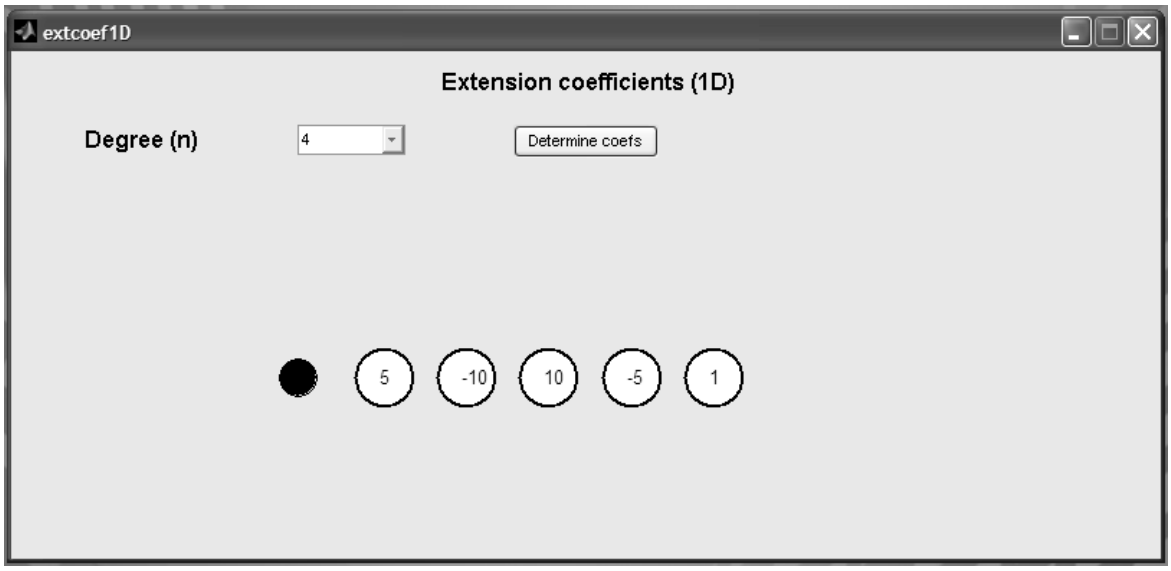

Figure 6.7. 1D extension coefficients

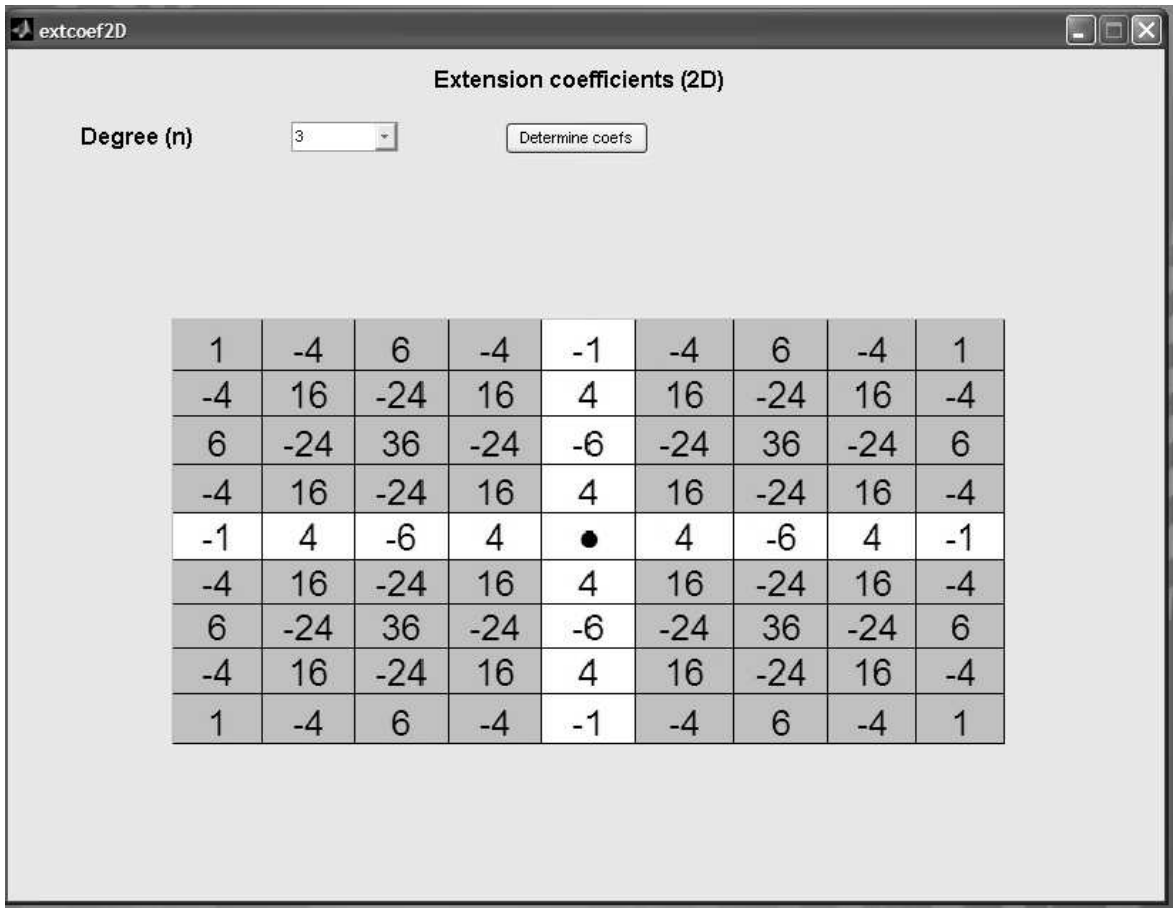

1	-4	6	-4	-1	-4	6	-4	1
-4	16	-24	16	4	16	-24	16	-4
6	-24	36	-24	-6	-24	36	-24	6
-4	16	-24	16	4	16	-24	16	-4
-1	4	-6	4	●	4	-6	4	-1
-4	16	-24	16	4	16	-24	16	-4
6	-24	36	-24	-6	-24	36	-24	6
-4	16	-24	16	4	16	-24	16	-4
1	-4	6	-4	-1	-4	6	-4	1

Figure 6.8. 2D extension coefficients

6.4. 1D Electromagnetic Applications

This section shows graphical user interfaces for one dimensional electromagnetics. First GUI, which is shown in Figure 6.9, finds the reflection coefficient from a metal dielectric slab while changing degree, grid width, and relative permittivity. Then, the program shows analytical reflection coefficient and numerical solution for comparison.

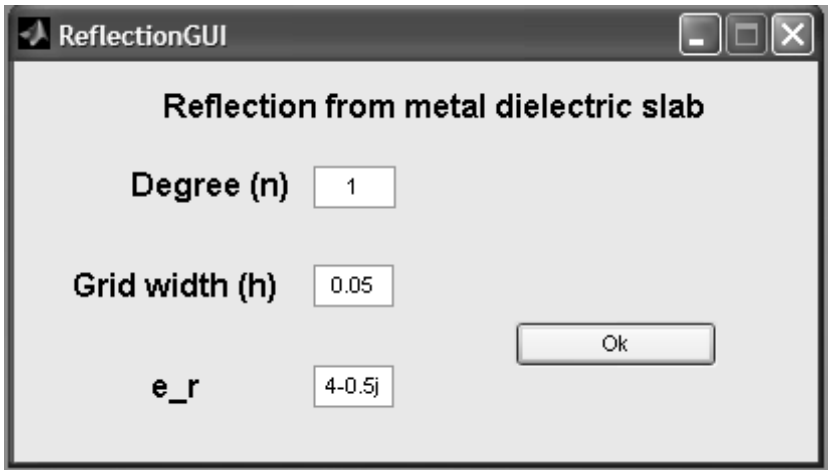

Figure 6.9. Reflection coefficient from a dielectric slab

Second GUI shows electric field between parallel plates, which is shown in Figure 6.11. The points show the approximated results and the line shows the analytical results. Input files (Figure 6.10) are written according to the following rule: The first two lines show the degree and grid width respectively. The third line shows the number of points for integration.

Then, the functions of PDE are entered $(p(x), q(x), f(x))$. For the end point, the position, boundary condition (0 for Dirichlet, 1 for Neumann), parameters for boundary condition (BNq, BNg for Neumann, u for Dirichlet) are entered on the fifth line. The same parameters are written for the starting point. If exact solution exists, it can be put on the last line for comparison.

The maximum errors, condition numbers, and L_2 errors for weighted b-splines and web-splines are shown for comparison.

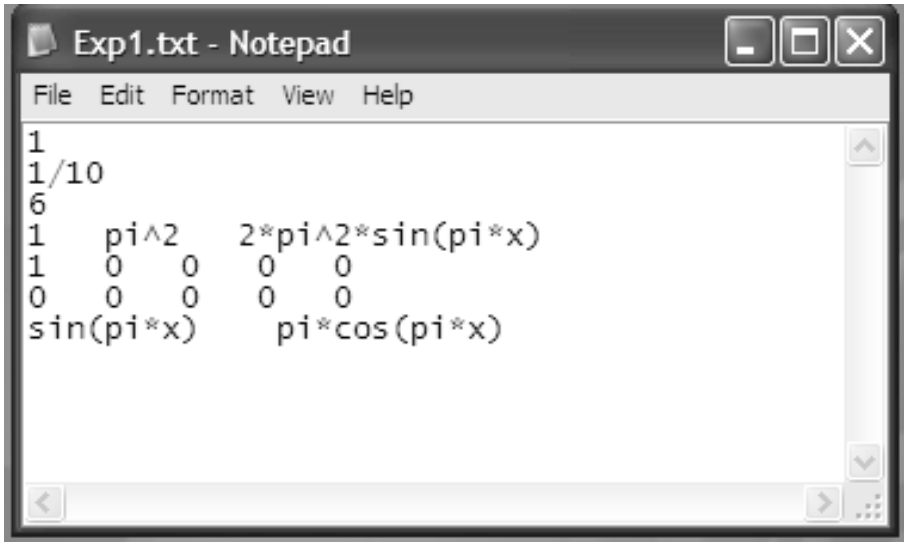

Figure 6.10. Input file for parallel plate application

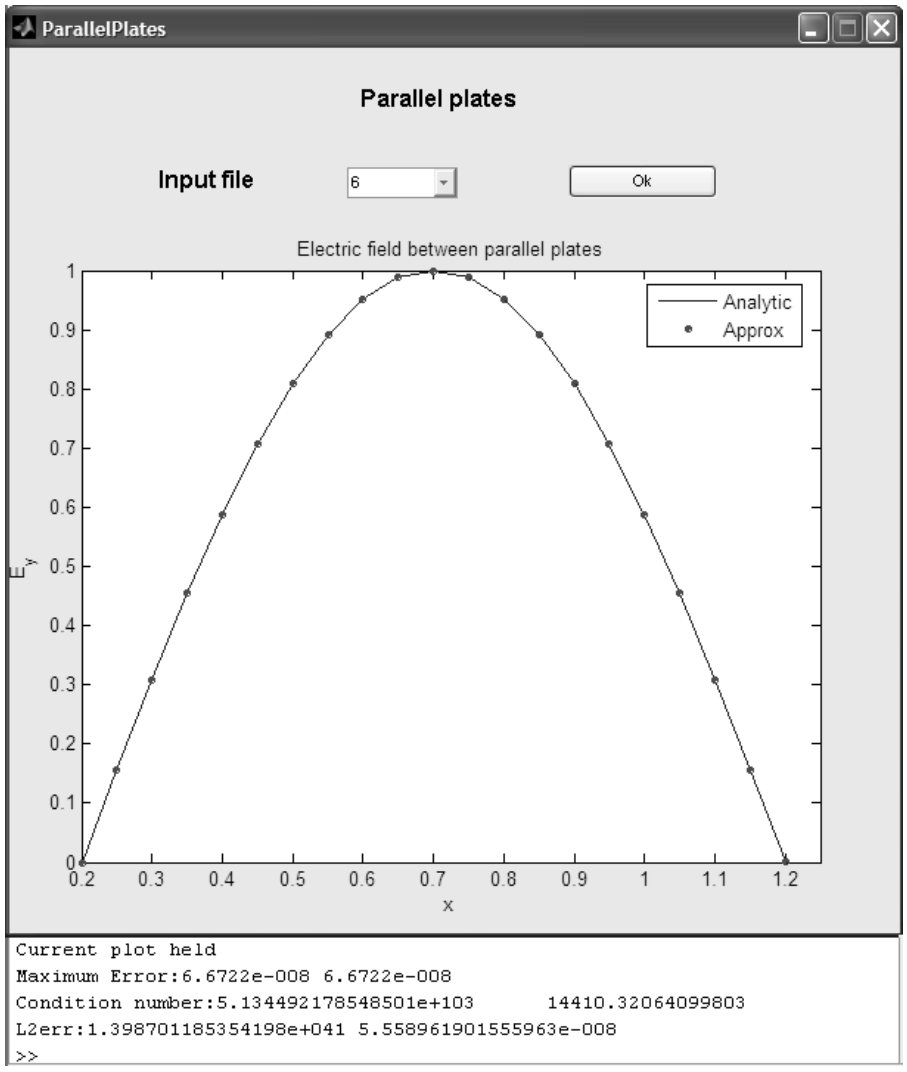

Figure 6.11. Electric field between parallel plates

6.5. 2D Electromagnetic Applications

This section shows graphical user interfaces for two dimensional electromagnetics. First and second GUIs, which are shown in Figures 6.12-6.13, show the electric fields using FEM with web-splines. The degree, the grid width, the square of wave number, and direction angle are changed easily. The user can see the effects of parameters for square and for circular domains.

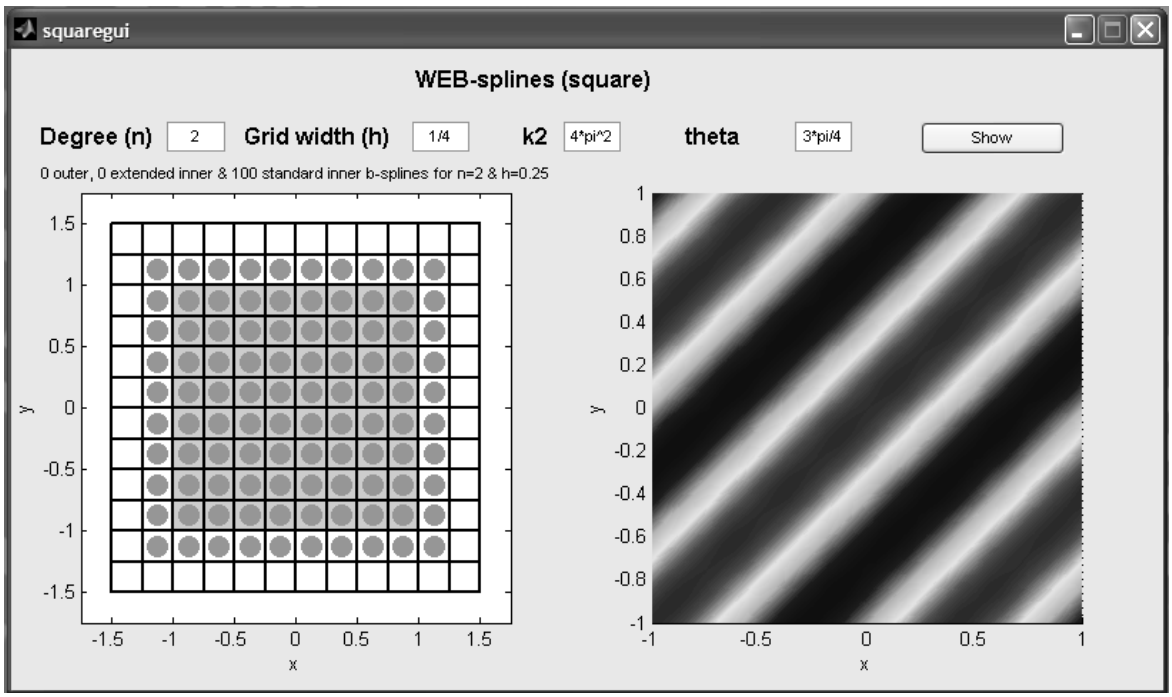

Figure 6.12. The web-spline application for square domain

The two dimensional rectangular, circular, and coaxial waveguide applications are shown by using GUI. Figures 6.14, 6.16, 6.18 show the analytical values of wave numbers. Other Graphical User Interfaces show the relative errors of wave numbers for various modes.

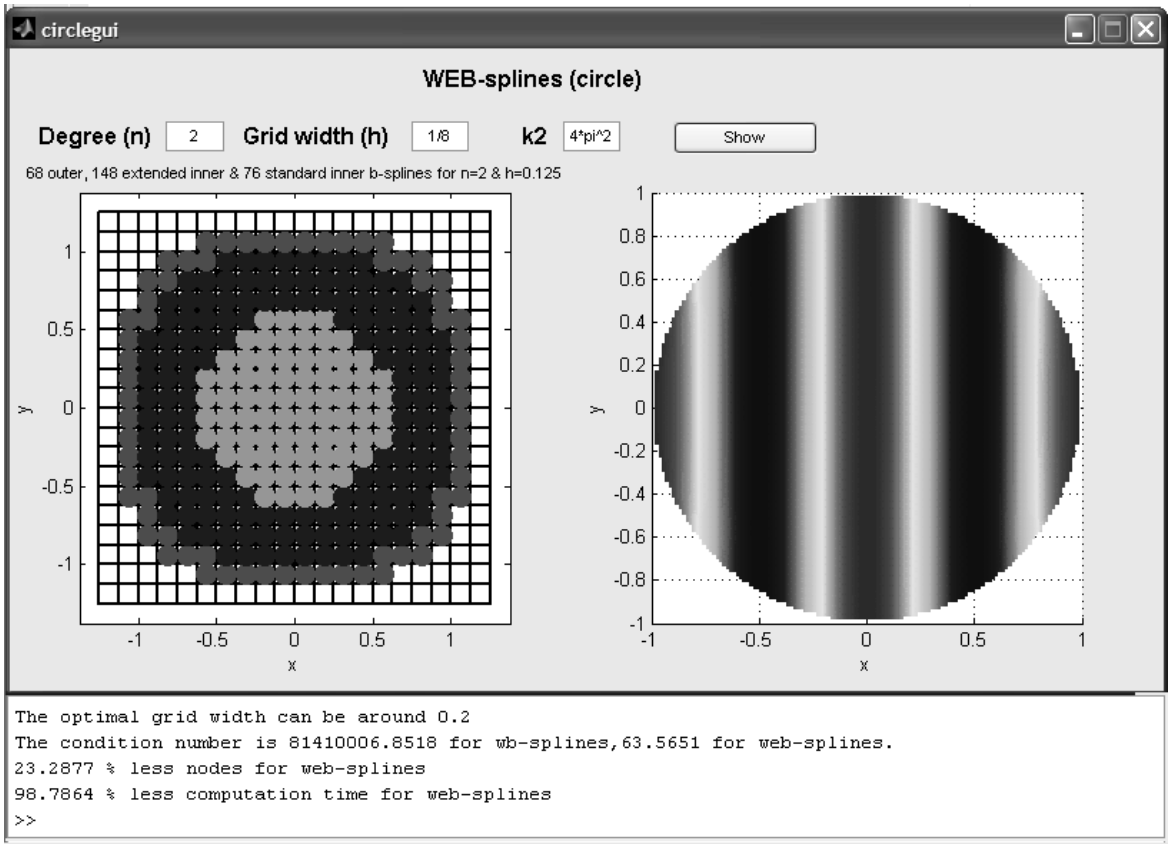

Figure 6.13. The web-spline application for circular domain

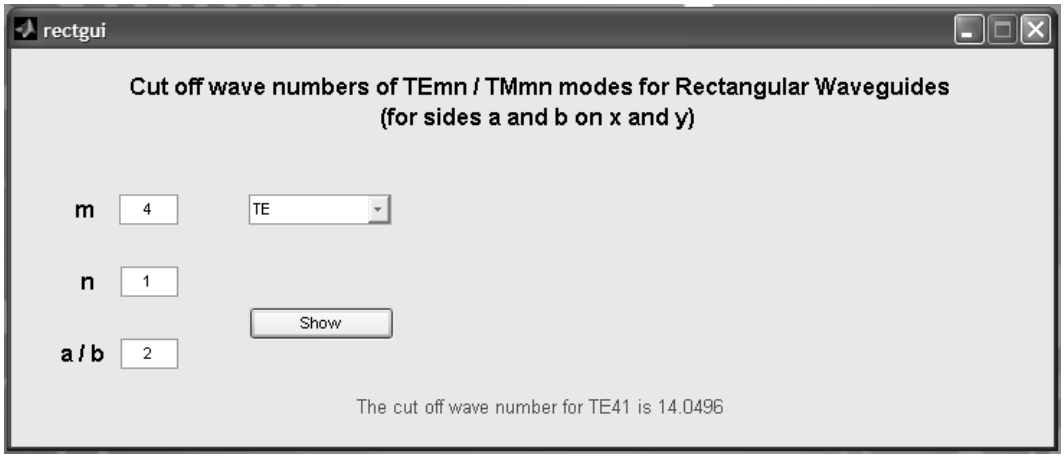

Figure 6.14. The analytical wave numbers for rectangular waveguide

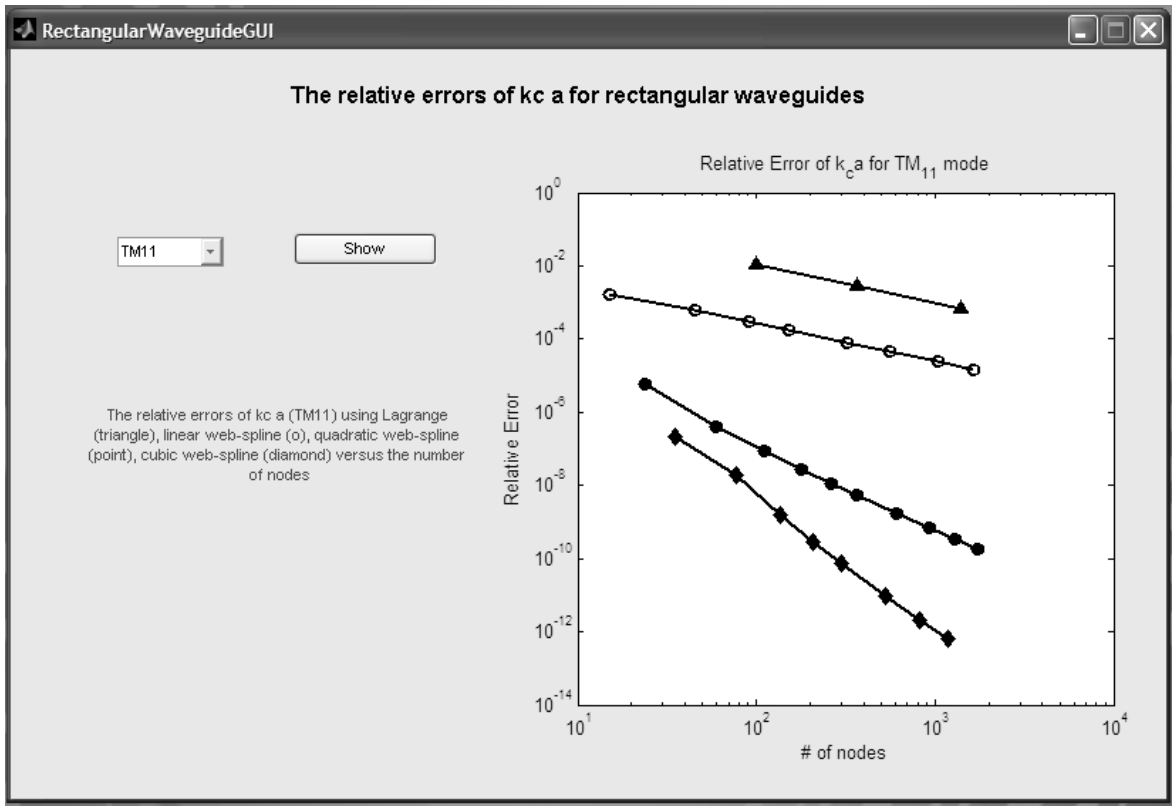

Figure 6.15. The relative errors of wave numbers for rectangular waveguide

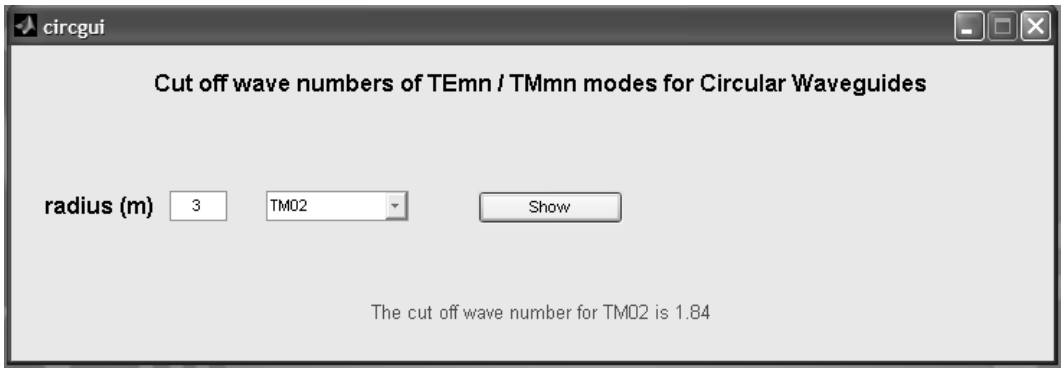

Figure 6.16. The analytical wave numbers for circular waveguide

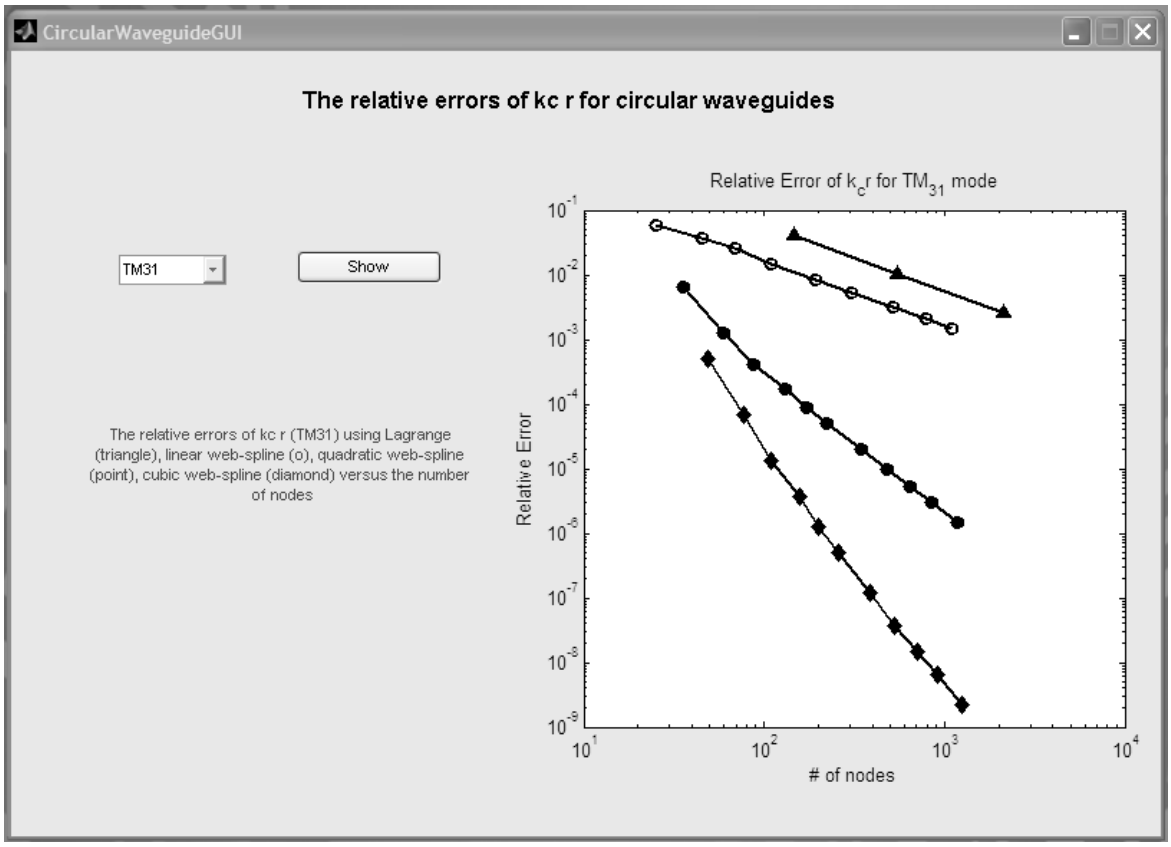

Figure 6.17. The relative errors of wave numbers for circular waveguide

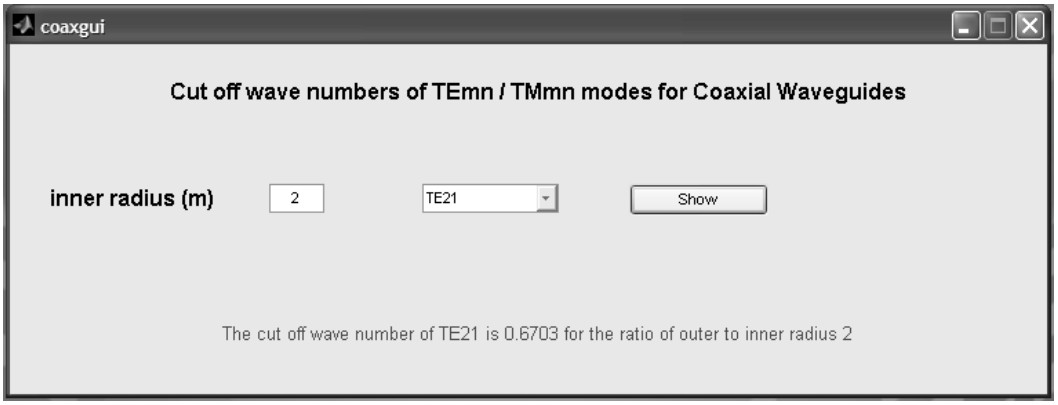

Figure 6.18. The analytical wave numbers for coaxial waveguide

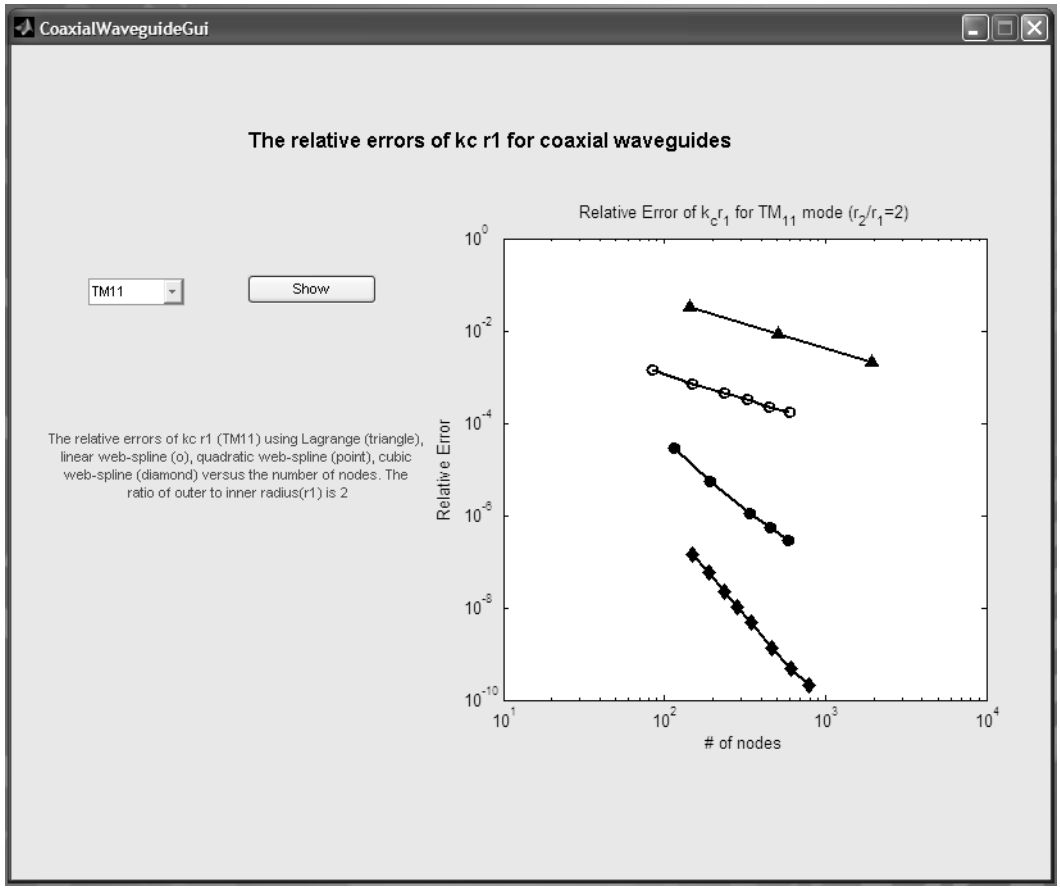

Figure 6.19. The relative errors of wave numbers for coaxial waveguide

7. CONCLUSIONS

Electromagnetics studies the behavior of electric and magnetic fields in different mediums. These mediums can be homogeneous or inhomogeneous, with or without losses. The Maxwell's equations form the foundations for the mathematical analysis of elecromagnetics. However, such analytical solutions to the Maxwell's equations are not trackable for many cases. Therefore, numerical approximation techniques have been developed and computational electromagnetics has been a popular field of study. Such approaches are based on numerical solutions of the partial differential equations that govern the electromagnetic properties, such as the wave equations.

The numerical computational electromagnetics in scattering, biomedical problems, and antenna design are taken into consideration in various journals and conferences. There are several numerical methods, which are given attention. One of the popular numerical methods is Finite Element Method, which is very effective for inhomogeneous materials and allows representing complex geometries very precisely. It is a versatile and flexible numerical technique that is often used in the analysis of geometrical complex structures. It is also used for scattering, radiation, and propagation problems.

This thesis proposed the use of extended and weighted extended b-spline method to numerically study the electromagnetic models. To our best knowledge, it is the first time that this method is considered in the context of electromagnetic computing. One and two dimensional solvers have been developed for simulations of electromagnetics. The wave equation has been solved easily and accurate results have been obtained by increasing the degree of basis function. Web-spline graphical user interface for Matlab has been completed. We have found that the approximation solution of waveguide applications using web-splines is possible at low computational cost. By increasing the degree of web-splines, the numerical solutions for electromagnetic problems can be easily obtained.

First, the finite element method using web-splines has been applied to one-dimensional electromagnetic problems. The simulation results have been compared with the literature and excellent agreement was found.

The finite element method which uses web-splines has then been extended to two-dimensional electromagnetic problems such as waveguides. The simulation results have been compared with the literature and excellent agreement was obtained. More accurate results have been obtained with fewer nodes using web-splines compared to the standard FEM. It has been observed that web-spline method is versatile and can be implemented easily for electromagnetic applications. Highly accurate results have been obtained without using mesh generation. 20-30 per cent improvement has been observed as compared to standard FEM. Therefore, it has been concluded that the web-splines based FEM is a successful computational method for electromagnetic simulations.

Web-splines have then been applied to coaxial waveguides. The numerical approximations have been compared with the analytical results. Accurate results have been obtained by using web-splines for different ratio of coaxial waveguides. Web-splines and extended b-splines have been used to find the wave numbers of TM and TE mode respectively. The relative errors for the TM modes are more accurate than those of the TE modes according to the error analysis. Finally, web-splines have been obtained more stable than normal basis splines functions in this work.

It was found that, FEM with web-spline is suitable for obtaining electromagnetic solution for different frequencies. The theoretical and simulation results have been compared with the literature and the model agrees very well with published results. These comparisons show that the method is valid when $k_0h < 0.79$ where k_0 is the free space wave number, h is the grid width for numerical computation. The simulation results have been tested with $0.198 < k_0h < 0.79$ and $0.792 < k_0a < 12.64$ where a is the maximum diameter of circle circumscribing domain. The criteria for choosing h depends on the domain and frequency. The necessary step, which has given attention, is to take k_0h value smaller than 0.8. This means, for high frequencies it is noted

that the grid width should be selected as small compared to wavelength. In addition, the maximum diameter of circle circumscribing domain should be small for higher frequencies in order to provide fast calculation. Figure 7.1 shows the effect of frequency on parameters using web-spline method.

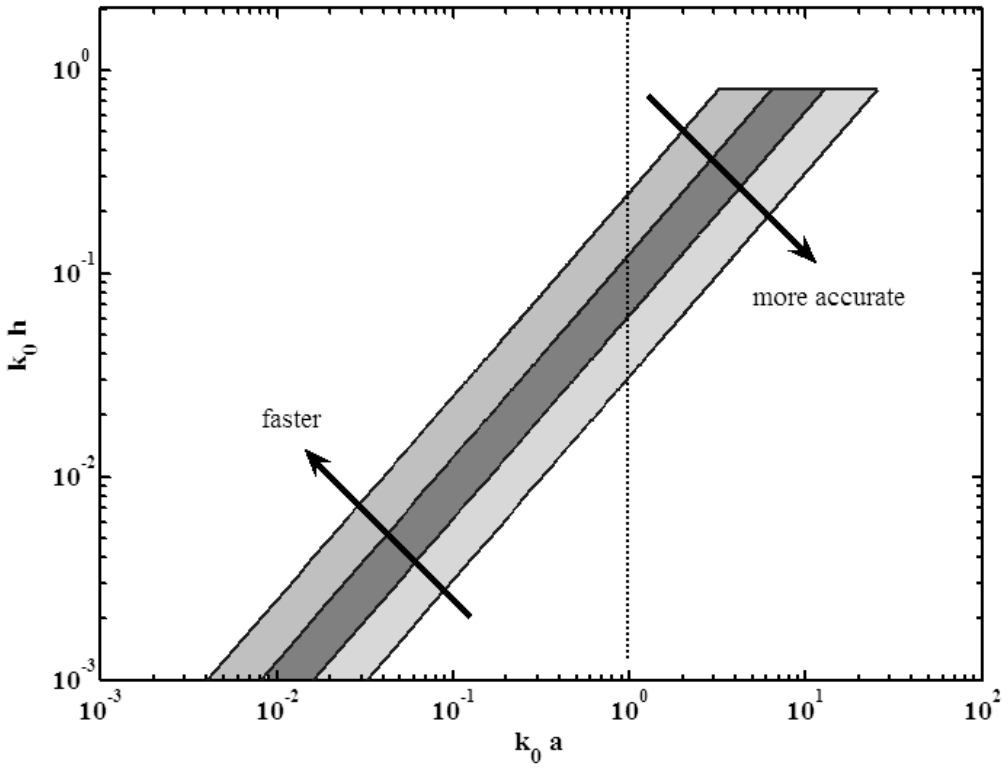

Figure 7.1. The effect of frequency on size parameters using web-spline method

This new approach for electromagnetics can be applied to various structures and more complex electromagnetic problems such as biomedical modeling and scattering problems. The results of this study show that the developed method is suitable for three dimensional electromagnetic problems as well.

APPENDIX A: GRADIENT AND CURL

A.1. Cartesian Coordinates

$$\nabla \cdot \mathbf{A} = \frac{\partial A_x}{\partial x} + \frac{\partial A_y}{\partial y} + \frac{\partial A_z}{\partial z} \tag{A.1}$$

$$\nabla \times \mathbf{A} = \left(\frac{\partial A_z}{\partial y} - \frac{\partial A_y}{\partial z}\right)\mathbf{a}_x + \left(\frac{\partial A_x}{\partial z} - \frac{\partial A_z}{\partial x}\right)\mathbf{a}_y + \left(\frac{\partial A_y}{\partial x} - \frac{\partial A_x}{\partial y}\right)\mathbf{a}_z \tag{A.2}$$

$$\nabla V = \frac{\partial V}{\partial x}\mathbf{a}_x + \frac{\partial V}{\partial y}\mathbf{a}_y + \frac{\partial V}{\partial z}\mathbf{a}_z \tag{A.3}$$

$$\nabla^2 V = \frac{\partial^2 V}{\partial x^2} + \frac{\partial^2 V}{\partial y} + \frac{\partial^2 V}{\partial z^2} \tag{A.4}$$

A.2. Cylindrical Coordinates

$$\nabla \cdot \mathbf{A} = \frac{1}{r}\frac{\partial (rA_r)}{\partial r} + \frac{\partial A_\phi}{r\partial \phi} + \frac{\partial A_z}{\partial z} \tag{A.5}$$

$$\nabla \times \mathbf{A} = \left(\frac{\partial A_z}{r\partial \phi} - \frac{\partial A_\phi}{\partial z}\right)\mathbf{a}_r + \left(\frac{\partial A_r}{\partial z} - \frac{\partial A_z}{\partial r}\right)\mathbf{a}_\phi + \frac{1}{r}\left(\frac{\partial (rA_\phi)}{\partial r} - \frac{\partial A_r}{\partial \phi}\right)\mathbf{a}_z \tag{A.6}$$

$$\nabla V = \frac{\partial V}{\partial r}\mathbf{a}_r + \frac{\partial V}{r\partial \phi}\mathbf{a}_\phi + \frac{\partial V}{\partial z}\mathbf{a}_z \tag{A.7}$$

$$\nabla^2 V = \frac{1}{r}\frac{\partial}{\partial r}\left(r\frac{\partial V}{\partial r}\right) + \frac{1}{r^2}\frac{\partial^2 V}{\partial \phi^2} + \frac{\partial^2 V}{\partial z^2} \tag{A.8}$$

A.3. Spherical Coordinates

$$\nabla \cdot \mathbf{A} = \frac{1}{R^2}\frac{\partial (R^2 A_R)}{\partial R} + \frac{1}{R\sin\theta}\frac{\partial (A_\theta \sin\theta)}{\partial \theta} + \frac{1}{R\sin\theta}\frac{\partial A_\phi}{\partial \phi} \tag{A.9}$$

$$\nabla \times \mathbf{A} = \frac{1}{R^2 \sin\theta}\begin{vmatrix} \mathbf{a}_R & R\mathbf{a}_\theta & R\sin\theta\mathbf{a}_\phi \\ \frac{\partial}{\partial R} & \frac{\partial}{\partial \theta} & \frac{\partial}{\partial \phi} \\ A_R & RA_\theta & R\sin\theta A_\phi \end{vmatrix} \tag{A.10}$$

$$\nabla V = \frac{\partial V}{\partial R}\mathbf{a}_R + \frac{\partial V}{R\partial \theta}\mathbf{a}_\theta + \frac{1}{R\sin\theta}\frac{\partial V}{\partial \phi}\mathbf{a}_\phi \tag{A.11}$$

$$\nabla^2 V = \frac{1}{R^2}\frac{\partial}{\partial R}\left(R^2\frac{\partial V}{\partial R}\right) + \frac{1}{R^2\sin\theta}\frac{\partial}{\partial \theta}\left(\sin\theta\frac{\partial V}{\partial \theta}\right) + \frac{1}{R^2\sin^2\theta}\frac{\partial^2 V}{\partial \phi^2} \tag{A.12}$$

APPENDIX B: VECTOR IDENTITIES AND INTEGRAL THEOREMS

$$\nabla \times (a\mathbf{b}) = \nabla a \times \mathbf{b} + a\nabla \times \mathbf{b} \tag{B.1}$$

$$\nabla \times \nabla \times \mathbf{a} = \nabla\nabla \cdot \mathbf{a} - \nabla^2\mathbf{a} \tag{B.2}$$

$$\int_\Omega \nabla^2 uv + \int_\Omega \nabla u \nabla v = \int_{\partial\Omega} \frac{\partial u}{\partial n} v \tag{B.3}$$

APPENDIX C: PROGRAM CODES

C.1. ONE DIMENSION

main1D:

This program considers FEM using web-splines for Electromagnetic problems.

Consider two-point boundary value problem for one dimension (1D)

$-d/dx\,(p(x)\,du/dx) + q(x)\,u = f(x)\; x_i < x < x_e$

Boundary Conditions (BC)

$u = u_d$ at $x = x_i$ or $x = x_e$ Dirichlet BC

$du/dx + BNq * u = BNg$ at $x = x_i or x = x_e$ Cauchy BC

input1D:

INPUT DATA

name: Application name

n: degree (1 for linear, 2 for quadratic, 3 for cubic etc.)

h: grid width

NP: number of points for integration

$-d/dx\,(px\,du/dx) + qx\,u = fx$

Boundary Conditions (BC)

u=bound.u at $x = x_i$ or $x = x_e$ Dirichlet BC

$du/dx + bound.BNq * u = bound.BNg$ at $x = x_i$ or $x = x_e$ Cauchy BC bound.BC: 0 for DRICHLET, 1 for NEUMANN

bound.x: position

bound.BNq: for NEUMANN

bound.BNg: for NEUMANN

bound.u: for DRICHLET

uexact: exact solution

duexact: derivative of exact solution

weight: weight function

weightt: derivative of weight function

deternode:

determination of the nodes

xx : position of nodes

xi,xe : initial and end points

detbspln:

determination of the classification of b-splines for 1D

D : all b-splines supporting the region

bb : inner(2) and outer(1) b-splines

gi : inner b-splines

gj : outer b-splines

showinoutmid:

plotting of the classification of b-splines for 1D

splines are marked in the middle of of their support

the inner and outer b-splines for w=1

the extended,normal inner and outer bsplines for w=2

detext:

determines the extended inner bsplines, computes coefficients

D=[i xx(i)]: all b-splines supporting the domain

bb: extended(3), inner(2) and outer(1) b-splines

gi, gj: inner and outer b-splines

E: extended matrix

webassemb:

assemble PDE for 1D

xx: position of grid cells

TH: the direction angle of wave

k: square of wave number

K,M,F,DNq,DNg: Matrices for assembly

webanal:

solve and plot results

webnorm:

maximum, L2 error norm analysis

gnodewt:

Gaussian Integration points and coefficients

bsplfunc:

loads data (up to degree 5)

(*) inner integral coefficients of b-splines for inner cells

(*) b-spline equations to compute integrals for boundary cells

splninteg:

find the finite element stiffness, mass, load coeff.

pbicgstab:

solves the linear system Ax=b using the BiConjugate Gradient Stabilized Method with

preconditioning

C.2. TWO DIMENSIONS

main2D:

This program considers FEM using web-splines for Electromagnetic problems.

input2D:

determines the region to be applied

C:boundary positions

xx yy:grid positions

h:grid width

n:degree

name:project name

boun:boundary data

bound.cont :'0' rectangle, '1' ellipse, '2' unarbitrary region

bound.con :'0' Dirichlet, '1' Neumann

detbspln:

determines the classification of b-splines for 2D

xx,yy, x,y(gridded): position of grid cells

D=[i j xx(i) yy(j)]: all b-splines supporting the region

bb: inner(2) and outer(1) b-splines

gi: inner b-splines

gj: outer b-splines

detext:

determines the extended inner bsplines and computes coefficients

bb: extended(3), inner(2) and outer(1) b-splines

E: extended matrix

webassemb:

assembles PDE for 2D using WEB-method

TH: the direction angle of wave

k2: square of wave number

K,M,F,DNq,DNg: Matrices for assembly

isinpoly:

Finds whether points with coordinates X and Y are inside or outside of a polygon with vertices XP, YP. Returns matrix ISIN of the same size as X and Y with 0 for points outside a polygon, 1 for inside points and 0.5 for points belonging to a polygon XP, YP itself.

showinoutmid:

plots the classification of b-splines for 2D

splines are marked at the center of their support

the inner and outer b-splines for w=1

the extended and normal inner and outer bsplines for w=2

showinout:

plots the classification of b-splines for 2D

splines are marked at the lower left position of their support

the inner and outer b-splines for w=1

the extended and normal inner and outer bsplines for w=2

C.3. OTHER NUMERICAL METHODS

FDM:

programming code which uses Finite Difference Method
applied to two-point boundary value problems

FEM:

programming code which uses Finite Element Method
applied to two-point boundary value problems

FVM:

programming code which uses Finite Volume Method
applied to two-point boundary value problems

bsplinecubic:

programming code which uses B-spline Cubic Interpolation Method
applied to two-point boundary value problems

REFERENCES

1. Faraday, M., *Experimental Researches in Electricity*, Seventh Series, Philosophical Transactions of The Royal Society, London, 1834.

2. Maxwell, J. C., *A Treatise on Electricity and Magnetism*, Dover Publications, New York, 1954.

3. Yee, K. S., "Numerical Solution of Initial Boundary Value Problems Involving Maxwell's Equations in Isotropic Media", *IEEE Transactions on Antennas and Propagation*, Vol. 14, No. 6, pp. 302-307, May 1966.

4. Gupta, O. P., *Finite and Boundary Element Methods in Engineering*, Taylor Francis, India, 1999.

5. Bochev, P. B. and M. D. Gunzburger, *Finite Element Methods of Least Squares Type*, SIAM Review, Vol. 40, 1998.

6. Belytschko, T., Y. Krongauz, D. Organ, M. Fleming and P. Krysl, "Meshless Methods: An Overview and Recent Developments", *Computation Methods in Applied Mechanics and Engineering*, Vol. 139, pp. 3-47, 1999.

7. Ho, S. L., S. Yang, J. M. Machado and H. C. Wong, "Application of A Meshless Method in Electromagnetics", *IEEE Transactions on Magnetics*, Vol. 37, No. 5, pp. 3198-3202, 2001.

8. Wendland, H., "Meshless Galerkin Methods Using Radial Basis Functions", *Mathematical Computations*, Vol. 68, No. 228, pp. 1521-1531, 2002.

9. De Boor, C., "On Calculating with B-splines", *Journal of Approximation Theory*, Vol. 6, pp. 50-62, 1972.

10. De Boor, C., *A Practical Guide to Splines*, Applied Mathematics Series 27, Springer-Verlag, New York, 1978.

11. Kipp, A., *Spline Galerkin Approximation*, Ph.D. Thesis, University of Stuttgart, 1998.

12. Zhou, X., "Physical Spline Finite Element (PSFEM) Solutions to One Dimensional Electromagnetic Problems", *Progress in Electromagnetics Research*, Vol. 40, pp. 271-294, 2003.

13. Han, J. G., W. X. Ren and Y. Huang "A Spline Wavelet Finite-Element Method in Structural Mechanics", *International Journal for Numerical Methods in Engineering*, Vol. 66, pp. 166-190, 2006.

14. Hubing, T. H., *Survey of Numerical Electromagnetic Modeling Techniques*, University of Missouri-Rolla EMC Lab, Intel Co, 1991.

15. Harrington, R. F., *Time Harmonic Electromagnetic Fields*, McGraw Hill. New York, 1961.

16. Volakis, J. L., A. Chatterjee and L. C. Kempel, *Finite Element Method for Electromagnetics*, IEEE Press, New York, 1998.

17. Jin, J., *The Finite Element Method in Electromagnetics*, John Wiley and Sons, 1993.

18. Petrovsky, I. G., *Lectures on Partial Differential Equations*, Dover Publication, New York, 1991.

19. Clough, R. W., "The Finite Element Method in Plane Stress Analysis", *Proceedings of the Second ASCE Conference on Electronic Computation*, Pittsburgh, PA, September 1960.

20. Zienkiewicz, O. C. and Y. K. Cheung, *The Finite Element Method in Structural and Continuum Mechanics*, McGraw-Hill Publication, London, 1967.

21. Holand, I. and K. Bell, *Finite Element Methods in Stress Analysis*, Tapir, Trondheim, Norway, 1969.

22. Tottenham, H. and C. A. Brebbia, *Finite Element Techniques in Structural Mechanics*, Stress Analysis Publication, Southampton, 1970.

23. Strang, G. and G. J. Fix, *An Analysis of The Finite Element Method*, Prentice Hall, Englewood Cliffs, 1973.

24. *Introduction to FEM (History, Advantages and Disadvantages)*, http://cee.uiuc.edu/paulino/cee478/handouts/introfem.pdf

25. Babushka, I., "The Finite Element Method with Penalty", *Mathematics of Computation*, Vol. 27, No. 122, pp. 221-228, 1973.

26. Babushka, I., "The Finite Element Method with Lagrangian multipliers", *Numerical Mathematics*, Vol. 20, pp. 179-192, 1973.

27. Xuebiao, L., J. Baidun and N. Guangzhen, "The B-spline Finite Element Method in Electromagnetic Field Numerical Analysis", *IEEE Transactions on Magnetics*, Vol. 23, No. 5, pp. 2641-2643, 1987.

28. Hollig, K., *Finite Element Methods with B-splines*, Frontiers in Applied Mathematics, Vol. 26, Society for Industrial and Applied Mathematics (SIAM), Philadelphia, 2003.

29. Hollig, K., U. Reif and J. Wipper, "Weighted Extended B-spline Approximation of Dirichlet Problems", *SIAM Journal on Numerical Analysis*, Vol. 39, No. 2, pp. 442-462, 2001.

30. Hollig, K., U. Reif and J. Wipper, *B-spline Approximation of Neumann Problems*, Mathematics Institute, University of Stuttgart, 2002.

31. Hollig, K., U. Reif and J. Wipper, "Multigrid Methods with Web-splines", *Numerishe Mathematik*, Vol. 91, No. 2, pp. 237-256, 2002.

32. Hollig, K., U. Reif and J. Wipper, "Error Estimates for the Web-method", *Mathematical Methods for Curves and Surfaces: Oslo 2000*, Vanderbilt University Press, Nashville, TN, pp. 195-209, 2000.

33. Hollig, K., *Handbook of Computer Aided Geometric Design: Finite Element Approximation with Splines*, Mathematics Institute, Elsevier, Amsterdam, pp. 283-308, 2002.

34. Hollig, K., C. Apprich and A. Streit, "Introduction to the Web-method and its Application", *Advances in Computational Mathematics*, Vol. 23, pp. 215-237, 2005.

35. Rvachev, V. L., "Analtical Description of some Geometric Objects", *Dokl AS USSR*, Vol. 153, No: 4, pp. 765-768, 1963.

36. Rvachev, V. L. and T. I. Sheiko, "R-functions in Boundary Value Problems in Mechanics", *Applied Mechanics Reviews*, Vol. 48, No: 4, pp. 151-188, 1996.

37. Rvachev, V. L., T. I. Sheiko, V. Shapiro and I. Tsukanov, "On Completeness of RFM Solution Structures", *Computational Mechanics*, Vol. 25, No: 1, pp. 305-316, 2000.

38. Shapiro, V. and I. G. Tsukanov, "Implicit Functions with Guaranteed Differential Properties", *Fifth ACM Symposium on Solid Modeling and Applications*, Ann Arbor, Michigan, pp. 258-269, 1999.

39. Rvachev, V. L., A. N. Shevchenko and V. V. Veretelnik, "Numerical Integration Software for Projection and Projection-grid Methods", *Cybernetics and System Analysis*, Vol. 30, pp. 154-158, 1994.

40. Press, W. H., S. A. Teukolsky, W. T. Vetterling and B. P. Flannery, *Numerical Recipes in C*, Cambridge University Press, 2nd Edition, 1992.

41. Chen, R. S., E. K. Yung, C. H. Chan, D. X. Wang and D. G. Fang, "Application of the SSOR Preconditioned CG Algorithm to the Vector FEM for 3D Full-wave Analysis of Electromagnetic Field Boundary Value Problems", *IEEE Transactions on Microwave Theory and Techniques*, Vol. 50, No: 4, pp. 1165-1172, 2002.

42. Van der Vorst, H. A., "A Fast and Smoothly Converging Variant of BI-CG For The Solution of Nonsymmetric Linear Systems", *SIAM Journal on Scientific and Statistical Computing*, Vol. 13, No: 2, pp. 631-644, 1992.

43. Fang, Q., T. Tsuchiya and T. Yamamoto, "Finite Difference, Finite Element and Finite Volume Methods Applied to Two-point Boundary Value Problems", *The Journal of Computational and Applied Mathematics*, Vol. 139, pp. 9-19, 2002.

44. Caglar, H., N. Caglar and K. Elfaituri, "B-spline Interpolation Compared with Finite Difference, Finite Element and Finite Volume Methods Which Applied To Two-point Boundary Value Problems", *Applied Mathematics and Computation*, Vol. 175, pp. 72-79, 2006.

45. Strouboulis, T., I. Babuska and R. Hidajat, "The Generalized Finite Element Method for Helmholtz Equation: Theory, Computation, and Open Problems", *Computer Methods in Applied Mechanics and Engineering*, Vol. 195, pp. 4711-4731, 2006.

46. Bao, G., G. W. Wei and S. Zhao, "Numerical Solution of The Helmholtz Equation with High Wave Numbers", *International Journal for Numerical Methods in Engineering*, Vol. 59, pp. 389-408, 2004.

47. Reddy, C. J., M. D. Deshpande, C. R. Cockrell and F. B. Beck, *Finite Element Method for Eigenvalue Problems in Electromagnetics*, NASA Langley Research Center, 1994.

48. Balanis, C. A., *Advanced Engineering Electromagnetics*, Arizona State University, John Wiley and Sons, 1989.

49. Marcuvitz, N., *Waveguide Handbook*, IET, 1986.